Environmental Implications of Hydroxyl Radicals (°OH)

Published version:

DOI:10.1021/cr500310b

Chemical Reviews, 115, 2015, 13051-13092
DOI: 10.1021/cr500310b

The environmental implications of hydroxyl radicals ($^{\bullet}OH$)

Sasho Gligorovski[1*], Rafal Strekowski[1], Stephane Barbati[1], Davide Vione[2,3*]

[1]Aix-Marseille University, CNRS, FRE 3416, 3 Place Victor Hugo, 13331 Marseilles, France
[2]Dipartimento di Chimica, Università di Torino, Via P. Giuria 5, 10125 Torino, Italy
[3]Centro Interdipartimentale NatRisk, Università di Torino, Via L. Da Vinci 44, 10095 Grugliasco (TO), Italy.

Re-submitted to *Chemical Reviews* on 29/09/2015

Corresponding authors:

*Davide Vione E-mail: *davide.vione@unito.it*

*Sasho Gligorovski E-mail: *saso.gligorovski@univ-amu.fr*

1. Introduction

Ubiquitous occurrence of hydroxyl radicals ($^{\bullet}$OH) in various types of environments that include natural waters, atmosphere, biological systems and interstellar space is now well established. Hydroxyl radicals were first discovered in 1934 by Haber and Weiss [1] in what is known today as the Fenton reaction [2]. It is now well known that under most atmospheric conditions, $^{\bullet}$OH radicals govern the oxidative capacity of the natural atmosphere. $^{\bullet}$OH radicals are composed of a hydrogen atom bonded to an oxygen atom which make them highly reactive, readily stealing hydrogen atoms from other molecules to form water molecule. $^{\bullet}$OH radical reactivity with various water pollutants, that include bacteria, organic and inorganic compounds, continues to be a subject of scientific and governing agency pollution prevention interest in waste water treatment processes. Water and waste water regulatory requirements have become more strict and demanding regarding the characterization and identification of toxic effects on humans and other living organisms of numerous xenobiotics that are released into the natural waters. Hazardous and toxic organic and inorganic pollutants present in waters and wastewater need to be removed, inactivated or transformed into secondary by-products that are less toxic than the parent molecules. Advanced oxidation processes (AOPs) are techniques with this capacity. AOPs are near ambient temperature water treatment processes that use highly reactive $^{\bullet}$OH radicals among others as primary oxidants. In AOP processes, $^{\bullet}$OH radicals are generated usually by coupled chemical and/or physical systems that include H_2O_2/Fe^{II} or H_2O_2/Fe^{III} (Fenton), H_2O_2/catalyst or peroxide/catalyst (Fenton-like), O_3 (ozonation), and H_2O_2/O_3 (peroxone) that are often associated with an irradiation technique, namely Vacuum-UV radiation, UV radiation, pulse radiolysis or ultrasound. The gas, liquid and heterogeneous phase reactions of $^{\bullet}$OH radicals with organic compounds are often complex chemical processes that proceed through a number of partially oxidized radical intermediates. To directly identify these reaction transients in different media, they have to be studied in “real time”, that is, on the time scale that they actually exist. Therefore, diagnostic techniques must respond to rapid changes in radical concentration and life-time. Pulse radiolysis combined with competition kinetics methods, laser induced fluorescence and electron spin resonance (ESR) associated with the spin trapping technique are a few of the sophisticated diagnostic tools with this capacity. Alternatively, $^{\bullet}$OH radicals may be detected indirectly using scavengers and the derived products or adducts may then be analyzed using more conventional techniques. All of the above listed $^{\bullet}$OH radical detection techniques are discussed in this review paper.

The postulated mechanisms of $^{\bullet}$OH radical reactions are highly complex and many atmospheric reactions remain uncertain. However, in general, under most conditions, $^{\bullet}$OH reacts *via* an addition to a carbon-carbon unsaturated bond, aromatic ring substitution, hydrogen atom abstraction or monoelectronic oxidation. All of the above listed hydroxyl radical oxidation processes are discussed in this review.

1.1. Scope of the review

The scope of this review is confined to $^{\bullet}$OH radicals' occurrence and reactivity in the laboratory setting and in the natural environment that includes natural waters and the indoor and outdoor atmosphere. The $^{\bullet}$OH radical production and detection techniques both in the liquid and gas phase will be discussed. The review is divided into 7 chapters and aims to critically asses recent developments reflecting $^{\bullet}$OH radical formation, scavenging and detection methods in different environments and under laboratory conditions. The authors follow a multidisciplinary approach underlying the abundant nature of hydroxyl radicals in the natural environment and under laboratory conditions.

The first chapter introduces $^{\bullet}$OH radical as one of the most important reactive oxygen species (ROS). The second chapter gives an overview of $^{\bullet}$OH radical formation and scavenging in diverse natural environments. The $^{\bullet}$OH radicals are key oxidant species responsible for the oxidative capacity of the atmosphere and of surface waters, which are involved in the chemical transformation of an important number of primary pollutants into secondary compounds. The third chapter discusses the generation of $^{\bullet}$OH radicals under laboratory conditions, in both aqueous solution and the gas phase. A number of existing methods and recent techniques and developments involved in direct and indirect $^{\bullet}$OH radical production in the laboratory are reviewed. Because some of these methods can also be used in AOPs, a chapter paragraph briefly outlines the role of $^{\bullet}$OH generation in advanced oxidation techniques. The fourth chapter reviews several $^{\bullet}$OH radical detection and production/detection methods that can be used under controlled laboratory conditions to study the reactivity of $^{\bullet}$OH, namely, laser flash photolysis (where the laser pulse generates $^{\bullet}$OH in the presence of a substrate S and one then monitors a radiation-absorbing intermediate of the reaction S + $^{\bullet}$OH), laser induced fluorescence and spin trapping coupled with electron spin resonance spectroscopy, as well as the use of probe molecules in more conventional detection techniques. The fifth chapter reviews $^{\bullet}$OH radical reaction kinetics in aqueous solution, including the use of competition kinetics to derive the second-order reaction rate constants and the kinetics of formation and reactivity of $^{\bullet}$OH in surface waters. The $^{\bullet}$OH reaction mechanisms with selected organic and inorganic compounds in both aqueous solution and the gas phase are discussed in the sixth chapter. Concluding remarks will be given in the seventh chapter.

2. Formation and scavenging of $^{\bullet}$OH radicals under different conditions

2.1. $^{\bullet}$OH radicals in an aquatic environment

Major aqueous phase $^{\bullet}$OH radical sources include the solar irradiation of nitrate (NO_3^-) and nitrite (NO_2^-) ions as well as chromophoric dissolved organic matter (CDOM). The $^{\bullet}$OH radical production mechanism by nitrite photolysis is similar to the nitrate photolysis one. However, since the NO_2^- ion has a greater absorption cross section that is known to extend into longer wavelengths than the NO_3^- ion absorption spectrum, and because the quantum yield for the photochemical $^{\bullet}$OH radical production from NO_2^- ions is greater than the quantum yield for the photochemical $^{\bullet}$OH radical production from NO_3^- ions, NO_2^- ions are about two orders of magnitude more efficient in producing $^{\bullet}$OH radicals in aqueous phase than NO_3^- ions given equivalent concentrations. This issue partially compensates (or more than compensates) for the often lower levels reached by nitrite compared to nitrate in natural waters.[3] Further, the photogenerated $^{\bullet}$OH can react with nitrite to yield NO_2 that can further produce NO_2^- and NO_3^-, thereby coupling the dynamic cycles of NO_2^- and NO_3^- photolysis.[4]

The liquid phase oxidative attack of H_2O_2 on dissolved metals in their reduced forms, such as Fe(II) and Cu(I) can also lead to the production of $^{\bullet}$OH radicals in the liquid phase. However, this process is limited to waters where important concentrations of reduced metals are observed.[5,6] The photolysis of H_2O_2 in natural waters represents a less important $^{\bullet}$OH radical liquid phase source, although the quantum yield of $^{\bullet}$OH radical generation (Φ_{OH}) is in the range between 0.96 and 0.98 for the wavelength region $308 < \lambda(\text{nm}) < 351$.[7] This is due to the very poor overlap of H_2O_2 absorption spectrum with the ground-level solar spectrum irradiance.

Another potential source of $^{\bullet}$OH radicals in natural waters arises from the direct (UV-vis) photolysis of chromophoric dissolved organic matter (CDOM).[8,9] Recently, it has been shown that $^{\bullet}$OH radicals may be formed in a photosensitized reaction process.[10,11] Clifford et al. [10] and Reeser et al. [11] have shown that the uptake of non-radical oxidants such as ozone and its interaction with photo-activated organic material such as chlorophyll can lead to a production of secondary oxidants, namely $^{\bullet}$OH, O_3^-, $Cl/Cl_2^{\bullet-}$, $Br/Br_2^{\bullet-}$ and $I/I_2^{\bullet-}$.

In the presence of solar light irradiation, the $^{\bullet}OH$ radical production is a result of a modified reaction process between ozone (O_3) and chlorophyll where O_3 accepts an electron from the photoexcited chlorophyll yielding an $^{\bullet}OH$ radical.

$O_3 + H^+ + e^- \rightarrow {}^{\bullet}OH + O_2$ (R 2-1)

In the presence of ozone, another reaction that could be significant involves $O_3 + O_2^{-\bullet}$. If these processes take place in seawater, $^{\bullet}OH$ radicals may then react directly with dissolved organic matter, dissolved halogen ions and halogen-containing organic compounds.[11] In the oceans, $^{\bullet}OH$ radicals react rapidly with Br^- (R 2-2) to produce ultimately $Br_2^{-\bullet}$ (R 2-3), which in turn reacts with carbonate to generate carbonate radicals (R 2-4).[12]

$^{\bullet}OH + Br^- \rightarrow Br^{\bullet} + OH^-$ $k = 1.1 \cdot 10^{10}\ M^{-1}\ s^{-1}$ (R 2-2)

$Br^{\bullet} + Br^- \rightarrow Br_2^{\bullet-}$ $k = 1.1 \cdot 10^{10}\ M^{-1}\ s^{-1}$ (R 2-3)

$Br_2^{-\bullet} + CO_3^{2-} \rightarrow 2\ Br^- + CO_3^{-\bullet}$ (R 2-4)

The carbonate radicals, on the other hand, may self-terminate in competition with oxidation by organic compounds (OC).

$2\ CO_3^{-\bullet} + 2\ H^+ \rightarrow 2\ CO_2 + H_2O_2$ $k = 10^6$ to$10^7\ M^{-1}\ s^{-1}$ (R 2-5)

$CO_3^{-\bullet} + OC \rightarrow OC_{ox} + CO_3^{2-}$ (R 2-6)

2.2. $^{\bullet}$OH radicals in the atmosphere

It is well recognized that under most atmospheric conditions, the oxidative capacity of the atmosphere is governed by the reactions that involve $^{\bullet}OH$ radicals.[13] Hydroxyl radicals, known as the “detergent” of the atmosphere are important reaction chain initiators in most oxidation processes involving organic compounds. $^{\bullet}OH$ radicals initiate chain reactions in both polluted and clean atmospheres, where the rates of termination are comparable with the rates of propagation. The atmospheric lifetime of $^{\bullet}OH$ radicals ranges between 0.01 and 1 s, and it has been argued that their mixing ratio and vertical profile are controlled only by the local concentrations of longer-lived species such as O_3, VOCs, and NO_x, independent of atmospheric transport.[14] Although the mixing ratio of $^{\bullet}OH$ radicals is less than one part per trillion (ppt), the global levels of an important greenhouse gas (CH_4) would be many orders of magnitude higher in the absence of $^\bullet OH$.[15] The $^\bullet OH$ concentrations are strongly affected by ozone, and in turn they affect substantially the ozone concentration.[16] In the upper troposphere, the $^\bullet OH$ radicals are produced by photolysis of gaseous ozone.[17]

$O_3 + h\nu\ (\lambda \leq 310\ nm) \rightarrow O(^1D_2) + O_2$ (R 2-7)

$O(^1D_2) + H_2O \rightarrow 2\ ^\bullet OH$ (R 2-8)

In the lower troposphere, the photo-initiated reaction of ozone as a source of $^\bullet OH$ radicals is less important due to the weaker overlapping between ozone's absorption band and the solar spectrum.

However, Ravishankara et al. [18] indicated that contrary to what was previously believed, oxygen atoms in their excited state, $O(^1D_2)$, can be formed at wavelengths $\lambda \leq 330$ nm by the photolysis of internally excited ozone molecules O_3 (IE).

$$O_3(IE) \xrightarrow{\lambda \leq 310nm} O(^1D_2) + O_2(^1\Delta_g) \qquad \text{(R 2-9)}$$

The importance of R 2-9 is emphasized by a threefold increase in solar radiation light intensity at the sea level in the wavelengths region $310 \leq \lambda\ (nm) \leq 330$.

In the rural unpolluted areas under low NOx concentrations (NOx< 10 ppb) the $^\bullet OH$ radicals are mainly consumed by reaction with either carbon monoxide (CO) or methane (CH_4) to produce peroxy radicals such as $HO_2^\bullet$ and $CH_3O_2^\bullet$.

$^\bullet OH + CO \rightarrow H + CO_2$ (R 2-10)

$H + O_2 \rightarrow HO_2^\bullet$ (R 2-11)

$^\bullet OH + CH_4 \rightarrow\ ^\bullet CH_3 + H_2O$ (R 2-12)

$^\bullet CH_3 + O_2 \rightarrow CH_3O_2^\bullet$ (R 2-13)

Then the formed hydroxyl peroxy radicals ($HO_2^\bullet$) can further react with ozone (O_3) leading to the formation of $^\bullet OH$ radicals.

$HO_2^\bullet + O_3 \rightarrow\ ^\bullet OH + 2O_2$ (R 2-14)

$^\bullet OH\ ^+ O_3 \rightarrow HO_2^\bullet + O_2$ (R 2-15)

$HO_2^\bullet$ radicals can also recombine with themselves leading to the formation of hydrogen peroxide (H_2O_2), which in turn represents a source of $^\bullet OH$ radicals by the photolytic cleavage of the O-H bond.

$HO_2^\bullet + HO_2^\bullet \rightarrow H_2O_2 + O_2$ (R 2-16)

Alternatively, hydrogen peroxide reacts with $^\bullet OH$:

$H_2O_2 + {}^\bullet OH \rightarrow HO_2^\bullet + H_2O$ (R 2-17)

or with NO which leads to catalytic production of NO_2

$HO_2^\bullet + NO \rightarrow {}^\bullet OH + NO_2$ (R 2-18)

The photolysis of NO_2 leads to the formation of ozone, as follows:

$NO_2 + h\nu(\lambda < 420nm) \rightarrow NO + O(^3P)$ (R 2-19)

$O(^3P) + O_2 \rightarrow O_3$ (R 2-20)

which in turn leads to the formation of $^\bullet OH$ radicals through R-2-7.

The ozone production efficiency is a balance between the propagation of the free radical interconversion cycle and the rate of termination of the cycle. Under polluted conditions when the ratio between NO_x and VOCs concentrations is high, the competing chain propagation and termination reactions are given as follows:

$^\bullet OH + RH \rightarrow R^\bullet + H_2O$ (R 2-21)

$^\bullet OH + NO_2 + M \rightarrow HNO_3 + M$ (R 2-22)

where R 2-21 leads to the ozone generation and R 2-22 represents an effective loss mechanism of both HO_x and NO_x.

Alternatively, Li et al. [17] suggested that $^\bullet OH$ radicals can be photo-chemically formed through the fast reaction of electronically excited NO_2 and water vapor, as follows:

$NO_2 + h\nu(\lambda > 420nm) \rightarrow NO_2^*$ (R 2-23)

$NO_2^* + H_2O \rightarrow {}^\bullet OH + HONO$ (k = $1.7 \cdot 10^{-10}$ cm^3 molecule^{-1} s^{-1}) (R 2-24)

However, Carr et al. [19] demonstrated that this reaction is feasible only in the boundary layer of the Polar Regions when the sun is mostly laying low on the horizon. Hence, this reaction may efficiently explain the discrepancy between the model and the real-life observations only with respect to the Polar Regions. To a lesser extent, the reaction of O_3 with alkenes can also contribute to the production of $^\bullet OH$ radicals, particularly in forested and urban environments.[20] In addition, in the remote (and particularly the upper) troposphere, photodissociation of volatile organic compounds such as peroxides, acetone and some other ketones, alcohols and aldehydes may produce atmospheric $^{\bullet}OH$ radicals.[21–25]

Other very important $^{\bullet}OH$ radical sources in the lower troposphere include the photolysis of nitrous acid (HONO),[26] which occurs at wavelengths smaller than 390 nm [27] according to the following reaction:

$HONO + h\nu \rightarrow NO + {}^{\bullet}OH$ (R 2-25)

This $^{\bullet}OH$ source is particularly important in urban polluted areas with high NO_x levels.[34] $^{\bullet}OH$ radicals may also react with atmospheric HONO to generate nitrogen dioxide (NO_2):

${}^{\bullet}OH + HONO \rightarrow NO_2 + H_2O$ (R 2-26)

The back reaction of $^{\bullet}OH$ radicals with nitrogen oxide (NO) in the presence of a third body (N_2 or O_2) (R 2-27) regenerates HONO:

$NO + {}^{\bullet}OH + M \rightarrow HONO + M$ (R 2-27)

In polluted urban area the high NO_x levels suppress the $^{\bullet}OH$ concentrations through the following reaction:[28]

${}^{\bullet}OH + NO_2 \rightarrow HO_2{}^{\bullet} + NO$ (R 2-28)

It is worth mentioning that one alternative important pathway of $^{\bullet}OH$ radical formation in the lower atmosphere is the ozonolysis of alkenes. The reactions of ozone with alkenes leads to the generation of $^{\bullet}OH$ radicals at yields between 7–100% depending on the structure of the alkene.

2.2.1. •OH radical budget in the lower troposphere

The $^{\bullet}OH$ concentrations on a global level determine the oxidative capacity of the atmosphere. As described above the HO_x and NO_x are intimately linked, which implies that the influence of NO_x on HO_x can be expressed by a simple conversion ratio between $^{\bullet}OH$ and $HO_2{}^{\bullet}$, as follows:

$$\frac{[HO_2{}^{\bullet}]}{[{}^{\bullet}OH]} = \frac{k_{{}^{\bullet}OH+CO}[CO] + k_{{}^{\bullet}OH+CH_4}[CH_4] + k_{HO_2{}^{\bullet}+O_3}[O_3]}{k_{HO_2{}^{\bullet}+NO}[NO] + k_{{}^{\bullet}OH+O_3}[O_3]} \qquad \text{(R 2-29)}$$

This conversion ratio simply shows that the reaction of $^{\bullet}OH$ with CO, CH_4 and O_3 converts $^{\bullet}OH$ into $HO_2{}^{\bullet}$ and the reactions of $HO_2{}^{\bullet}$ with NO or O_3 convert $HO_2{}^{\bullet}$ into $^{\bullet}OH$.

As mentioned in the previous section, under polluted urban conditions $^{\bullet}$OH is primarily formed by photolysis of HONO (R 2-25). Recent studies [29–34] estimated that the contribution of HONO photolysis to the integrated $^{\bullet}$OH radical yield is 60%.

Soergel et al. [35] have shown that even in unpolluted forested regions the contribution of HONO photolysis to the $^{\bullet}$OH formation is higher than the contribution of ozone photolysis (R 2-8). Namely, the contribution of HONO is higher in the morning and evening hours, due to the longer wavelengths (up to ~400 nm) associated with HONO photolysis, compared to the contribution of ozone photolysis which occurs at $\lambda \leq 310$nm (R 2-7). Although the average HONO mixing ratios (ca. 30 ppt) are three orders of magnitude lower than mean O_3 mixing ratios around noon (ca. 35 ppb), and although $^{\bullet}$OH production rates by $O(^1D)$ exceed those of HONO photolysis by about 50% around noon, $^{\bullet}$OH radical production from HONO photolysis is about 20% larger than ozone photolysis in the lower troposphere, when integrated over the duration of a day (Figure 2).

Insert Figure 2

It has been shown that in highly polluted cities such as Santiago de Chile [36,37] the most important primary source of $^{\bullet}$OH radicals is the photolysis of HONO, comprising 81% and 52% of the $^{\bullet}$OH initiation rate during winter and summer, respectively, followed by ozonolysis of alkenes (12.5% and 29%), photolysis of formaldehyde (6.1% and 15%), and photolysis of ozone (<1% and 4%). During both winter and summer periods there was a balance between the $^{\bullet}$OH secondary production ($HO_2^{\bullet}$+NO) and destruction ($^{\bullet}$OH +VOCs), showing that initiation sources of $RO_2^{\bullet}$ and $HO_2^{\bullet}$ are no net $^{\bullet}$OH initiation sources. Therefore, the total rates of radical initiation and termination can be calculated by considering only the net radical sources and sinks which are implemented in the simple photostationary steady state model (PSS). [36,37]

$$^{\bullet}\mathrm{OH}_{\mathrm{PSS}} = \left(\frac{\mathrm{J\,(HONO)\,[HONO]} + \sum \mathrm{k}_{\mathrm{O_3+alkenes}}\mathrm{[alkenes][O_3]}\Phi_{^{\bullet}\mathrm{OH}} + J(O^1D)[O_3]\Phi_{^{\bullet}OH} + 2J(HCHO_{radical})[HCHO]}{\left(\mathrm{k}_{^{\bullet}\mathrm{OH+NO_2}}\mathrm{[NO_2]} + \mathrm{k}_{^{\bullet}\mathrm{OH+NO}}\mathrm{[NO]}\right)} \right) \quad \text{(Eq 2-1)}$$

where J(HONO), $J(O^1D)$ and $J(HCHO_{radical})$ are the photolysis frequencies of nitrous acid, ozone and formaldehyde (radical channel), respectively. For the ozonolysis of alkenes, $\Phi_{^{\bullet}OH}$ is the formation yield of $^{\bullet}$OH radicals which describes the amount of $^{\bullet}$OH produced when 1 molecule of ozone reacts with 1 molecule of a given alkene. For the photolysis of ozone, $\Phi_{^{\bullet}OH}$ is defined as the fraction of O^1D that will react with H_2O

rather than being quenched to ground state O^3P. $k_{O_3+\text{alkenes}}$, $k_{^\bullet OH+NO_2}$ and $k_{^\bullet OH+NO}$ are the rate constants for the reactions between ozone and alkenes, $^\bullet$OH and NO_2 and $^\bullet$OH and NO, respectively.

An excellent agreement between the $^\bullet$OH concentration profiles obtained by the more elaborate MCM (master chemical mechanism) model and PSS models confirmed that indeed the main $^\bullet$OH radical sources and sinks are integrated in the PSS model, with respect to the polluted urban areas.

Regarding the moderately polluted areas such as the pristine rainforest of Amazon, a recent study [38] revealed that the photo-oxidation of unsaturated hydroperoxy-aldehydes (HPA, products of isoprene oxidation) represents an important $^\bullet$OH source. These investigators suggested that the HPA photolysis initiates a hydroxyl radical production cascade that is limited by the reaction of HPA with the $^\bullet$OH radical itself. Significantly higher $^\bullet$OH radical concentrations than expected by the model calculations were also detected during chamber experiments, providing direct evidence for a strong $^\bullet$OH radical enhancement due to the additional recycling of radicals in the presence of isoprene. [39] However, the $^\bullet$OH recycling observed in the chamber study is not sufficient to explain the unexpectedly high concentrations of $^\bullet$OH radicals reported in moderately polluted areas such as the Amazon basin, the Pearl River Delta and Borneo, among others.[38,40–42]

However, the proposed $^\bullet$OH recycling mechanism could contribute significantly to the oxidizing capacity of the atmosphere under isoprene-rich conditions.

Petters and his coworkers[43] proposed novel peroxy radical pathways in isoprene oxidation at low and moderate NO levels, with the aim of justifying the observed $^\bullet$OH regeneration in moderately polluted regions.

The suggested isomerization reactions of isoprene peroxy radicals were found to result in an increase of the modeled $^\bullet$OH levels in the planetary boundary layer by up to a factor of 3, in agreement with the experimental observations during the field campaign in the Amazon basin.

A recent study [44], however, estimated negligible variations of $^\bullet$OH concentrations (ranging from 2 to 3%) on a global level. These estimations were based on atmospheric measurements, in the period 1998-2007, of a trace gas (methyl chloroform) whose predominant sink is the reaction with $^\bullet$OH.

Regarding the global $^\bullet$OH levels, another study [45] determined the Northern to Southern Hemispheric (NH/SH) $^\bullet$OH concentration ratio with the help of methyl chloroform data and an atmospheric transport model, which accurately describes interhemispheric transport and modeled emissions. These investigators found that for the period 2004-2011, the model predicted an annual-mean NH-SH gradient of methyl chloroform that is a linear function of the modeled NH/SH ratio in annual-mean $^{\bullet}$OH. They [45] determined a NH/SH $^{\bullet}$OH ratio of 0.97±0.12 during this time period, by optimizing global total emissions and mean $^{\bullet}$OH abundance to fit methyl chloroform data from two surface measurements networks and aircraft campaigns.

In a short period of time, the large emissions of reactive gases such as methane could swamp the $^{\bullet}$OH radicals and induce large variations. For example, variations in $^{\bullet}$OH concentrations of up to 20% have been estimated from ^{14}CO, in the period of few months. [46] However, a long-term study carried out between 1999 and 2003 [17] at the Meteorological Observatory Hohenpeissenberg in southern Germany revealed that the $^{\bullet}$OH concentrations are linearly dependent on solar ultraviolet radiation. These authors claimed that the intensity of UVB radiation is sufficient to predict $^{\bullet}$OH concentrations more accurately than current, complex atmospheric models that take into account factors such as temperature, ozone and the concentrations of the atmospheric pollutants, pointing to the fact that the current theory fails to explain the oxidative chemistry of the lower atmosphere.

A comprehensive understanding of the $^{\bullet}$OH radical behavior in the atmosphere and its reactions with other organic and inorganic compounds is of paramount importance to improving the accuracy of atmospheric models. In the future, the increased pollution induced by the anthropogenic factor coupled with a climate change could lead to significant changes in the $^{\bullet}$OH radical budget. To better understand these issues, investigators need models that have higher resolution, include interactive coupling with biosphere processes and climate change, and draw on improved emission inventories.

Clearly, further studies need to be performed in order to make a conclusion about the $^{\bullet}$OH radical budget in the troposphere. With this respect recent advances regarding the measurements of $^{\bullet}$OH reactivity allow deeper understanding of the $^{\bullet}$OH radical budget. The measurements of $^{\bullet}$OH reactivity can be performed with three existing techniques (laser induced fluorescence, differential optical absorption spectroscopy and chemical ionization mass spectrometry) that have been detailed in a review by Heard and Pilling.[47]

2.3. $^{\bullet}$OH radicals in the indoor atmospheres

Whereas the $^{\bullet}$OH radical concentrations in the troposphere have been a topic of intense research, the $^{\bullet}$OH radical within indoor environments has received little attention. Considering the extremely short lifetime of $^{\bullet}$OH radicals, the outdoor-to-indoor transport can be neglected. However, the possibility must not be ignored that $^{\bullet}$OH radicals can be formed by indoor chemistry. A modeling study by Nazaroff and Cass [48] suggested that $^{\bullet}$OH radicals with concentration of $5.4 \cdot 10^4$ cm^{-3} can be generated indoors by gas-phase reactions between ozone and alkenes. Their overall kinetic mechanism included a generic reaction that yields $^{\bullet}$OH radicals, as follows:

$$\text{Alkenes} + O_3 \rightarrow RCHO + HCHO + HO_2^{\bullet} + RO_2^{\bullet} + {}^{\bullet}OH + RO^{\bullet} \qquad \text{(R 2-30)}$$

The model of Weschler and Shields [49] predicted an $^{\bullet}$OH concentration of $1.7 \cdot 10^5$ cm^{-3}, at ozone mixing ratio of 20 ppb and assuming average indoor mixing ratios of the alkenes. Based on the idea that ozonolysis of alkenes represents an important indoor $^{\bullet}$OH source, Weschler and Shields [50] performed the first indirect $^{\bullet}$OH measurements by use of 1,3,5-trimethylbenzene as a reactive $^{\bullet}$OH radical tracer. To determine an average $^{\bullet}$OH concentration, 1,3,5-trimethylbenzene was emitted into the indoor environment at a known rate assuming that it reacts exclusively with $^{\bullet}$OH. These measurements were performed applying rather high ozone mixing ratio, in the range between 62 and 192 ppb. As a result an average $^{\bullet}$OH concentration of $7 \cdot 10^5$ cm^{-3} was obtained, that is about six times higher than the previous model calculations [49]. Sarwar et al. [51] using the comprehensive SAPRC-99 atmospheric chemistry model predicted an $^{\bullet}$OH concentration of $1.2 \cdot 10^5$ cm^{-3} for a base case scenario, again assuming that gas-phase reaction between ozone and alkenes is a main $^{\bullet}$OH source. A MCM chemistry model performed by Carslaw [52] predicted maximum daytime $^{\bullet}$OH concentration of $4 \cdot 10^5$ cm^{-3}. Although this value is similar to the $^{\bullet}$OH levels obtained by chemical tracers, the initial ozone mixing ratios which were considered in the model were much lower, hence more realistic (3-13 ppb). White et al. [53], based on chemical tracers of indoor $^{\bullet}$OH radical, performed indirect measurements in two seminar rooms in UK. These measurements confirmed that the indoor $^{\bullet}$OH concentrations range in the order between 10^4 to 10^5 cm^{-3} in agreement with all the previous modeling and indirect studies.

It was believed [48] that the sunlight that penetrates indoors through the windows is largely attenuated, especially in the UV region. Consequently, the photochemical formation of $^{\bullet}$OH radicals within indoor environments has been completely ignored until 2013, when Gligorovski and his coworkers [54] directly measured $^{\bullet}$OH concentrations of $1.8 \cdot 10^{6}$ cm^{-3} in a real-life indoor environment. This elevated $^{\bullet}$OH level was associated with the photolysis of HONO (Figure 3) and it is an order of magnitude higher than former indoor $^{\bullet}$OH radical concentration estimates. Indeed, it is comparable to the $^{\bullet}$OH levels of a typical urban environment [14].

Insert Figure 3

The work of Gligorovski et al. presented some truly innovative results since it tested all the previous theories and models mentioned above. Another study performed by the same investigators [55] with chamber experiments showed that even higher $^{\bullet}$OH concentrations (up to $1.6 \cdot 10^{7}$ cm^{-3}) emerge from the photolysis of HONO directly emitted by combustion processes such as burning candle.

These results are not surprising considering that HONO has strong absorption bands in the near-UV region extending up to ~390 nm.[27] Recent studies [56,57] demonstrated that these wavelengths (λ>340nm) are available indoors and that they can initiate efficient photochemistry. Moreover, significant HONO levels can be directly emitted by combustion processes which exceed those in the polluted urban regions.[58] The heterogeneous reactions of gaseous NO_2 towards adsorbed water layers on various indoor surfaces (R 2-31) can also contribute to the indoor HONO levels.[59]

$$2NO \; + H_2O \rightarrow HONO + HNO_3 \qquad \text{(R 2-31)}$$

Bartolomei et al. and Gomez Alvarez et al. [60,61] revealed a “new” source of high levels of indoor HONO in the photosensitized heterogeneous reactions of gas-phase NO_2 with indoor surfaces such as glass, detergent, paint and lacquer. In the case of lacquer, one of its constituents is benzophenone that is a known photo-sensitizer [62] and was suggested as a reason for the enhanced HONO production. The generated HONO surface flux under light irradiation of the surface covered with lacquer was $2.8 \cdot 10^{10}$ molecules cm^{-2} s^{-1}, which is of similar magnitude to $2.5 \cdot 10^{10}$ molecules cm^{-2} s^{-1} obtained by the heterogeneous reactions of NO_2 with humic acid, that is a soil constituent [63]. Gandolfo et al. [64] reported an HONO surface flux of $2.9 \cdot 10^{10}$ molecules cm^{-2} s^{-1} produced under realistic indoor integrated UV (340 nm<λ<400nm) light irradiation (10 W m^{-2}) of a surface covered with photocatalytic paint. The latter contained 7 % of TiO_2 (w/w) at 30 % relative humidity, in the presence of 40 ppb of NO_2. Applying this HONO surface flux in a dynamic mass balance model and considering the photolysis of HONO as a main sink, a steady day-time state mixing ratio of HONO of 5.6 ppb has been obtained [65]. While our understanding of indoor photochemistry is still in its infancy, these results suggest that it is an area that warrants further studies. [66]

2.3.1. Estimation of the $^{\bullet}$OH radical budget in the indoor air

$^{\bullet}$OH radical concentrations in the order of 10^6-10^7 cm^{-3} produced by the photolysis of HONO can control the oxidative capacity of indoor atmospheres. During the reactions of $^{\bullet}$OH radicals with the indoor VOCs, reactive intermediate species are formed. Finally, secondary pollutants such as ozone, secondary aerosols and VOCs oxidation products would be produced within indoor environments. In order to accurately describe the oxidative capacity of indoor atmospheres and effectively evaluate human exposure to the reactive intermediates and secondary organic pollutants, a quantitative knowledge of $^{\bullet}$OH radical concentrations is of paramount importance. [66] The $^{\bullet}$OH radical budget can be determined using the zero dimensional photochemical box model based on the Master Chemical Mechanism, MCMv3.1 [67,68] and a simple quasi-photostationary state model (PSS) [36,37,54]. Regarding a polluted urban atmosphere, in Santiago de Chile (see section 2.2) it has been established [36,69] an excellent agreement between the $^{\bullet}$OH concentration profiles obtained by both the MCM and PSS models. Therefore, the main $^{\bullet}$OH radical sources and sinks are incorporated in the PSS model. Photolysis of ozone and formaldehyde can be neglected within indoor environments because the glass window filters out the wavelengths $\lambda < 340$ nm [56,57]. Therefore, with respect to the indoor atmospheres, Eq 2-1 can be reduced to Eq 2-2:

$$^{\bullet}OH_{PSS} = \left(\frac{J_{HONO}[HONO] + \sum k_{O_3+alkenes}[alkenes][O_3]\Phi_{^{\bullet}OH}}{\left(k_{^{\bullet}OH+NO_2}[NO_2] + k_{^{\bullet}OH+NO}[NO]\right)} \right) \qquad \text{(Eq 2-2)}$$

Gomez Alvarez et al. [54] tested the PSS model for the indoor atmosphere by plotting the measured $^{\bullet}$OH radical concentrations against the $^{\bullet}$OH values estimated by Eq 2-2. The obtained slope of 0.6 indicated an underestimation of the measured $^{\bullet}$OH concentrations. This underestimation emerged from the photolysis frequencies (J) of HONO (J(HONO)) which were spanning in the range between 1.0 and $1.5 \cdot 10^{-4}$ s^{-1}. These values were calculated based on direct measurements of the spectral irradiance by a spectroradiometer with flat collector (LiCOR Li-1800). The measured spectral irradiances were used to estimate the actinic fluxes assuming that the solar flux reflected by the indoor surfaces is isotropous, in the case when the spectroradiometer was in the shed. When the spectroradiometer was irradiated, only the direct solar flux was considered and the reflected flux was neglected. The estimated actinic flux was then used to determine the J(HONO) values. Despite the possibility of using advanced algorithms to convert the spectral irradiance into actinic flux, it has been recommended that if the actinic flux is the primary radiation quantity of interest, it should be measured in preference to the irradiance because there can be a factor of 3 to 5 difference depending on the surface.[70] Indeed, Bartolomei et al. [55] demonstrated an excellent agreement between the measured $^{\bullet}OH$ concentrations and the PSS model, whereas the J(HONO) values were measured by Metcon 2π spectral radiometer with an electronically cooled Charge Coupled Device (CCD) detector, confirming that **the** PSS model is an appropriate tool to model the measured $^{\bullet}OH$ concentrations in indoor atmosphere with NO_x levels higher than 10 ppb, which is common in the urban environment.

Moreover, these investigators demonstrated that in indoor environments in the presence of combustion sources such as burning candle, the photolysis of HONO is the main source of $^{\bullet}OH$ radicals. Hence, the Eq-2-2 can be rewritten as follows:[66]

$$^{\bullet}OH_{PSS} = \left(\frac{J_{HONO}[HONO]}{\left(k_{^{\bullet}OH+NO_2}[NO_2] + k_{^{\bullet}OH+NO}[NO] + k_{^{\bullet}OH+HONO}[HONO]\right)} \right) \qquad \text{(Eq-2.3)}$$

Considering that the photolysis of HONO is a primary $^{\bullet}OH$ source and using the photolysis frequency J(HONO)= $7.2 \cdot 10^{-4}$ s^{-1} [64] of a typical indoor environment under direct solar radiation, the obtained $^{\bullet}OH$ production rate of 10.4 ppb h^{-1} is 10 times higher than the value of 1.1 ppb h^{-1} resulting from the fastest reaction between ozone and d-limonene, assuming a typical ozone mixing ratio of 10 ppb, in the absence of ozone-based air purifiers. For this calculation, an average mixing ratio of ca. 7 ppb of d-limonene was applied considering that, typically, the background indoor mixing ratio of d-limonene is between 5 and 10 ppb. [71]

A similar $^{\bullet}OH$ production rate of 0.9 ppb h^{-1} was obtained by Weschler and Shields [49] based on the reaction between ozone and d-limonene, assuming a relatively high ozone mixing ratio (20 ppb) and 2.9 ppb of d-limonene.

This comparison of the $^{\bullet}$OH formation rates emphasizes the importance of nitrous acid towards the oxidative capacity of indoor atmospheres. [72]

3. Generation of $^{\bullet}$OH radicals under controlled laboratory conditions

This section compares and contrasts the laboratory methods currently employed to produce $^{\bullet}$OH radicals under controlled conditions, that is, experimental conditions where the quantum yield of $^{\bullet}$OH radicals produced is known. It is not possible to provide an all-inclusive description of all datasets, therefore, this section will focus on representative techniques used in atmospheric and environmental sciences that include water and wastewater treatment technologies.

Heterogeneous and photocatalytic $^{\bullet}$OH radical production processes are not reviewed since these $^{\bullet}$OH radical reaction mechanisms remain largely uncertain and the $^{\bullet}$OH radical production quantum yields cannot be established with certainty.[73–75] In addition, there have been a number of recent publications and reviews that specifically cover heterogeneous photocatalytic and other similar $^{\bullet}$OH radical production processes.[76,77] However, few advanced oxidation process (AOP) techniques that involve heterogeneous photocatalytic $^{\bullet}$OH radical production of environmental interest will be discussed at the end of this chapter.

3.1. Generation of $^{\bullet}$OH radicals in the aqueous phase

3.1.1. Nitrate (NO_3^-)/UV

The nitrate anion NO_3^- absorbs UV radiation up to around 340 nm, with absorption maxima in the UVC and UVB. Radiation absorption by nitrate produces $^{\bullet}$OH through several pathways that can be activated in different wavelength intervals. A general overview of the $^{\bullet}$OH radical formation processes that result from nitrate photolysis is the following: [78,79]

$NO_3^- + h\nu \rightarrow [O^{-\bullet} + {}^{\bullet}NO_2]_{cage} \rightarrow O^{-\bullet} + {}^{\bullet}NO_2$ (R 3-1)

$O^{-\bullet} + H^+ \leftrightarrows {}^{\bullet}OH$ (R 3-2)

$NO_3^- + h\nu \rightarrow ONOO^-$ (R 3-3)

$ONOO^- + H^+ \leftrightarrows ONOOH$ (R 3-4)

$ONOOH \rightarrow {}^{\bullet}OH + {}^{\bullet}NO_2$ (R 3-5)

The process that is described by reactions (R 3-1, R 3-2) plays an important role as ${}^{\bullet}OH$ source in natural waters (*vide infra*, section 5.2).[80] Note that ${}^{\bullet}OH$ has $pK_a \approx 12$, thus its conjugated base $O^{-\bullet}$ would not occur to a significant extent at lower pH values. Therefore, the ${}^{\bullet}OH$ production process by (R 3-1, R 3-2) would not show a significant pH dependence in the ~neutral range, despite the involvement of H^+ in reaction (R 3-2).[81] Possible pH effects in such a range have to be explained differently (*vide infra*).

A major feature of reaction (R 3-1) is the fact that the photoproducts $O^{-\bullet} + {}^{\bullet}NO_2$ are initially formed inside a cage of water molecules, where they can either recombine to nitrate or diffuse into the solution bulk.[82] The quantum yield of bulk $O^{-\bullet}/{}^{\bullet}OH$ generation in (R 3-1) has been found to vary with wavelength, from 0.2 at 200 nm to 0.01 at 300 nm [83] and above, [84] probably because of the involvement of different transitions connected to different nitrate absorption bands.[85] The reported values actually represent the yield of ${}^{\bullet}OH$ that reaches the solution bulk by diffusion/protonation after escaping recombination with ${}^{\bullet}NO_2$. The quantum yield of the primary process that gives $[O^{-\bullet} + {}^{\bullet}NO_2]_{cage}$ would be higher, and it can be assessed by using hydroxyl scavengers in excess that should be able to react with cage $O^{-\bullet}$ in addition to reacting with bulk ${}^{\bullet}OH$. By monitoring either the oxidation products of the ${}^{\bullet}OH$ scavengers (suitable scavengers may be *e.g.* 2-propanol and bromide) [86] or the transformation of compounds undergoing selective reactions with ${}^{\bullet}NO_2$ (*e.g.* phenol → 2-nitrophenol),[87] it was possible to determine that the quantum yield of $[O^{-\bullet} + {}^{\bullet}NO_2]_{cage}$ would be 3-5 times higher than that of bulk ${}^{\bullet}OH$. Indeed, the recombination of $[O^{-\bullet} + {}^{\bullet}NO_2]_{cage}$ to nitrate would be faster than their diffusion into the solution bulk.[87]

When studying the formation of ${}^{\bullet}OH$ upon nitrate photolysis as a function of pH, it is often found that the relevant yield decreases with increasing pH in the ~neutral range. This issue cannot be accounted for by reaction (R 3-2), which would rather cause a pH dependence in the basic range (around pH 12). The ~neutral pH trend would reflect the formation of $ONOO^-/ONOOH$ in reactions (R 3-3, R 3-4) and the homolysis of the latter in (R 3-5).[88] Indeed, ONOOH has $pK_a \approx 6.6\text{-}7$ that is consistent with the observed pH trend. Moreover $ONOO^-$, differently from ONOOH, does not yield ${}^{\bullet}OH$ upon further transformation.[89]

In the presence of irradiated nitrate, organic compounds would mainly undergo transformation because of reaction with ${}^{\bullet}OH$.[90] However, the process also yields nitrating agents such as ${}^{\bullet}NO_2$ and ONOOH, which can induce the formation of nitroderivatives in the presence of electron-rich substrates (*e.g.* phenol) or even with unsubstituted aromatics.[90,91] Photonitration reactions induced by ${}^{\bullet}NO_2$ are enhanced by elevated concentration values of ${}^{\bullet}OH$ radical scavengers that can react with cage $O^{-\bullet}$, inhibit the recombination of $O^{-\bullet} + {}^{\bullet}NO_2$ to nitrate, and favor the release of ${}^{\bullet}NO_2$ in the solution bulk.[87] The nitrating agent ONOOH operates with higher yields in acidic conditions, possibly because of the formation of $ONOOH_2^+$.[92] A further nitrating (and nitrosating) agent that is produced by irradiated nitrate in acidic solution is HNO_2, [92] which is particularly effective towards electron-rich aromatics such as some phenols and anilines.[93] The production of nitrous acid is due partially to the direct photochemical generation of nitrite (R 3-6, minor process with quantum yield 0.001) [84] followed by protonation, and partially to the hydrolysis of photogenerated ${}^{\bullet}NO_2$:

$$NO_3^- + h\nu \rightarrow NO_2^- + O \qquad \text{(R 3-6)}$$

$$NO_2^- + H^+ \leftrightarrows HNO_2 \qquad \text{(R 3-7)}$$

$$2\,{}^{\bullet}NO_2 \leftrightarrows N_2O_4 \xrightarrow{H_2O} NO_3^- + H^+ + HNO_2 \qquad \text{(R 3-8)}$$

3.1.2. Nitrite (NO_2^-) /UV

The nitrite anion (NO_2^-) absorbs UV radiation with maxima in the UVC and UVA. In the UV range nitrite has actually three absorption bands, but the intermediate one (which spans UVC and UVB) is the least intense and only gives a shoulder between 270 and 300 nm. The presence of multiple bands can explain why the quantum yield of ${}^{\bullet}OH$ production upon nitrite photolysis varies with wavelength, from ~0.065 at or below 300 nm to ~0.025 above 350 nm. The production of ${}^{\bullet}OH$ upon nitrite photolysis can be described as follows:[78,81]

$$NO_2^- + h\nu \rightarrow O^{-\bullet} + {}^{\bullet}NO \qquad \text{(R 3-9)}$$

$$O^{-\bullet} + H^+ \leftrightarrows {}^{\bullet}OH \qquad \text{(R 3-10)}$$

Also in this case, pH would play an important role in the $O^{-\bullet}/{}^{\bullet}OH$ equilibrium only in the basic range (~12). Under neutral conditions, reaction (R 3-10) equilibrium is shifted toward products, that is, toward ${}^{\bullet}OH$ radical production. Contrary to nitrate anions, nitrite anions react with ${}^{\bullet}OH$ radicals to produce nitrogen dioxide:[81]

$NO_2^- + {}^\bullet OH \rightarrow {}^\bullet NO_2 + OH^-$ (R 3-11)

The above reaction is responsible for the effective formation of nitroderivatives, when nitrite is irradiated in the presence of organic and most notably of aromatic molecules.[92,94]

Under UV irradiation, nitrite can additionally undergo photoionization with very low quantum yield ($< 10^{-3}$):[81]

$NO_2^- + h\nu \rightarrow {}^\bullet NO_2 + e^-$ (R 3-12)

The most interesting effect of pH on nitrite photolysis is observed in the acidic range and it is the consequence of the acid-base equilibrium between HONO and NO_2^- ($pK_a \approx 3.3$). Because nitrous acid exhibits much higher $^\bullet OH$ quantum yield (0.35) compared to nitrite, and because it absorbs radiation to a comparable extent (although with a significantly different absorption spectrum, which shows clear vibrational bands even in solution), the formation of $^\bullet OH$ radicals upon photolysis of HONO/NO_2^- significantly increases below pH 5.[95,96]

$HONO + h\nu \rightarrow {}^\bullet OH + {}^\bullet NO$ (R 3-13)

A major consequence of the production of $^\bullet OH$ upon nitrite photolysis is the hydroxylation of dissolved organic compounds. However, irradiated nitrite is also an effective nitrating and nitrosating agent.[92,96,97] These processes are induced by $^\bullet NO_2/N_2O_4$ and N_2O_3 [98] and they require the formation of $^\bullet NO_2$, which is produced by nitrite oxidation (R 3-11). Nitrogen dioxide (formed in R 3-11) can in fact dimerize or react with $^\bullet NO$ (formed in R 3-9) to give the nitrosating agent N_2O_3. Interestingly, aromatic nitroderivatives can also be formed through a nitrosation/oxidation pathway.[92] Moreover, HONO is also an effective nitrating agent for phenolic compounds in the dark.[92]

Photonitration and photonitrosation reactions induced by nitrite are strongly favored at elevated nitrite concentrations, which enhances (R 3-11), and they are inhibited by $^\bullet OH$ radical scavengers that inhibit the same reaction.[94]

3.1.3. Hydrogen peroxide (H_2O_2)/UV

Hydrogen peroxide absorbs radiation in the UVC (100-280 nm) region of the solar spectrum, but it features an absorption tail that spans the UVB (280-315 nm) and part of the UVA (315-400 nm) regions of the solar spectrum. However, the molar absorption coefficient above 300 nm is quite low, and competition for irradiance with other radiation-absorbing compounds is often unfavorable toward H_2O_2 photolysis. Therefore, for practical purposes the photolysis of H_2O_2 is mostly exploited under UVC irradiation, and the Hg emission line at 253.6 nm is the most popular photolysis wavelength source because of its low cost. A more expensive method to generate $^\bullet$OH radicals by H_2O_2 photolysis includes a discharge-pumped KrF laser that operates at 248 nm wavelength.

The photolysis of a H_2O_2 molecule yields two $^\bullet$OH radicals. Given a rather elevated photolysis quantum yield ($\Phi \approx 0.5$ in an aqueous solution), the H_2O_2 photolysis is a fairly attractive way of generating $^\bullet$OH in an aqueous solution.[99] A potential drawback is the scavenging of $^\bullet$OH by H_2O_2 itself. However, the $^\bullet$OH by H_2O_2 reaction has been reported to have a relatively low rate constant ($k_{R3\text{-}15} = 2.7 \cdot 10^7\ M^{-1}\ s^{-1}$).[100] To maximize the effectiveness of solute degradation by $^\bullet$OH radicals, the concentration of H_2O_2 should be maintained at values where its ability to scavenge hydroxyl radicals is limited compared to the other water constituents and the reaction should be carried out at pseudo steady-state-conditions, that is, [$^\bullet$OH]<<[Reactant]. By further increasing the concentration of H_2O_2, the degradation rates of substrates/pollutants would reach a “plateau” or even decrease with increasing H_2O_2 concentration.[101,102]

$$H_2O_2 \xrightarrow{h\nu} 2^\bullet OH \qquad \text{(R 3-14)}$$

$$H_2O_2 + {}^\bullet OH \rightarrow HO_2^\bullet + H_2O \qquad \text{(R 3-15)}$$

Interestingly, the quantum yield of $^\bullet$OH radicals in the photolysis of H_2O_2 (R 3-14) is reported to be $\Phi_{^\bullet OH} = 2.09 \pm 0.36$ in the gas phase [103] and $\Phi_{^\bullet OH} \sim 1$ in an aqueous solution. The primary event of H_2O_2 photolysis yields two $^\bullet$OH, which are “free” in the gas phase but are surrounded by the solvent molecules in an aqueous solution. This solvent “cage” favors geminate recombination ($2\,^\bullet OH \rightarrow H_2O_2$) that competes with $^\bullet$OH diffusion into the solution bulk (R 3-16). Measurements of photolysis quantum yields usually consider bulk

$^{\bullet}$OH, thus the geminate recombination within the solvent cage would decrease the observed yield of the photolysis process.[3]

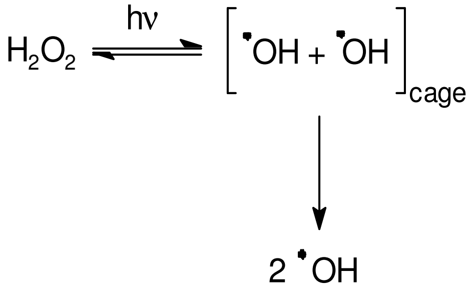

(R 3-16)

The kinetics of the transformation reactions induced by photogenerated $^{\bullet}$OH radicals depend on the concentration of H_2O_2, because absorbed radiation (and photolysis rate as a consequence) reaches saturation with increasing $[H_2O_2]$, while $^{\bullet}$OH scavenging does not.[104] The generation rate of $^{\bullet}$OH upon H_2O_2 photolysis can be expressed as follows:[105]

$$R_{^{\bullet}OH}(\lambda) = \Phi_{^{\bullet}OH} \cdot \frac{\varepsilon(\lambda) b [H_2O_2]}{A(\lambda)+\varepsilon(\lambda) b [H_2O_2]} \left[p^{\circ}(\lambda)\left(1-10^{-A(\lambda)-\varepsilon(\lambda) b [H_2O_2]}\right)\right] \qquad \text{(Eq 3-1)}$$

In equation 3-1 above, $p^{\circ}(\lambda)$ is the photon flux emitted by the radiation source (which for simplicity could be considered monochromatic), $(\varepsilon(\lambda) b [H_2O_2]) \cdot (A(\lambda)+\varepsilon(\lambda) b [H_2O_2])^{-1}$ is the fraction of the solution absorbance that is accounted for by H_2O_2, $\varepsilon(\lambda)$ is the molar absorption coefficient of H_2O_2, $A(\lambda)$ is the total absorbance of the solution before the addition of H_2O_2, and *b* is the optical path length within the irradiated solution. The steady-state $[^{\bullet}OH]$ depends on the formation-transformation budget, because $^{\bullet}$OH is consumed by both H_2O_2 and the other scavengers and impurities present in solution (with *S* as the relevant scavenging rate constant).[106] The transformation rate of a generic pollutant would be proportional to $[^{\bullet}OH]$, which can be expressed as follows:

$$[^{\bullet}OH] = \frac{R_{^{\bullet}OH}(\lambda)}{k_{R3-2}\,[H_2O_2]+S} = \frac{\Phi_{^{\bullet}OH}\left[p^{\circ}(\lambda)\left(1-10^{-A(\lambda)-\varepsilon(\lambda) b [H_2O_2]}\right)\right]}{k_{R3-2}\,[H_2O_2]+S} \cdot \frac{\varepsilon(\lambda) b [H_2O_2]}{A(\lambda)+\varepsilon(\lambda) b [H_2O_2]} \qquad \text{(Eq 3-2)}$$

Considering that $p^{\circ}(\lambda)$ will vary under different experimental conditions, one can define the ratio $\Re = [^{\bullet}OH]\,[p^{\circ}(\lambda)]^{-1}$ that would make modeling easier. The equation that describes $\Re$ is the following:

$$\Re = \frac{\Phi_{^{\bullet}OH}\left(1-10^{-A(\lambda)-\varepsilon(\lambda) b [H_2O_2]}\right)}{k_{R3-2}\,[H_2O_2]+S} \cdot \frac{\varepsilon(\lambda) b [H_2O_2]}{A(\lambda)+\varepsilon(\lambda) b [H_2O_2]} \qquad \text{(Eq 3-3)}$$

At a given value of $p°(\lambda)$, $\Re$ is directly proportional to the decay constant observed upon reaction of the dissolved substrate with $^{\bullet}OH$. Assuming that irradiation is monochromatic, one can use $\varepsilon(\lambda)\ b = 50\ M^{-1}$ (which is a reasonable value under UVC irradiation with b in the cm range), **a** scavenging rate constant $S \leq 2 \cdot 10^5\ s^{-1}$, and the total absorbance of the solution before the addition of H_2O_2, $A(\lambda) = 1$.[107,108] **Under these assumptions, the** plot of $[H_2O_2]$ and S versus $\Re$ is shown in Figure 4.

Insert Figure 4

As shown in Figure 4, the maximum value of $\Re$ *vs.* $[H_2O_2]$ is located at higher H_2O_2 concentration values when S is higher. This is reasonable because the higher the S, the less important is the relative role of H_2O_2 as a scavenger. The reason for having a maximum is that elevated $[H_2O_2]$ values tend to saturate absorption and to induce important $^{\bullet}OH$ scavenging. Indeed, at $[H_2O_2] > 0.02$ M, $\varepsilon(\lambda) b [H_2O_2] > A(\lambda)$. Also, as shown in Figure 3, $\Re$ decreases with increasing S, which measures the overall $^{\bullet}OH$ scavengers that are present in solution (with the exception of H_2O_2).

3.1.4. Fenton reaction

The name of "Fenton reaction" encompasses a complex and to date only partially understood reaction sequence that involves the reaction of hydrogen peroxide in an acidic solution with metal ions, namely Fe^{2+} ion and (to a lesser extent) Fe^{3+} or Cu^{2+} ions. Similar processes (Fenton-like) take place in the presence of other peroxides and/or of iron (hydr)oxides.[109,110]

Back in the 30's, the Fenton process was essentially regarded as a variant of the Fe-catalyzed Haber-Weiss reaction ($O_2^{-\bullet} + H_2O_2 \rightarrow {}^{\bullet}OH + OH^- + O_2$). Today, the simplest and most widely accepted (but also strongly discussed and questioned) Fenton reaction sequence is still the following:[111]

$$Fe^{2+} + H_2O_2 \rightarrow FeOH^{2+} + {}^{\bullet}OH \text{ (or } Fe^{3+} + OH^- + {}^{\bullet}OH) \qquad \text{(R 3-17)}$$

$$Fe^{2+} + {}^{\bullet}OH \rightarrow FeOH^{2+} \text{ (or } Fe^{3+} + OH^-) \qquad \text{(R 3-18)}$$

$$H_2O_2 + {}^{\bullet}OH \rightarrow HO_2^{\bullet} + H_2O \qquad \text{(R 3-19)}$$

$$FeOH^{2+} + HO_2^{\bullet} / O_2^{\bullet-} \rightarrow Fe^{2+} + O_2 + H_2O / OH^- \qquad \text{(R 3-20)}$$

$$FeOH^{2+} + H_2O_2 \rightarrow Fe^{2+} + H_2O + HO_2^{\bullet} \qquad \text{(R 3-21)}$$

Reaction sequence (R 3-17) to (R 3-21) is not exhaustive but a reasonable representation of what is expected to take place under given experimental conditions for the Fenton reaction (pH ~ 3). Here, dissolved pollutants will be degraded or transformed by $^{\bullet}OH$ radicals generated in the Fenton reaction sequence (R 3-17) to (R 3-21) listed above.[112,113] Note that in reaction (R 3-18), the Fe^{2+} cation scavenges $^{\bullet}OH$ radical in competition with other solutes, and it is detrimental to degradation processes. In reaction (R 3-19), H_2O_2 also scavenges $^{\bullet}OH$ radical, but it yields $HO_2^{\bullet}/O_2^{-\bullet}$ that enhances the recycling of $FeOH^{2+}$ to Fe^{2+} in reaction (R 3-20). Further recycling takes place in reaction (R 3-21), but the reaction (R 3-20) is faster. Therefore, the scavenging of $^{\bullet}OH$ by H_2O_2 in reaction (R 3-19) would partially inhibit and partially favor (the net outcome depending on the experimental conditions) the overall Fenton degradation.[114] The recycling of Fe(III) to Fe^{2+} can be enhanced by some dissolved organic compounds including humic substances, which could increase the rate of the Fenton degradation of pollutants despite their ability to act as $^{\bullet}OH$ scavengers.[115,116]

The Fe^{2+} cation is typically used as a catalyst in the Fenton process, despite the fact that reaction (R 3-17) between Fe^{2+} and H_2O_2 is stoichiometric. Indeed, a high amount of Fe^{2+} would induce significant $^{\bullet}OH$ scavenging (R 3-18) and thus decrease the process efficiency. If the initial $[Fe^{2+}] < [H_2O_2]$, excess H_2O_2 would still occur after Fe^{2+} oxidation. However, recycling of $FeOH^{2+}$ to Fe^{2+} in reactions (R 3-20, R 3-21) ensures continued production of $^{\bullet}OH$ until H_2O_2 is completely consumed. Anyway, because the reaction (R 3-17) is much faster than reactions (R 3-20) and (R 3-21), the rate of the Fenton process decreases considerably after Fe^{2+} consumption.[114]

Reaction (R 3-21) accounts for the fact that the Fenton process also works in the presence of Fe(III) + H_2O_2. This approach to Fenton degradation is supported by the lower cost of ferric compared to ferrous salts, but it has the substantial drawback that the generation rate of $^{\bullet}OH$ by the Fe(III) + H_2O_2 reaction is much lower compared to Fe^{2+} + H_2O_2 process.[117] For this reason, several approaches have been attempted to increase the rate of $^{\bullet}OH$ generation by the Fe(III) + H_2O_2 reaction that are based on an enhanced Fe(III) reduction (application of light, electrical potential or ultrasound as discussed later).

An important issue to be considered is that the reactions (R 3-17) to (R 3-21) are just an approximation to the actual system. For example, the reaction (R 3-17) between Fe^{2+} and H_2O_2 is actually far more complex and proceeds through formation of highly oxidized iron species (*e.g.* ferryl, often indicated as FeO^{2+} by omitting several ligands), which might or might not result in the $^{\bullet}OH$ radical formation.[118] The conversion efficiency of ferryl to $^{\bullet}OH$ is highly uncertain but is estimated to be around 60% at pH 2,[119] and it becomes very low under ~neutral conditions.[120] Further, although less than $^{\bullet}OH$ radicals, ferryl is also reactive and it can be involved in electron-transfer processes. To maximize the yield of $^{\bullet}OH$ at the expense of less reactive ferryl species the Fenton reaction process is carried out under acidic conditions.[121,122] Actually, the details of the reaction depend strongly on solution pH, as well as on the ligands around the Fe ions.[111]

3.1.5. Photo-Fenton processes

Several Fe(III) complexes are able to absorb UV light and even visible radiation of the solar spectrum to produce Fe^{2+} by ligand-to-metal charge transfer. In this way, the Fe(III) + H_2O_2 system under irradiation can photochemically produce the Fenton reagent. In the most general case the photo-Fenton system involves reaction (R 3-22) plus all the typical Fenton processes described in section 3.1.4, and most notably reaction (R 3-17):[123–125]

$$Fe^{III}\text{-}L + h\nu \rightarrow Fe^{2+} + L^{+\bullet} \qquad \text{(R 3-22)}$$

The $^{\bullet}OH$ radical production of the reaction (R 3-17) is greatest at pH 3. At this value of pH, the Fe(III) ions are largely present in the form of the hydroxocomplex $FeOH^{2+}$. The UV photolysis of the $FeOH^{2+}$ ions results in the $^{\bullet}OH$ radical production quantum yield of around 0.2:[126]

$$FeOH^{2+} + h\nu \rightarrow Fe^{2+} + {}^{\bullet}OH \qquad \text{(R 3-23)}$$

The main drawback to use the $FeOH^{2+}$ ion as an $^{\bullet}OH$ radical source in the aqueous phase is that this ion has an absorption maximum in the UVB region of the solar spectrum and can absorb only a limited fraction of the natural sunlight. Therefore, other aqueous phase $^{\bullet}OH$ radical sources have been proposed that include Fe(III) ion complexes with oxalate, citrate, ethylenediaminetetraacetic acid (EDTA) and ethylenediamine-N,N'-disuccinic acid (EDDS).[127] These Fe(III) ion complexes undergo photolysis (see reaction (R 3-22)) through one-electron oxidation of the organic ligand (L). The reaction (R 3-22) does not directly produce $^{\bullet}OH$ radicals. $^{\bullet}OH$ is only generated *via* reaction (R 3-17) that follows (R 3-22). However, the Fe(III) ion complexes with organic compounds (Fe(III)-L) absorb in the visible region of the solar spectrum and extend the solubility of Fe(III) ions to higher pH values. Because, in addition, the $^{\bullet}OH$ radical production quantum yields from Fe(III)-L complex photolysis can be higher compared to $FeOH^{2+}$ ions,[128,129] there is a definite advantage in the use of organic complexes of Fe(III) in the photo-Fenton process.

After Fe^{2+} has been photochemically generated, the reactions taking place in the photo-Fenton system are quite similar to those involved in the dark Fenton process. Similarities include optimum pH and the possible formation of ferryl. However, in the photo-Fenton system, Fe^{2+} reaches a relatively low steady-state concentration [130] and the scavenging of $^{\bullet}OH$ by ferrous iron (reaction (R 3-18)) is not important.

3.1.6. Other Fenton systems

The photochemical conversion of the Fe(III) ion into Fe^{2+} is only one of the means needed to activate the Fenton reaction. Other activation approaches include the electro-Fenton system.[131–133] The electro-Fenton system reaction mechanism is believed to proceed through the simultaneous generation of Fe^{2+} and H_2O_2 upon cathodic reduction of Fe(III) and O_2, respectively.[131]

$$\mathrm{Fe(III)} + e^- \rightarrow Fe^{2+} \qquad \text{(R 3-24)}$$

$$O_2 + 2\,e^- + 2\,H^+ \rightarrow H_2O_2 \qquad \text{(R 3-25)}$$

In the electro-Fenton system, a small amount of the Fe^{2+} catalyst salt is added to initiate the process. The ferrous salt reacts with the electrochemically generated H_2O_2 and the additional reduction of Fe(III) to Fe^{2+} becomes important when a large fraction of the initial Fe^{2+} has been consumed.[134] Reaction (R 3-24) is important because it accelerates the recycling of Fe(III) to Fe^{2+} compared to reactions (R 3-20) and (R 3-21). Cathodes in electro-Fenton system are usually made up of graphite or glassy carbon.[135] The anodic reaction (oxidation of water to O_2) is often carried out in the laboratory using Pt electrodes.[136]

$$2\,H_2O \rightarrow O_2 + 4\,e^- + 4\,H^+ \qquad \text{(R 3-26)}$$

An alternative approach does not require the addition of any Fenton reactant, because Fe^{2+} is produced by oxidation of sacrificial Fe anodes. In this case, reactions (R 3-25) and (R 3-27) are followed by the classic Fenton cycle (see section 3.1.4), and most notably by reaction (R 3-17). Recycling of Fe(III) to Fe^{2+} by reaction (R 3-24) is also operational.[137]

$Fe \rightarrow Fe^{2+} + 2\ e^-$ (R 3-27)

Another way to produce the Fenton reagent is the application of high-frequency ultrasounds within aqueous solutions to split water into $^{\bullet}OH + H^{\bullet}$ (sonochemistry is discussed in section 3.1.8).[138] Briefly, ultrasound is applied to solutions containing Fe(III) ions, allowing for sonochemical production of both Fe^{2+} and H_2O_2:[139]

$H^{\bullet} + Fe(III) \rightarrow Fe^{2+} + H^+$ (R 3-28)

$H^{\bullet} + O_2 \rightarrow HO_2^{\bullet}$ (R 3-29)

$HO_2^{\bullet} \leftrightarrows O_2^{\bullet-} + H^+$ (R 3-30)

$Fe(III) + O_2^{\bullet-} \rightarrow Fe^{2+} + O_2$ (R 3-31)

$HO_2^{\bullet} + O_2^{\bullet-} + H^+ \rightarrow H_2O_2 + O_2$ (R 3-32)

Often, ferrous salts are initially added to the reaction system followed by ultrasound irradiation. Here, H_2O_2 is generated sonochemically and reactions (R 3-28) to (R 3-31) have been postulated to play a role in the Fe^{2+} cation regeneration after the initial amount of added Fe^{2+} has been largely consumed.[140,141] In this system, $^{\bullet}OH$ is produced both by water sonochemistry and the Fenton reaction. Interestingly, there is evidence that the two $^{\bullet}OH$ sources may have comparable importance.[132]

The Fenton reaction may also play some role in the context of the zero-valent iron reduction (ZVI).[142] The ZVI technique has been proposed to detoxify target pollutants such as chlorinated organics by means of dechlorination carried out by metallic Fe, Fe°.[143,144] It may be surprising that a strong oxidant such as $^{\bullet}OH$ radical can be produced in a reductive environment, but the addition of Fe° to an aerated aqueous solution enables the following reactions to take place:[145,146]

$2\ Fe^{\circ} + O_2 + 4\ H^+ \rightarrow 2\ Fe^{2+} + 2\ H_2O$ (R 3-33)

$Fe^{2+} + O_2 \rightarrow Fe(III) + O_2^{\bullet-}$ (R 3-34)

$2\ O_2^{\bullet-} + 2\ H^+ \rightarrow H_2O_2 + O_2$ (R 3-35)

The above reaction sequence (R 3-33) to (R 3-35) is not complete and, several additional reactions occur in the presence of ZVI and organic compounds.[147] The reaction sequence (R 3-33) to (R 3-35) is not considered to be a “clean” $^{\bullet}OH$ radical source. However, the possibility to generate hydroxyl radicals in aerated aqueous solution should be taken into account when using ZVI for reductive purposes.[148]

3.1.7. Ozonation

Ozone is a widely used disinfectant in the fields of drinking water production and wastewater treatment.[149] Ozone disinfectant qualities have gained in popularity in recent years given that chlorination water treatment produces a wide range of potentially harmful disinfection by-products.[150] However, ozone water treatment is not free of inherent by-product formation.[151,152]

The production of ozone is energy intensive because it requires the vacuum ultra-violet (VUV) irradiation of, or the application of high-voltage electric discharges to, dry air or oxygen.[153] Ozone is an effective disinfectant, but its instability and elevated toxicity make it unsuitable as residual disinfectant for drinking water. Therefore, in water treatment plants the primary ozonation has to be associated to a secondary disinfection stage.[154] Despite these drawbacks, ozone is reported to be effective in the depollution of water from selected organic contaminants.[155] Ozone is particularly reactive toward alkenes (leading to the breaking of C=C bonds), amines and electron-rich aromatic compounds.[156]

However, ozone shows negligible reactivity toward saturated organic compounds, electron-poor aromatics and several functional groups, which strongly limits the O_3 ability to act as a generic solution for water depollution. A possible way to extend the action of ozone towards a wider range of water pollutants is to use techniques that produce $^{\bullet}OH$ radicals from ozone itself.[157] The relevant processes will be described in the next paragraphs.

3.1.7.1. Reactivity of O₃ under alkaline conditions

The reactivity of O_3 toward dissolved organic pollutants can be further enhanced by inducing the formation of $^{\bullet}OH$ under alkaline conditions. Two different mechanisms (R 3-36 + R 3-37 or R 3-38 + R-3.39, see below) have been proposed for the reaction sequence:[158,159]

$$O_3 + OH^- \rightarrow HO_2^{\bullet} + O_2^{-\bullet} \qquad \text{(R 3-36)}$$

$$O_3 + O_2^{-\bullet} + H_2O \rightarrow [HO_3^{\bullet} + O_2 + OH^-] \rightarrow {}^{\bullet}OH + 2\,O_2 + OH^- \qquad \text{(R 3-37)}$$

$$O_3 + OH^- \rightarrow HO_2^- + O_2 \qquad \text{(R 3-38)}$$

$$O_3 + HO_2^- + H_2O \rightarrow [HO_2^{\bullet} + O_3^{-\bullet} + H_2O] \rightarrow {}^{\bullet}OH + O_2 + HO_2^{\bullet} + OH^- \qquad \text{(R 3-39)}$$

A further proposal ($O_3 + OH^- \rightarrow O_3^{-\bullet} + {}^\bullet OH$) looks less likely because ${}^\bullet OH$ is a much stronger oxidant than O_3. The formation of ${}^\bullet OH$ under alkaline conditions usually causes an increase of the transformation rate of dissolved compounds, and particularly of those that react poorly with O_3.[160] One of the limits of oxidation by ozone alone (*e.g.* under pH conditions where the reactions (R 3-36) to (R 3-**39**) are negligible) is that, while decreasing the Chemical Oxygen Demand (COD) of treated wastewater, the Total Organic Carbon (TOC) is affected to a much lesser extent.[161] In other words, ozone oxidizes but it does not totally eliminate (mineralize) organic compounds, with an additional possibility to form harmful transformation intermediates.[151,162] In contrast, ${}^\bullet OH$-induced processes cause both the COD and the TOC of wastewater to decrease, even leading up to total mineralization.[163]

3.1.7.2. O_3 /H_2O_2

Another technique to produce ${}^\bullet OH$ in the presence of O_3 includes the addition of hydrogen peroxide, H_2O_2. The following reactions (R 3-38) and (R 3-39) are involved in the ozone-peroxide system (note than R 3-41 is a short-hand way to indicate R 3-39):[164]

$$H_2O_2 \leftrightarrows H^+ + HO_2^- \qquad \text{(R 3-40)}$$

$$HO_2^- + O_3 \rightarrow {}^\bullet OH + O_2 + O_2^{\bullet -} \qquad \text{(R 3-41)}$$

Also note that in the presence of ${}^\bullet OH$, H_2O_2 would be oxidized to $HO_2^\bullet$ / $O_2^{-\bullet}$ (R 3-15), thus also reaction (R 3-37) would be operational. The ${}^\bullet OH$ radical is both consumed and produced by the latter reactions, thus the reaction sequence (R 3-15) + (R 3-37) would correspond to $H_2O_2 + O_3 \rightarrow 2\ O_2 + H_2O$, catalyzed by ${}^\bullet OH$.

3.1.7.3. O_3 /UV

As in the gas-phase, the photolysis of O_3 in aqueous solution occurs at $\lambda \leq 320$ nm yielding $O(^1D_2)$. In water the process yields H_2O_2, thus reactions (R 3-40) and (R 3-41) would follow to produce ${}^\bullet OH$. Moreover, depending on the irradiation wavelength, the photolysis of H_2O_2 to ${}^\bullet OH$ (R 3-14) can occur to some extent.

$$O_3 \xrightarrow{h\nu} O_2 + O(^1D_2) \qquad \text{(R 3-42)}$$

$$O(^1D_2) + H_2O \rightarrow H_2O_2 \qquad \text{(R 3-43)}$$

The photochemical formation of oxygen atoms in their electronically excited state (O^1D_2) is essential for $^{\bullet}OH$ generation. The UV photolysis of ozone can also be used to produce $^{\bullet}OH$ radicals in water treatment facilities, to obtain a more powerful reactant than O_3 towards the degradation of organic compounds.[164]

3.1.7.4. $O_3/H_2O_2/UV$

This process is a combination of the already described O_3/UV, H_2O_2/UV and O_3/H_2O_2, thus the relevant reactions involved are the sum of those operational in the three separate systems. The advantage is that the production of $^{\bullet}OH$ is both chemical and photochemical, which can overcome the shortcomings of either system. Moreover, the poor radiation absorption of H_2O_2 is compensated for by the fact that its photolysis is not the only $^{\bullet}OH$ source.[165]

3.1.8. Water sonolysis

The application of high-frequency ultrasound (in the approximate range of 100 kHz to 1 MHz) to aqueous solutions induces the formation of cavitation bubbles containing dissolved gases and water vapor. Bubbles undergo various cycles of expansion and compression until implosive collapse. The sudden collapse of the bubbles is adiabatic and causes the internal temperature to reach extremely high values of the order of several thousand Kelvin. Under such conditions, the compounds present in the gas phase of the imploding bubbles (including poorly hydrophilic and/or volatile solutes and water vapor) undergo pyrolysis processes.[166] High-temperature pyrolysis of H_2O yields $^{\bullet}OH$ radicals and $H^{\bullet}$ atoms, the steady-state concentration of which reaches quite high values in a confined volume.[167–169] For this reason, differently from the vast majority of the other techniques used to produce $^{\bullet}OH$ radicals (in which the hydroxyl radicals are predominantly scavenged by organic and inorganic solutes), radical-radical recombination reactions prevail in sonochemistry.[170]

The main primary processes occurring in aqueous solutions exposed to ultrasound (represented by ")))" in reaction (R 3-44)) are listed below. Reactions (R 3-48) to (R 3-49) apply in air-equilibrated solutions, before the prolonged application of ultrasounds removes dissolved gases, or in systems where continuous air supply is provided.[171]

$$H_2O \xrightarrow{)))} {}^{\bullet}OH + H^{\bullet} \qquad \text{(R 3-44)}$$

$^{\bullet}OH + H^{\bullet} \rightarrow H_2O$ (R 3-45)

$2\ ^{\bullet}OH \rightarrow H_2O_2$ (R 3-46)

$2\ H^{\bullet} \rightarrow H_2$ (R 3-47)

$H^{\bullet} + O_2 \rightarrow HO_2^{\bullet}$ (R 3-48)

$2\ HO_2^{\bullet} \rightarrow H_2O_2 + O_2$ (R 3-49)

The radical-radical recombination occurs in the gas phase or at the air-water interface of collapsing bubbles, and it constitutes a considerable limit to the energy efficiency by which sonochemistry can carry out the degradation of dissolved compounds. Indeed, most of the energy required to form reactive radicals is lost during recombination. Degradation processes of solutes involve either pyrolysis of gas-phase molecules within the bubbles, or migration of $^{\bullet}OH$ to the solution bulk, where transformation of hydrophilic and/or poorly volatile compounds can take place.[172]

The application of sonochemistry to induce pollutant degradation has been the focus of several recent studies.[166] Investigation in the field of sonochemistry has been further stimulated by the finding that cavitation processes such as those caused by ultrasound can also be induced by hydrodynamic phenomena, a technique that is more energy-effective.[173,174]

Dissolved inorganic solutes such as HCO_3^-, CO_3^{2-}, NO_2^-, Br^- and I^- can act as $^{\bullet}OH$ scavengers, but their occurrence is not always detrimental to sonodegradation processes. Indeed, such species are also present at the air-bubble interface where they can "intercept" a fraction of $^{\bullet}OH$ that would otherwise undergo radical-radical recombination. The relevant scavenging process yields reactive transients upon anion oxidation ($CO_3^{\bullet-}$, $^{\bullet}NO_2$, $Br_2^{\bullet-}$ and $I_2^{\bullet-}$, much less reactive than $^{\bullet}OH$), which can take part in the transformation of easily oxidized compounds. Therefore, depending on the reactivity of organic pollutants toward the radical species mentioned above, the anions HCO_3^-, CO_3^{2-}, NO_2^-, Br^- and I^- could in some cases even enhance the degradation reactions.[170,175] However, particular attention is to be paid to the possible formation of secondary pollutants in the presence of transients such as $^{\bullet}NO_2$, $Br_2^{\bullet-}$ and $I_2^{\bullet-}$, which have the potential to respectively nitrate and halogenate aromatic compounds.[176]

3.1.9. VUV photolysis of water

Water and air are almost transparent above 200 nm, but the picture changes dramatically for wavelengths shorter than 190 nm. This spectral range is usually called vacuum ultra-violet (VUV) because radiation of this wavelength cannot travel in air due to absorption by oxygen, which is subsequently transformed into ozone by photolysis. Therefore, spectral measures in the VUV range are usually carried out under vacuum or in an inert (non-absorbing) gas atmosphere.[177] In addition to being a possible source of ozone by air (or oxygen) irradiation, as an alternative to electrochemical O_3 generation,[178] VUV radiation is also a suitable technique to produce $^{\bullet}OH$ upon water photolysis.[179]

Historically, VUV photolysis has first been applied to water vapor as a source of gas-phase hydroxyl radicals for kinetic studies.[180,181] The VUV photolysis of water vapor results in the following process:[182,183]

$$H_2O + h\nu \rightarrow H^{\bullet} + {}^{\bullet}OH \qquad \text{(R 3-50)}$$

Water vapor can be photolyzed using a VUV flash lamp that was first developed by Norrish and Porter in Cambridge in the late 1940's and for which they received the Nobel prize in 1967.[184] The flash lamp is operated using an inductive energy store and the discharge occurs through a spark gap [185] or a hydrogen thyratron.[186,187] The lamp discharge flash is coupled into the reaction volume through a LiF window that transmits radiation longer than 104 nm.

Reaction (R 3-50) would also take place in the presence of liquid water, but here the photolysis of OH^- (R 3-51) would be operational as well:

$$OH^- + h\nu \rightarrow {}^{\bullet}OH + e^- \qquad \text{(R 3-51)}$$

The production of $^{\bullet}OH$ from H_2O/OH^- by VUV irradiation has been made easier by the availability of cost-effective excilamps, based on excimers or exciplexes of Xe_2, Cl_2, I_2, XeBr, KrCl and XeCl.[188] These lamps also opened up the possibility for water photolysis to be considered among the potential oxidation processes for wastewater treatment, although the Hg emission line at 185 nm is more often used in laboratory applications.[189,190] Absorption of VUV radiation splits H_2O/OH^- into $^{\bullet}OH$ and $H^{\bullet}$ or $^{\bullet}OH$ and e^-. The reductive character of hydrogen atoms and solvated electrons, which could compensate for the oxidizing activity of $^\bullet$OH, is minimized in aerated aqueous solutions by O_2 scavenging to yield $HO_2^\bullet/O_2^{-\bullet}$.[191]

A consequence of the fact that $^\bullet$OH is produced by irradiation of the solvent is that the water ability to absorb VUV radiation, combined with its high molar concentration, make H_2O an optically thick medium in the VUV range. This means that VUV radiation penetrates only sub-mm water layers, and that the optical path length of the illuminated solution has to be kept to a minimum to avoid important diffusion-limitation effects.[192] Another issue is that air is also non-transparent in the VUV, thus the irradiation lamps should be immersed in solution [193] and not placed over it, as is allowed for instance in the case of UV (including UVC) irradiation.

3.1.10 The $^\bullet$OH radical in advanced oxidation processes (AOPs)

Several of the techniques that can be used to produce $^\bullet$OH in the laboratory, and that are described in this chapter, can also be applied to the decontamination of polluted water and wastewater. This section will give a brief overview of the present applications of $^\bullet$OH-based advanced oxidation processes (AOPs) in the field of water treatment.

Ozone is a widespread oxidant that is extensively used for the disinfection of water and wastewater. Its applications have increased enormously since the discovery that the reaction between chlorine and organic matter yields harmful trihalomethanes as disinfection by-products.[194] Not surprisingly, the diffusion of the ozone-based technologies provides a considerable advantage to the techniques that produce $^\bullet$OH from ozone (*i.e.* operation in basic solution, UV irradiation, addition of H_2O_2). From this point of view, the generation of $^\bullet$OH from ozone can be seen as a useful upgrade that considerably enhances the O_3 depollution potential.[157,195,196]

The Fenton reaction is also extensively used in water treatment. In addition to the thermal process, much interest has recently been raised by the solar photo-Fenton techniques. They consist in Fe(III)-based systems where the addition of ligands extends radiation absorption into the visible range. One such ligands is citrate, which is particularly useful thanks to its environmental friendliness. The solar photo-Fenton technology has recently proven its considerable potential in water treatment.[197–199] Moreover, a very important application is related to the cheap production of safer water for human use in developing countries, the so-called solar disinfection (SODIS) technique. The SODIS operation is very simple: raw water (usually contaminated by potentially harmful bacteria and viruses) is placed in a clear, transparent polyethylene bottle and placed under sunlight over an inclined undulated metal plate surface (*e.g.* a roof).[200] The disinfection carried out by UV radiation and heating can be enhanced with additives such as H_2O_2 and/or juice from a squeezed lemon. The latter, in addition to creating pH conditions that are unfavorable to bacteria, can aid the solar photo-Fenton process. The iron that is naturally contained in water is complexed by citrate, thereby absorbing sunlight and yielding Fe^{2+} upon photolysis, which reacts with H_2O_2 to yield $^{\bullet}OH$.[200–202] Day-long water treatment under sunlight considerably reduces the potential of water to induce disease, because $^{\bullet}OH$ and related oxidants kill bacteria, viruses, parasite larvae and eggs. Although the final product could not be really considered as drinking water by western standards and legislation, SODIS is currently the only feasible treatment option in several rural communities in developing countries. Therefore, it could give a considerable help to reduce the worldwide diffusion of waterborne disease.[200]

Heterogeneous photocatalysis (especially that based on titanium dioxide, TiO_2), while not a “clean” system to produce $^{\bullet}OH$ in laboratory conditions, is another potentially important technique to photodegrade pollutants. Presently its application to water treatment suffers from the successful competition by ozone-based systems and the solar photo-Fenton, but titanium dioxide is becoming an important tool for the abatement of airborne pollutants. Indeed, many commercial applications concern air rather than water treatment.[203,204]

The heterogeneous photocatalysis makes use of semiconductor materials (usually metal oxides) that absorb radiation in the UV-visible range. The most successful material to date is anatase TiO_2, which can absorb the UVB and UVA components of sunlight. Radiation absorption promotes electrons from the valence to the conduction band of the semiconductor, leaving electron vacancies (holes) in the valence band. Most photogenerated electrons and holes recombine in the semiconductor bulk, which constitutes the main limit of the photocatalytic process. However, some electrons and holes escape bulk recombination and migrate to the semiconductor surface, where they can be trapped by surface and sub-surface groups. Recombination of (sub)surface-trapped electrons and holes is possible but it is much slower than in the bulk, which enables chemical reactivity. Holes can be trapped by surface $\equiv Ti^{IV}\text{-}OH^{-}$ and sub-surface $\equiv Ti^{IV}\text{-}O^{2-}\text{-}Ti^{IV}\equiv$ to produce oxidizing agents ($\equiv Ti^{IV}\text{-}^{\bullet}OH$ and $\equiv Ti^{IV}\text{-}O^{\bullet -}\text{-}Ti^{IV}\equiv$, respectively). Electrons can be trapped by surface $=Ti^{IV}=$ to produce $=Ti^{III}\text{-}$, a reducing agent. The latter could for instance react with dissolved O_2 to yield superoxide. Interestingly, such a reductive pathway finally yields free $^{\bullet}OH$ through the following reaction scheme:[205,206]

$=Ti^{III}\text{-} + O_2 \rightarrow =Ti^{IV}= + O_2^{\bullet -}$ (R 3-52)

$2\ O_2^{\bullet -} + 2\ H^+ \rightarrow H_2O_2$ (R 3-53)

$H_2O_2 + h\nu \rightarrow 2\ ^{\bullet}OH$ (R 3-54)

$H_2O_2 + =Ti^{III}\text{-} \rightarrow =Ti^{IV}= + ^{\bullet}OH + OH^-$ (R 3-55)

The species $\equiv Ti^{IV}\text{-}^{\bullet}OH$, $\equiv Ti^{IV}\text{-}O^{\bullet -}\text{-}Ti^{IV}\equiv$ and $^{\bullet}OH$ are all involved in pollutant degradation (and in some cases, also the reducing agent $=Ti^{III}\text{-}$ can play an important role). The main limits of the process are the poor use of sunlight (TiO_2 does not absorb visible radiation) and the low quantum yield/photon efficiency, because of the effective bulk recombination processes between electrons and holes.[207,208]

The irradiation of H_2O_2 alone, despite its straightforwardness and the high $^{\bullet}OH$ quantum yield, is not so frequently used in remediation processes. The main reasons are the limited ability of hydrogen peroxide to absorb sunlight, and its not-so-high absorption coefficients in the UVC region. In the latter spectral interval, important spectral interference with the natural water matrix may take place.[209] However, H_2O_2 under irradiation is often used in combination with O_3 or in photo-Fenton processes.

The practical applications of sonochemistry are strongly limited by the elevated costs of the technique, which presently has very low energy efficiency. However, sonochemical cavitation is often proposed in combination with other techniques (*e.g.* those based on irradiation) to improve the treatment efficiency and keep operational costs to a reasonable level.[210,211] In these cases as well, however, the development of the technique has not gone far beyond the laboratory stage.

The VUV photolysis of water also has a limit represented by the operational costs. While the use of mercury lamps emitting at 185 nm allows a cost-effective production of VUV photons, a major problem is connected with the elevated cross section of water that allows only limited volumes to be treated. Therefore, further development and an additional decrease of the radiation energy costs could be required before the technique reaches operational maturity.[212]

3.2. The laboratory $^{\bullet}$OH production in the gas phase

3.2.1. Reaction of ozone with alkenes

The reaction of ozone with alkenes represents an important source of $^{\bullet}$OH radicals in the gas-phase, especially in the urban and forested regions. In 1992, Paulson et al. [213], Paulson and Seinfeld [214], and Atkinson et al. [215] demonstrated that the $^{\bullet}$OH radical can be efficiently generated under laboratory conditions produced from the gas-phase reaction of ozone with isoprene, 1-octene, ethene, and a series of monoterpenes. The $^{\bullet}$OH radicals are formed in a multistep process whose chemistry has been detailed by Atkinson et al. [216]. Briefly, an ozonide is formed during the ozonolysis of the alkenes that rapidly decomposes into one of two possible combinations of a carbonyl and a biradical. The energy rich biradical then rearranges or reacts via a number of different pathways. Two of the possible pathways, the ester channel and the hydroperoxide channel, lead to the formation of $^{\bullet}$OH. The yield of $^{\bullet}$OH formation describes the $^{\bullet}$OH quantity produced while one molecule of ozone reacts with one molecule of a given alkene. On the other hand, the alkenes are removed by $^{\bullet}$OH; hence, the concentrations of $^{\bullet}$OH radical are governed by competition between the production rate of the ozone/alkene reaction and the elimination rate by the $^{\bullet}$OH /alkene reaction. The steady state concentration of $^{\bullet}$OH radical can be presented as a ratio between the source and the sink: [217]

$$[^{\bullet}\mathrm{OH}]=\frac{k_{\mathrm{O_3+alkene}}\Phi_{^{\bullet}\mathrm{OH}}[\mathrm{O_3}][\mathrm{alkene}]}{k_{^{\bullet}\mathrm{OH+alkene}}[\mathrm{alkene}]+k_{^{\bullet}\mathrm{OH+O_3}}[\mathrm{O_3}]} \qquad \text{(Eq 3-4)}$$

where $k_{\mathrm{O_3+alkene}}$ is the rate constant for the reaction between the ozone and the alkene, $\Phi_{^{\bullet}\mathrm{OH}}$ is the yield of $^{\bullet}$OH formation, $k_{^{\bullet}\mathrm{OH+alkene}}$ is the rate constant for the reaction between the $^{\bullet}$OH and the alkene, and $k_{^{\bullet}\mathrm{OH+O_3}} = 7.3 \cdot 10^{-14}$ cm^3 molecule^{-1} s^{-1} [218] is the rate constant for the reaction between ozone and $^{\bullet}$OH. The $^{\bullet}$OH yield is highly variable between 0.08 for the reaction between ozone and 1,3-butadiene and 0.91 for the reaction between ozone and α-terpinene.[219] The accuracy of this method depends on associated uncertainties of the rate constants and ozone concentrations measured with commercial ozone analyzers.

3.2.2. Photolysis of hydrogen peroxide (H_2O_2)

The photolysis of hydrogen peroxide (H_2O_2) is a very common method used for laboratory generation of $^\bullet OH$ radicals in the gas phase. This method is unique because under dark conditions, H_2O_2 acts as an $^\bullet OH$ radical scavenger, converting $^\bullet OH$ to $HO_2^\bullet$ but under light irradiation efficiently generates $^\bullet OH$ radicals.

H_2O_2 is photolyzed in a 248 nm excimer laser pulse to produce ground state $^\bullet OH$ radicals with a quantum yield of 2 (R 3-54).[220] The generated $^\bullet OH$ radicals will then react quite rapidly with the remaining excess of H_2O_2, with the rate constant $k = 1.7 \cdot 10^{-12}$ cm^3 $molecules^{-1}$ s^{-1}.[218] The exponential decay of $^\bullet OH$ allows one to estimate the [H_2O_2]. The temporal evolution of [$^\bullet OH$] can be described by the integrated rate law for first-order kinetics.

3.2.3. Photolysis of nitrous acid (HONO)

Photolysis of gaseous HONO at wavelengths below ~ 400 nm is another important $^\bullet OH$ source, especially in the chamber experiments of atmospheric relevance (R 2-25).[221]

However, this source is insufficient to maintain an effectual $^\bullet OH$ concentration, especially in the presence of high concentrations of VOCs. Therefore, a regeneration of $^\bullet OH$ from $HO_2^\bullet$ radicals is crucial.

$HO_2^\bullet + NO \rightarrow {}^\bullet OH + NO_2$ (R 3-56)

$HO_2^\bullet + O_3 \rightarrow {}^\bullet OH + 2O_2$ (R 3-57)

$HO_2^\bullet$ can be formed during the reactions of $^\bullet OH$ with the VOCs or indirectly from the organic peroxy radicals ($RO_2^\bullet$) after another reaction step involving NO:

${}^\bullet OH + VOC \rightarrow RO_2^\bullet$ (R 3-58)

$RO_2^\bullet + NO \rightarrow RO^\bullet + NO_2$ (R 3-59)

$RO^\bullet + O_2 \rightarrow R'O + HO_2^\bullet$ (R 3-60)

The presence of NO leads to a propagation of the radical chain and counteracts terminating $HO_2^{\bullet}$ and $RO_2^{\bullet}$ self- and cross-reactions. The $^{\bullet}OH$ radicals can be also recycled during the reactions of $HO_2^{\bullet}$ with $RO_2^{\bullet}$:

$$RO_2^{\bullet} + HO_2^{\bullet} \rightarrow RO^{\bullet} + O_2 + {}^{\bullet}OH \qquad \text{(R 3-61)}$$

An important number of simulation chamber studies observed a significant so called “background” $^{\bullet}OH$ production in a clean environment that could not be attributed to known $^{\bullet}OH$ radical precursors [222]. A heterogeneous formation of HONO and its subsequent photolysis was suggested to explain this so called background reactivity within the simulation chambers [223–226]. It was postulated that HONO is formed, at least in part, by the heterogeneous dark hydrolysis of NO_2 on the humid chamber surfaces [227–232] and by a photo-enhanced HONO formation [223–226], the mechanism of which is still under discussion.

This background HONO production could differ at varying lighting conditions. Higher irradiation conditions would increase the photo-enhanced HONO formation but would also cause higher photolysis of the HONO formed. The balance can only be determined by especially dedicated experiments in identical conditions, not only of light irradiation but also of other experimental parameters, such as RH (%).[221]

Therefore, the investigations on $^{\bullet}OH$ radical budget in the chamber experiments have to be performed under well controlled conditions.

4. Production and production-detection of $^{\bullet}$OH radicals in the laboratory, in the gas phase and in the aqueous phase

Hydroxyl radicals have a very short lifetime because of their high reactivity, and consequently their concentration in aqueous solution is very low, typically below 10^{-12} M.[233] In order to study aqueous-phase $^{\bullet}$OH chemistry, certain precautions must be taken. First, radical species must be produced using the cleanest possible way (*e.g.* Fenton and photo-Fenton reactions may generate potential interferences). Second, transient radical concentrations ought to be low enough in order to avoid unwanted complications from the secondary chemistry (*e.g.* recombination reactions). Such considerations have led over the years to the development and validation of well established experimental methods such as pulse radiolysis and laser flash photolysis techniques. These laboratory techniques, coupled with spectroscopic or competition kinetics methods, combine the production and the detection of $^{\bullet}$OH radicals and they allow, *inter alia*, the study of reaction kinetics.

The approaches used to investigate the reaction kinetics in the liquid phase are similar to those in the gas phase, that is, the use of diverse spectroscopic techniques to follow the loss of one reactant (or the build-up of one product) in the presence of a large excess of the second reactant. UV-visible spectroscopy is a primary tool for following both stable species and radicals in solution.

The exciplex laser is used to generate $^{\bullet}$OH radical, which is located in a cell configured with white optics used to obtain long total pathlengths using a shorter base path. The time dependence of the concentrations of the $^{\bullet}$OH radical can be followed by using the absorption of light from a laser. According with the nature of the investigations the detection system can be a photodiode, a monochromator-photomultiplier or a photodiode array detector spectrometer.

Due to the very low concentrations of $^{\bullet}$OH ($< 5\times10^{7}$ cm^{-3}) and $HO_2^{\bullet}$ ($< 5\times10^{9}$ cm^{-3}) and to the very high reactivity of the $^{\bullet}$OH radicals, their in situ measurements are rather difficult. In the last 20 years, two techniques have been developed that are suitable to measure $^{\bullet}$OH with sufficiently high sensitivity (about 10^{5} cm^{-3}) and time resolution (less than 1 min): laser induced fluorescence, LIF, also known as fluorescence assay by gas expansion (FAGE), and chemical ionization mass spectrometry (CIMS). Being very sensitive, both methods require meticulous field calibration that limits the accuracy of the measurements, which is normally about 30%.

In addition, a number of factors have been identified for both techniques that may interfere with radical measurements and influence their accuracy, e.g. the influence of high NO concentrations for the CIMS technique or humidity variability for the FAGE. The role of such interferences may be more important for the measurements conducted in polluted environments in the presence of a large number of organic compounds at high concentrations. Under such conditions, the intercomparison of the two techniques becomes the only method to test their reliability.

The concept of laser flash photolysis (LFP) is very simple. A short pulse of light at a certain wavelength is made to interact with a sample that has been placed in the optical path of a spectrometer. The result of this interaction can be either a transient absorption or an emission process. The changes in detector signal that follow laser excitation may be due to a variety of processes such as electronic excitation producing a triplet state, cleavage of a molecule producing radicals, electron transfer, molecular rearrangement etc.

The laser flash photolysis technique can be applied for kinetic analysis and for transient absorption measurements. In both cases an excimer laser is used as an excitation and probe source, and a combination of monochromator, photomultiplier or CCD spectrograph can be used as a detection system.

A common LFP $^{\bullet}OH$ radical precursor is hydrogen peroxide, H_2O_2. The H_2O_2 is typically photolyzed using an excimer laser at λ=248 nm. The $^{\bullet}OH$ radicals are generated via the following reaction with a quantum yield of ~2 in the gas phase and ~1 in aqueous solution.[103]

$$H_2O_2 + h\nu\ (\lambda=248\ \text{nm}) \rightarrow {}^{\bullet}OH + {}^{\bullet}OH \qquad \text{(R 4-1)}$$

The combination of LFP and laser-induced fluorescence (LIF) is a suitable method to study the $^{\bullet}OH$ reactions in the gas phase, while LFP can be used to study comparable processes in aqueous solution. Detection of $^{\bullet}OH$ by electron paramagnetic resonance (EPR) and with probe molecules are more often used in solution.

4.1. Detection of $^\bullet$OH radicals in the gas phase by chemical ionization mass spectrometry (CIMS)

The $^\bullet$OH radical in the gas phase can be effectively measured by chemical ionization mass spectrometry (CIMS) The measurement of the hydroxyl radical by CIMS is carried out by titrating $^\bullet$OH into H_2SO_4 in a timescale that is shorter compared to the $^\bullet$OH lifetime. The isotopically labeled $^{34}SO_2$ is used to distinguish between the H_2SO_4 and $H_2{}^{34}SO_4$ which is derived by $^\bullet$OH.

The titration takes place in a 1.9 cm diameter tube by adding $^{34}SO_2$ through two transverse and opposed 0.011 cm ID injectors. The titration reactions are given as follows[234]

$^\bullet OH + {}^{34}SO_2 + M \rightarrow H^{34}SO_3^\bullet + M$ (R 4-2)

$H^{34}SO_3^\bullet + O_2 \rightarrow {}^{34}SO_3 + HO_2^\bullet$ (R 4-3)

$^{34}SO_3 + H_2O + M \rightarrow H_2{}^{34}SO_4 + M$ (R 4-4)

As was emphasized by Eisele and Tanner, the interference from the $^\bullet$OH regeneration may be reduced by shortening the $^\bullet$OH to H_2SO_4 conversion time, which is of the order of several tens of milliseconds. Considering the importance of CIMS for the $^\bullet$OH measurements, it is important to optimize a CIMS instrument for polluted conditions. In this sense, a more recent version of this analytical technique was successfully applied in several field and chamber measurements[235,236]. In brief, the $^\bullet$OH radical is measured by titrating sampled $^\bullet$OH radicals into H_2SO_4 by addition of SO_2 into a chemical conversion reactor in the presence of water vapor and oxygen. H_2SO_4 is detected by using mass spectrometry as an HSO_4^- ion, produced by chemical ionization with NO_3^- in an ion-molecule reactor. The concentration of total peroxy radicals ($RO_2^\bullet$) is measured by converting them into $^\bullet$OH radicals via reactions with NO. The short conversion time of $^\bullet$OH to H_2SO_4 employed in this instrument (about 3 ms) ensures minimum interference on the $^\bullet$OH measurements by high NO ambient concentrations. The calibration of the instrument for the $^\bullet$OH and $RO_2^\bullet$ measurements is based on the production of controlled concentration of $^\bullet$OH and $RO_2^\bullet$ radicals in a turbulent flow reactor by photolysis of water vapor at 184.9 nm. The calibration uncertainty (2σ) is estimated to be of 25% for $^\bullet$OH and of 30% for $HO_2^\bullet$. A lower limit of detection for $^{\bullet}OH$ radical measurements is 8×10^5 molecule cm^{-3} for one 2-min $^{\bullet}OH$ point at a signal-to-noise ratio of 3. The typical precision of the 15-min averaged data corresponds to a standard random deviation better than ± 15% for $^{\bullet}OH$ concentrations higher than 10^6 molecule cm^{-3}, and better than ± 5% for $RO_2^{\bullet}$ levels higher than 10^8 molecule cm^{-3}. Accounting for the calibration uncertainties and measurement precision, the overall 2σ uncertainty of the 15 min averaged measurements of $^{\bullet}OH$ and $RO_2^{\bullet}$ is estimated to be 30% and 36%, respectively.

4.2. Production and detection of $^{\bullet}OH$ radicals in the gas phase by LFP and LIF

LFP can be carried out using lasers with specific wavelengths and pulse durations of nanoseconds to femtoseconds. The intense light pulse of the laser creates short lived photo-excited intermediates such as excited states, radicals and ions. The advantages of lasers reside in the use of specific wavelengths, which minimizes the simultaneous photolysis of reactants or products that can occur with broadband light sources, and in the availability of higher light intensities to generate larger radical concentrations. Excimer lasers such as ArF at 193 nm, KrF at 248 nm, XeCl at 308 nm and XeF at 351 nm have been proven especially useful in the characterization and generation of free radicals.

The LFP technique has been proven as one of the most frequently used methods for the production of $^{\bullet}OH$ radicals in the gas phase. Whilst flash lamp photolysis is still used in kinetic experiments to produce $^{\bullet}OH$ radicals, the laser flash photolysis (LFP) technique offers high-energy shorter pulse durations, higher repetition rates, a narrow, precisely defined wavelength range and a well-defined profile, at the cost of greater experimental complexity and price tag. Since the laser pulse duration is much shorter than the flash lamp pulse, LFP has an advantage to study reactions on much smaller timescales. That is, it is the duration of the photolysis pulse that places a limit on the timescale of reactions that can be studied. The high beam energies of excimer lasers are also of great importance because high amounts of $^{\bullet}OH$ radicals can be produced from low precursor concentrations which, in turn, simplify the overall secondary reactions of the transient with the precursor. Disadvantages of LFP include ionization and superexcitation of the photolyzed species caused by high-energy laser pulse.

A KrF excimer laser at $\lambda = 248$ nm, causes decomposition of HNO_3 and H_2O_2 to generate $^{\bullet}OH$ radicals and the third harmonic of Nd:YAG laser at $\lambda = 355$ nm induces dissociation of HONO and produces $^{\bullet}OH$ radicals. An ArF excimer laser which operates at 193 nm can be used to generate $^{\bullet}OH$ radicals by decompositon of N_2O, as follows:

$N_2O + h\upsilon\ (\lambda=193\ nm) \rightarrow O(^1D_2) + N_2$ (R 4-5)

$O(^1D_2) + H_2O \rightarrow 2\ ^{\bullet}OH$ (R 4-6)

The laser induced fluorescence can be used to detect the $^{\bullet}OH$ radical in the gas phase. Typically, the gas phase LIF experiments involve time-resolved detection of $^{\bullet}OH$ ($X^2\pi$, v"=0) by pulsed laser-induced fluorescence spectroscopy at $\lambda \sim 282$ nm (1-0 band of the $A^2\Sigma^+$ - $X^2\pi$ system). Temporal profiles of ground state $^{\bullet}OH$ radicals are then mapped out by varying the time delay between the photolysis laser flash and the 282 nm probe pulse. The geometry of the experimental system is such that it allows for the photolysis laser and the probe laser beams to enter perpendicular to one another and the photomultiplier tube (PMT) detector to be orthogonal to the overlapping beams.

In a typical LIF experiment, an excimer laser ($\lambda = 308$ nm) is used to pump a second probe dye laser. When Coumarin-540A dye is employed, the dye laser output at $\lambda \sim 564$ nm is frequency doubled to obtain tunable radiation at $\lambda \sim 282$ nm. The tunable radiation excites the $Q_1 1$, $Q_1 1'$ and R_2^3 lines in the (1,0) band of the ($A^2\Sigma^+$, v'=1) $\leftarrow$ ($X^2\pi$, v"=0) transition of the $^{\bullet}OH$ radical around 282 nm. The probe laser is triggered at a variable delay time after the photolysis pulse. Fluorescence in the 0-0 and 1-1 bands at $\lambda = 308 - 314$ nm is collected by a quartz lens on the axis normal to both the photolysis laser beam and the probe laser beam, passed through one or two 309 nm interference filters, then through another lens that images the transmitted radiation onto the photocathode of a PMT.

A LFP system coupled to a LIF apparatus is commonly used technique for measuring the rate constants of gas phase reactions of $^{\bullet}OH$ radical.[237,238] Ambient or artificial air is introduced into a reaction cell. $^{\bullet}OH$ radicals are generated by the photolysis of O_3 (see R 2-7 and R 2-8) with a pump laser beam passing through the flow tube. The generated $^{\bullet}OH$ radicals are mixed and react with the reactants in the reaction cell.

The change in concentrations of $^{\bullet}$OH radicals generated by the pump laser (LFP) is probed by using a time-resolved LIF technique. [239] Considering the reaction of $^{\bullet}$OH with acetone as a typical example of atmospheric relevance, the decay of $^{\bullet}$OH concentrations can be described with the following equation:

$$[^{\bullet}\mathrm{OH}]_t = [^{\bullet}OH]_0 \exp[-(k_{^{\bullet}OH+CH_3COCH_3}[CH_3(CO)CH_3] + k_{^{\bullet}OH+NO_2}[NO_2] + d)t\}] \quad \text{(Eq 4-1)}$$

where $[^{\bullet}\mathrm{OH}]_t$ is the concentration of $^{\bullet}$OH at time *t* and $[^{\bullet}\mathrm{OH}]_0$ is the initial concentration of $^{\bullet}$OH radicals at t = 0, while *d* is the rate coefficient for diffusion out of the reaction area. When the concentrations of acetone which reacts with $^{\bullet}$OH are in excess compared to those of $^{\bullet}$OH radicals, the decrease of the $^{\bullet}$OH concentration can be expressed by the pseudo-first order decay rate constant k', and it is related to the desired rate constant, $k_{^{\bullet}OH+CH_3COCH_3}$, as follows:

$$k' = k_{^{\bullet}OH+CH_3COCH_3}[CH_3(CO)CH_3] + k_{^{\bullet}OH+NO_2}[NO_2] + d \quad \text{(Eq 4-2)}$$

The decay rate of $^{\bullet}$OH due to the reaction with NO_2 emerges from the intercept in the plot of k' versus $[CH_3COCH_3]$.

4.3. Production and detection of $^{\bullet}$OH radicals in the aqueous phase by laser flash photolysis

The formation of $^{\bullet}$OH radicals in the aqueous phase is based on the laser flash photolysis of three possible precursors, *i.e.* nitrate, nitrite and hydrogen peroxide in the range between 248 and 390 nm. The absolute quantum yields for the above-mentioned $^{\bullet}$OH precursors are reported in a review article by Herrmann.[78] It has been shown that in general the absolute values for the $^{\bullet}$OH-quantum yield at 298 K, based on the photolysis of hydrogen peroxide, are one order of magnitude higher compared to the quantum yields obtained from the photolysis of nitrate and nitrite.

Herrmann and his coworkers largely used the LFP technique to study the $^{\bullet}$OH reactivity in aqueous phases of atmospheric relevance. A series of reactions with various classes of organic compounds were studied and the results were summarized in a review article by Herrmann. [240]

To overcome the limits associated with the weak absorption of $^{\bullet}$OH radical in the aqueous phase, the group of Herrmann developed a "direct" method to study the $^{\bullet}$OH reactivity by monitoring the build-up of the associated peroxy radicals, formed by the reaction between $^{\bullet}OH$ and target organic substrates. In this case, the $^{\bullet}OH$ radicals are formed by photolysis of water at 193 nm by an excimer laser based on ArF as an active medium.

$H_2O + h\nu\ (\lambda=193\ nm) \rightarrow H^{\bullet} + {}^{\bullet}OH$ (R 4-7)

The absorption spectra of $^{\bullet}OH$ radicals were detected by CCD camera. The obtained extinction coefficient of $^{\bullet}OH$ radical in the aqueous phase at 244 nm is then used to observe the formation of peroxy radicals ($RO_2^{\bullet}$), taking into account the interference by $HO_2^{\bullet}$ radicals that absorb light at 244 nm and the decay of $^{\bullet}OH$ radicals. An internal frequency doubled Argon-ion laser with an output at λ=244 nm is used as an analyzing source of $^{\bullet}OH$ radicals and a sensitive photo-diode connected to a digital osciloscope is used as a detection system.

This methodology was applied to study the aqueous phase reactions of $^{\bullet}OH$ radicals with a series of organic compounds at different temperatures and ionic strengths.

4.4. Detection of $^{\bullet}$OH radicals by electron paramagnetic resonance

Electron paramagnetic resonance (EPR) or electron spin resonance (ESR) spectroscopy [241,242] offers the possibility to detect free radicals directly. Similarly to nuclear magnetic resonance (NMR) spectroscopy, this technique is based on the interaction between the electronic magnetic moment of radicals, placed in the EPR cavity of the spectrometer, and the externally applied magnetic field. One condition for observing an EPR signal is that the stationary state concentration of radicals has to rise above the detection limit of the spectrometer. However, $^{\bullet}$OH radicals are short-lived species reacting fast and often at a rate close to the diffusion-control limit: their direct detection is then rather difficult. The spin trapping technique overcomes this dilemma by transforming short-lived radicals into more persistent paramagnetic species, thus permitting EPR detection. It consists upon the addition to the reaction system of a diamagnetic acceptor agent (spin trap) having high affinity for reactive radicals, in order to produce a sufficiently persistent adduct (spin adduct) that can be readily observed by ESR spectroscopy at room temperature.[243,244] Analysis of EPR spectra provides characteristic parameters that are the hyperfine coupling constants and the *g*-factor, permitting to identify the initial trapped radicals.

The spin traps are generally nitroso or nitrone compounds that yield aminoxyls (or nitroxides) after trapping the radical Y (Scheme 1). Nitrones are generally preferred to nitroso compounds, which are less soluble in water and unstable because of their high sensitivity to light and temperature. The most common used nitrones are the cyclic nitrones dimethypyrroline *N*-oxide (DMPO), *N*-*t*-Butyl-Phenylnitrone (PBN) and 2,2,6,6-Tetramethylpiperidine-N-Oxyl (TEMPO). More than 100 derivatized DMPO/PBN spin trap agents have been synthesized and they have been compiled by Tordo and Clément,[245] who reported that phosphorylated (DEPMPO) and ethoxycarbonylated (EMPO) analogues of DMPO enhanced the spin adducts life-time. The rate constant of $^{\bullet}$OH trapping by DMPO has been determined as $3.3 \cdot 10^{9}$ $M^{-1}s^{-1}$.[246] The apparent rate constants of $^{\bullet}$OH trapping by DEPMPO and EMPO in competition with ethanol were determined to be $(4.83 \pm 0.34) \cdot 10^{9}$ and $(4.99 \pm 0.36) \cdot 10^{9}$ M^{-1} s^{-1}, respectively.[247] Half-lives of the $^{\bullet}$OH adducts of DMPO, DEPMPO and EMPO were measured as 55, 127 and 132 min, respectively. [247] It has also been reported that the signal half-time of trifluoroacetate may be enhanced at pH 6.15,[248] or in the presence of dihydroxybenzene.[249] A compilation of hyperfine coupling constants characterizing various spin trap/$^{\bullet}$OH adducts for different experimental conditions has been provided by Buttner.[250]

Scheme 1. Spin trapping by nitroso and nitrone compounds

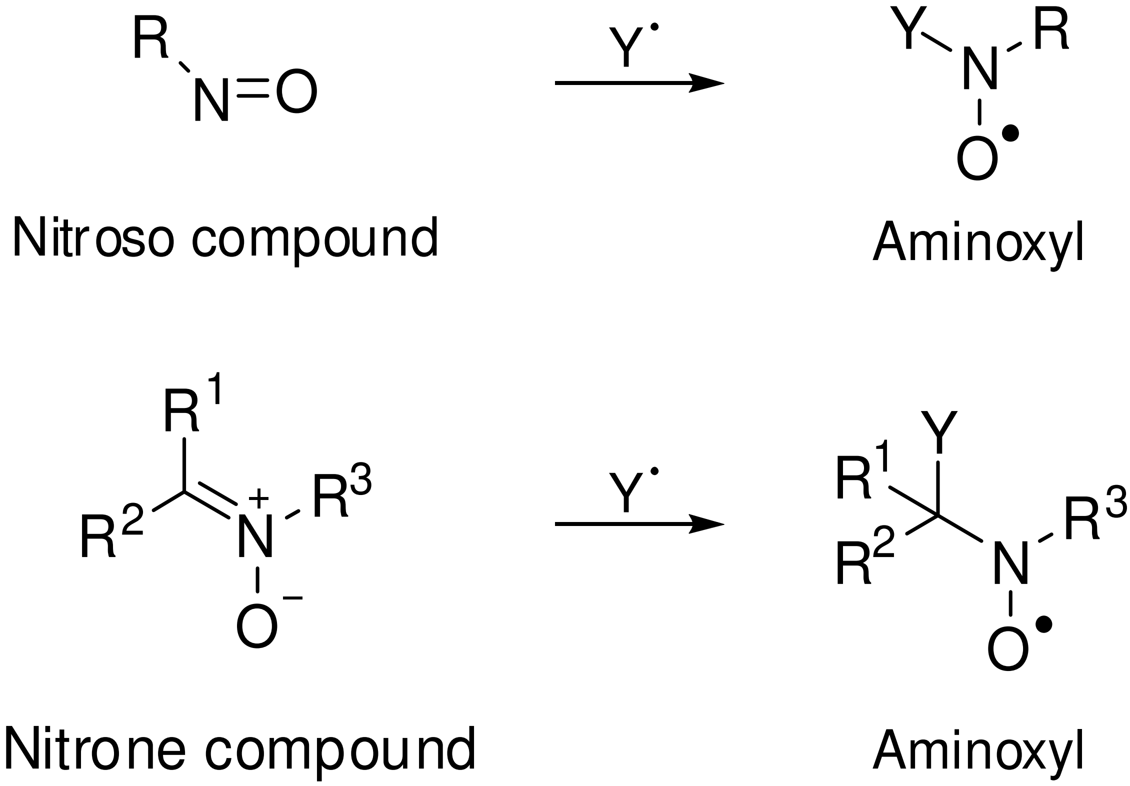

Scheme 2. Example of common spin traps (DMPO, PBN, TMPO) and more recent spin traps (DEPMPO, EMPO)

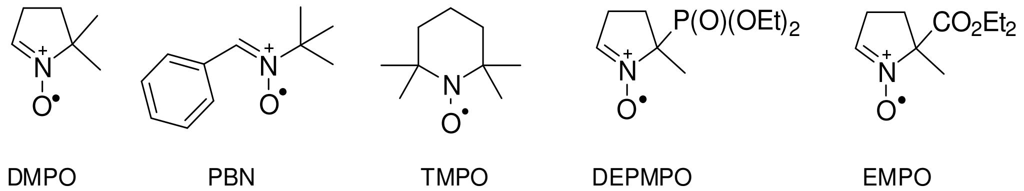

Spin trapping experiments coupled with EPR analysis require careful handling due to possible artifact signals which could lead to wrong attribution of the $^{\bullet}$OH spin adduct. For example, reverse spin trapping can occur in oxidant milieu in the presence of spin trap (ST). The ST can undergo electron abstraction into the radical cation $ST^{\bullet+}$, which can add water by nucleophilic addition yielding a ST/$^{\bullet}$OH-like spin adduct.[251] Spin trap/$^{\bullet}$OH-like spin adduct can also occur from intramolecular rearrangement of the nitrone into the corresponding oxaziridine which, similarly to the ring opening of epoxide, may be hydrolyzed. The resulting hydroxylamine is then readily oxidized into the same aminoxyl as formed by $^{\bullet}OH$ trapping.[252,253] Conventional methods permitting to eliminate artifact events and to verify the presence of $^{\bullet}OH$ use classical inhibitors such as alcohols.

The first application of spin trapping coupled with EPR spectroscopy for identifying $^{\bullet}OH$ generated from the catalyzed photodecomposition of water in the presence of TiO_2 was reported by Jaeger and Bard.[254] This technique has been particularly used in the 90's to characterize $^{\bullet}OH$ radicals in the photooxidation of chlorophenols in the presence of H_2O_2,[255] in TiO_2-H_2O_2-photocatalytic systems for the decomposition of *p*-toluenesulfonic acid [256] or alkylphenols,[257] in TiO_2-water-oxygen systems for the mineralization of *p*-cresol,[258] or to demonstrate the implication that $^{\bullet}OH$ produced in Fenton system originates exclusively from hydrogen peroxide.[259] More recently, intermediates in wet air oxidation, including $^{\bullet}OH$, were successfully identified from real effluent containing Nuclear-Fuel-Chelating compounds [260] or model effluent containing cellulose.[261]

4.5. Indirect $^{\bullet}OH$ detection with probes

Here, a selection of probes aimed to characterize the $^{\bullet}OH$ radicals in the aqueous phase, is presented. The method of indirect $^{\bullet}OH$ detection is based on the introduction of a molecular probe which reacts selectively (trapping) with $^{\bullet}OH$ to form stable hydroxyl radical-derived adducts. Thus, the monitoring of the probe decreasing or of the derived by-product increasing is an indirect method to measure the $^{\bullet}OH$ concentration. The probe should be easy to measure and especially stable, as well as non-reactive with the surrounding matrix, which may contain other organic and non-organic compounds which may interfere with or inhibit the identification. The choice of the probe is determined by the system under study, taking into account the solubility of the probe, the complexation properties with possible elements in the matrix (metals), and its toxicity toward microorganisms (for biological systems). Compared to the direct detection techniques, the probe-trapping method is a readily available and economically useful technique, permitting identification and measurement of the $^{\bullet}OH$ radical concentration for routine analysis. Common probes are salicylic acid, para-chlorobenzoic acid, benzoic acid, terephthalic acid, benzene or more generally aromatic compounds, and alternatively dimethylsulfoxide (DMSO). The product resulting from the reaction of hydroxyl radicals with the probe is generally separated by high performance liquid chromatography (HPLC) coupled with detection techniques, which generally include ultra-violet spectrophotometry and/or fluorescence, chemiluminescence, and mass spectrometry (MS). Electrochemical detection (ECD), developed in 1984,[262] has been also proposed particularly in biological-related systems,[263] allowing high sensitivity and selectivity. The sensitivity of ECD was reported to be 1000 times higher than the optical detection. Other separation techniques have also been described, particularly capillary zone electrophoresis (CZE) coupled with electrochemical detection [264,265] and micellar electrokinetic capillary chromatography (MECC) coupled with UV detection.[266] However, the CZE-ECD technique requires a precise pH control for the separation and analysis of components.[267]

The detection of $^{\bullet}$OH by hydroxylation of aromatic compounds has been known for a long time,[268] and salicylic acid (SA) represents probably one of the most popular probes in free-radical experiments. SA is known to react with hydroxyl radicals at a rate constant of $2.2 \cdot 10^{10}$ $M^{-1}s^{-1}$,[269] producing quantitatively 2,3-dihydrobenzoate (2,3-DHBA), 2,5-dihydroxybenzoate (2,5-DHBA) and, to a lesser extent, pyrocatechol (Scheme 3).

Scheme 3. Hydroxylation of salicylic acid (SA)

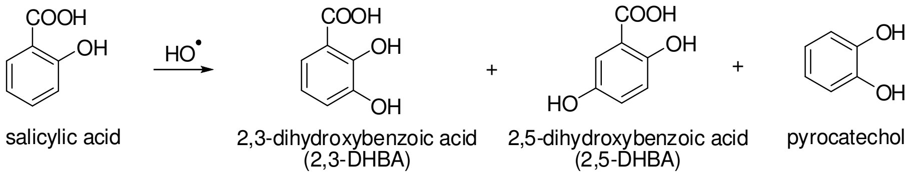

The quantitative determination of the primary hydroxylated derivatives of SA allows to assess, in a relative way, the $^{\bullet}$OH radical concentrations. SA has often been used in free radical research,[267] and in particular in studies related to biological systems where the absolute amount of 2,3-DHBA and 2,5-DHBA was measured to assess free radical damage. As example, Coudray *et al.* used SA as an *in vivo* marker of oxidative stress,[263] obtaining quite low detection limits (0.37 nM and 0.62 nM for 2,3-DHBA and 2,5-DHBA, respectively) with an electrochemical detector (ECD). Recently, this technique was applied for the detection of $^{\bullet}$OH in the atmosphere where lower detection limits were reached (0.3 nM and 0.15 nM for 2,3-DHBA and 2,5-DHBA, respectively) with a coulometric detector. [270] SA has been used successfully in AOPs by Jen *et al.*,[271] who determined indirectly the relative concentration of $^{\bullet}$OH generated from a Fenton system (Table 1), and by Karnik *et al.* in an ozone-membrane filtration hybrid process.[272]

Table 1. Probes, detected adducts with detection limit, and experimental conditions for indirect detection of hydroxyl radical

(Yan et al. 2005)Probe	Detected species	Separation/detection	Observation conditions	pH	Detection limit	Ref.
SA (245-729 μM)	2,3-DHBA 2,5-DHBA	HPLC/ECD	*In Vivo* (plasma)		0.37 nM (2,3-DHBA) 0.62 nM (2,5-DHBA)	273
SA (250 μg/mL)	2,3-DHBA 2,5-DHBA Pyrocatechol	HPLC/UV	Fenton: H_2O_2 (50 μg/mL), Fe^{2+} (5 μg/mL)	2.0-5.0 Optimum: 3.5	0.1 ng	271
SA (20 mM)	2,3-DHBA 2,5-DHBA	CZE/AD	Fenton: H_2O_2 (2 mM), Fe^{2+} (1 mM), EDTA (1 mM)	7.4	20 nM (2,3-DHBA) 20 nM (2,5-DHBA)	266
SA (50 μM)	2,3-DHBA 2,5-DHBA	HPLC/ECD	Atmosphere		3 nM,[a] 0.3 nM[b] (2,3-DHBA) 2 nM,[a] 0.15 nM[b] (2,5-DHBA)	270
p-HBA (0.3 mM)	3,4-DHBA	CZE/ECD	Fenton-type: $CuSO_4$ (1 mM), Vitamin C (2 mM), H_2O_2 (10 μM)	7.1-8.6	1.5 μM	274
p-CBA (1.92 μM)	*p*-CBA	HPLC/UV	TiO_2 (0.1-2.0 $g.L^{-1}$/hν(300-420 nm)	5.7,7.1,8.2		275
DMSO (250 mM)/ DNPH (240 μM)	HCHO	HPLC/UV	AOPs:[c] H_2O_2 (8 mM), $Fe^{2+/3+}$ (0.2 mM)	2-6	0.54 μM	276
TA (4.25 mM)	2-HOTA	/FL	Fenton: H_2O_2 (2.5-50 μM), Fe^{2+} (50 μM)		5 nM	277
TA (5 mM)	2-HOTA	/FL	Fenton: H_2O_2 (1-30 μM), Fe^{2+} (1-30 μM)	7.4	0.2 pM	278
Luminol (0.2 μM)	Aminophtalate	/CL	Catalyst: DPC (20 μM), H_2O_2 (100 pM)	11	41 pM	279

Abbreviations: SA: Salicylic acid, DHBA: Dihydroxybenzoic acid, HPLC: High pressure liquid chromatography, ECD: Electrochemical detection, *p*-HBA: parahydroxybenzoic acid, *p*-CPA: parachlorobenzoic acid: DMSO: Dimethysulsoxide, DNPH: 2,4-Dinitrophenylhydrazine, TA: Terephthalic acid, HOTA: Hydroxyterephthalic acid, FL: Fluorolumunescence, CL: Chemiluminescence.

[a] Amperometric detection.

[b] Coulometric detection.

[c] Fe^{2+}/H_2O_2; Fe^{3+}/H_2O_2; Fe^{2+}-EDTA/H_2O_2; Fe^{3+}-EDTA/H_2O_2; Fe^{2+}-bipyridine/H_2O_2; Fe^{3+}-bipyridine/H_2O_2; UV/H_2O_2; UV-Fe^{2+}/H_2O_2.

A number of other aromatic compounds have been employed to identify $^{\bullet}$OH radicals, and we give here some examples like benzene for the identification of $^{\bullet}$OH sources and sinks upon irradiation of natural waters,[280–282] phenol in Fenton systems,[283] *para*-chlorobenzoic acid (*p*-CBA) to correlate $^{\bullet}$OH with the inactivation of *E. Coli* bacteria in TiO_2 photocatalysis disinfection,[275] benzoic acid in natural water for the evaluation of $^{\bullet}$OH in aqueous iron-hydrogen peroxide reaction,[284] and para-hydroxybenzoic acid (*p*-HBA) for the determination of the antioxidant capacity of flavonids compared to the $CuSO_4$-Vitamin C system.[265]

Dimethylsulfoxide (DMSO) reacts rapidly with $^{\bullet}$OH at a rate constant $k = 6.6 \cdot 10^9$ M^{-1} s^{-1},[285] yielding methanesulfinic acid and methyl radical (reaction 4-8).

Scheme 4. Reaction of DMSO with hydroxyl radical

$$^{\bullet}OH + (CH_3)_2SO \rightarrow CH_3SO_2H + H_3C^{\bullet} \qquad \text{(R 4-8)}$$
$$H_3C^{\bullet} + H - R \rightarrow CH_4 + R^{\bullet} \qquad \text{(R 4-9)}$$
$$H_3C^{\bullet} + O_2 \rightarrow CH_3OO^{\bullet} \qquad \text{(R 4-10)}$$
$$2CH_3OO^{\bullet} \rightarrow HCHO + CH_3OH + O_2 \qquad \text{(R 4-11)}$$

Methanesulfinic acid detection and quantification after derivatization with diazonium salts has been used by Babbs and Gale to identify the $^{\bullet}$OH action on DMSO.[286] Tai et al.[276] proposed an alternative and sensitive method for the determination of hydroxyl radicals based on their reaction with DMSO in the presence of 2,4-dinitrophenylhydrazine (DNPH). The $^{\bullet}$OH radical reacts with DMSO to produce formaldehyde (HCHO), which then reacts with DNPH to give the corresponding hydrazone. The authors indicated the experimental conditions satisfying the optimal $^{\bullet}$OH detection by measuring the HCHO-DNPH derived-byproduct by HPLC (detection limit of 0.54 mmol L^{-1} - Table 1), avoiding side reactions like the scavenging effect of methanol (reaction 4-11). In addition, methanol itself has been used to detect $^{\bullet}$OH radicals, instead of DMSO. In this case, $^{\bullet}$OH reacts with methanol producing HCHO which is detected, in the same way as previously reported, in the presence of DNPH.[287]

In the last decade, the fluorescence spectroscopy technique has attracted considerable attention as a highly sensitive detection tool for reactive oxygen species.[288–290] Numerous fluorescent probes have been used to identify $^{\bullet}OH$ radicals generated by Fenton [291] or Fenton-like [292] systems, or by photoexcitation of catalyst.[293] Terephthalic acid (benzene-1,4-dicarboxylic acid) has been reported to add hydroxyl radical in *ortho*-position yielding the stable and fluorescent hydroxylated 2-hydroxy terephthalate (Scheme 5A).[294–296] Other probes have been described as specific $^{\bullet}OH$ markers and they have been reviewed by Gomes *et al.*,[288] including the relevant 4-(9-Anthroyloxy)-2,2,6,6-tetramethylpiperidine-1-oxyl (ATPO), coumarin-3-carboxylic acid (3-CCA), 3-CCA's succinimidyl ester (SECCA), 2-[6-(4'-hydroxy)phenoxy-3H-xanthen-3-on-9-yl]benzoic acid (HPF), 2-[6-(4'-amino)phenoxy-3H-xanthen-3-on-9-yl]benzoic acid (APF), and Fluorescein (Scheme 5B-D). Several of these specific fluorescence probes are the so-called "positive" fluorogenic probes, consisting in non-fluorescent (or weakly fluorescent) compounds yielding fluorescent adducts upon reaction with ROS. The probe ATPO shows an indirect sensitive response to $^{\bullet}OH$ radicals in the presence of DMSO. The reaction of $^{\bullet}OH$ with DMSO produces quantitatively the methyl radical, which then combines with ATPO to produce stable fluorescent *O*-methylhydroxylamine. The compounds 3-CCA and SECCA react directly with $^{\bullet}OH$ yielding an aromatic hydroxylation product (Scheme 5C),[297] similarly to terephthalic acid. According to Setsukinai *et al.*[291] the probes HPF and APF are capable of detecting $^{\bullet}OH$ radicals generated by a Fenton reaction with high selectivity. The authors reported that the reactive species H_2O_2, NO, $O_2^{\bullet-}$, $^1O_2$ and $ROO^{\bullet}$ did not influence the fluorescence intensity of the probes. The mechanism of the reaction involves the *O*-dearylation of HPF and APF that originate fluorescein (Scheme 5D). On the other hand, fluorescein (FL) is a so-called "negative" fluorogenic probe, a well-known fluorescent compound that is prone to be oxidized by $^{\bullet}OH$ into a non-fluorescent product. This probe was used by Ou *et al.*,[292] who assessed the antioxidant activity of natural compounds. The measurements were performed by monitoring the decrease of fluorescence induced by $^{\bullet}OH$, generated by a Fenton-like system using Co(II) with an antioxidant. Rhodamine has also been proposed as spectrophotometric indicator of $^{\bullet}OH$ scavenging in Fenton systems, in order to compare the antioxidant free-radical scavenging capacity of various flavonids, ascorbic acid [298] or some tea, using the resonance scattering and synchronous fluorescence technique.[299]

The $^{\bullet}OH$ addition rate constant and yields of fluorescent products have been determined for some benzoate, coumarin and phenoxazine derivatives. They range between $2\cdot10^9$ - $2\cdot10^{10}$ L mol^{-1} s^{-1} and 5-11%, respectively.[300] Fluorescent probes are very sensitive and generally permit very low detection limits for [$^{\bullet}$OH], *e.g.* 0.5 pM for *in vitro* measurement of $^{\bullet}$OH generated by a Fenton system.[278] However, the detection conditions are sensitive to pH and, generally, fluorescent probes require precise pH control.[288]

Scheme 5. Fluorescent probes

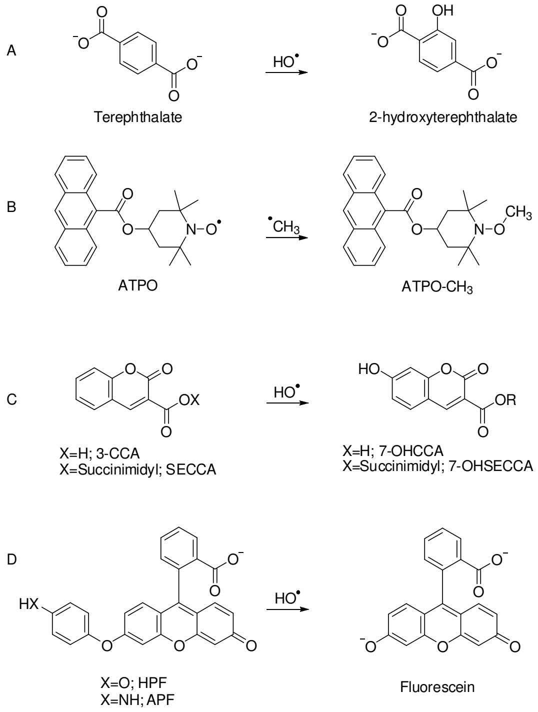

The chemiluminescence (CL) technique has been applied for the detection of ROS [289,301] and has received increasing interest because of its high sensitivity, simplicity, and a wide linear detection range. Luminol-amplified CL represents a common way to identify the involvement of hydrogen peroxide, superoxide radical anion and peroxynitrite in reaction mechanisms. According to Baj and Krawczyk,[279] luminol combined with a strong oxidant including horseradish peroxidase (HRP) and H_2O_2, cobalt, iron, and copper undergoes catalytic oxidation to yield the luminol radical. The latter reduces O_2 to superoxide, yielding an unstable intermediate (diazaquinone) that subsequently reacts with $O_2^{\bullet-}$ and decomposes, after an intramolecular substitution, into N_2 and electronically excited aminophthalate, which originates luminescence upon decay to the ground state (Scheme 6).

Scheme 6. Simplified mechanism of luminol oxidation by hydrogen peroxide (adapted from White et al. [302])

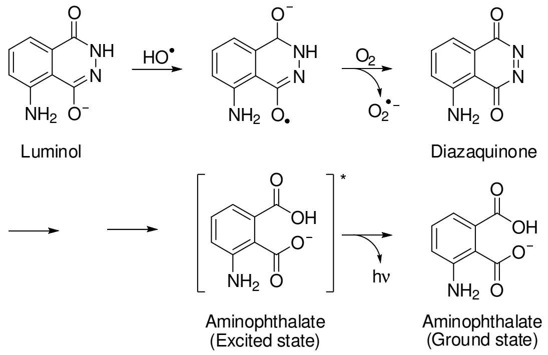

To the best of our knowledge, there is only one paper related to the indirect quantification of $^{\bullet}OH$ produced in ultrasonic systems with luminol/HRP, which permitted the quantification of H_2O_2 originated from $^{\bullet}OH$ recombination.[303] Other CL probes have been proposed, but they concern in their majority the detection of $O_2^{\bullet-}$, H_2O_2, $^1O_2$ or $ONOO^-$. In 2001, the first CL probe specific for hydroxyl radicals was proposed by Tsai *et al.*[304] The authors used the indoxyl-*β*-glucuronide (IBG) (Scheme 7) to characterize $^{\bullet}OH$ produced by the Fenton reagent, and they detected 16200±200 count/s for a system containing 3 μM IBG, 1 mM Fe^{2+}, 3% H_2O_2 in phosphate buffer (pH 7.4) with the presence of EDTA (10 mM). The controls demonstrated that this probe was insensitive to Fe^{2+}, $O_2^{\bullet-}$ and H_2O_2.

Scheme 7. Chemiluminescent probe

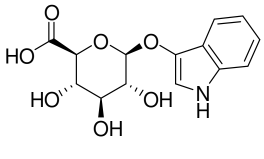

Indoxyl-*β*-glucuronide

Recently, a qualitative test for the nearly immediate detection of hydroxyl radical generated by a Fenton system, based on methylene blue (MB) dye was described by Satoh *et al.*[305] The reaction proceeds *via* an electron transfer from MB to $^{\bullet}OH$ producing the corresponding colorless MB radical cation and hydroxyde ion, respectively. Otherwise, yeast RNA was used as a probe for generation of hydroxyl radicals by earth minerals.[306] The authors have compared the effect on the RNA degradation of various mineral samples having an equivalent Brunauer-Emmett-Teller (BET) surface area. After having positively characterized the mineral-induced production of ROS in the presence of the fluorescent probe APF, the authors demonstrated the use of yeast RNA as a probe for mineral-generated hydroxyl radical.

5. Kinetic properties of hydroxyl radical in aqueous solution

5.1 Determination of reaction rate constants with the competition kinetics method

The $^{\bullet}OH$ radical absorbs weakly in the UV region of the spectrum, with only a small extinction coefficient ($\varepsilon \sim 600$ L $mol^{-1}cm^{-1}$ at $\lambda \sim 235$ nm).[307] Thus, it is extremely difficult to follow the $^{\bullet}OH$ radical concentration (see section 4.2). Usually, competition kinetics method is applied, in which the relative concentration, rather than the rate, of a product formed is determined. In this way, the reaction rate constant with $^{\bullet}OH$ of a studied compound can only be expressed relative to some other reference rate constant, which itself has to be determined absolutely by some other method. Therefore, the reliability of the obtained rate constant depends strongly on the accurate knowledge of the overall reaction system. Despite these difficulties, the competition kinetics method was used in many studies and very useful kinetic data sets have been obtained. In principle, two methods are employed for the determination of the relative $^{\bullet}OH$ rate constants in stationary state systems. In the first method, the kinetic analysis is based on the effect of an additive on the yield of a stable product, which results from the reaction of $^{\bullet}OH$ with the reactant. In the second method, the competition is measured by the effect of the additive on the rate of removal or modification of the reactant.

Few competition methods are also available when the pulse radiolysis and the laser flash photolysis technique are used to obtain the relative $^{\bullet}OH$ rate constants. As in the case above, the validity of the absolute rate constant depends on the accuracy with which the $^{\bullet}OH$ reactivity towards the reference compound can be determined. In principle, two spectrophotometric methods are available. If the reference compound has suitable absorption properties, the reaction of $^{\bullet}OH$ can be measured by monitoring the bleaching of this absorption, provided the transient product has a weaker absorption in the relevant region of the spectrum. The reaction of a competitive reactant is indicated by the reduction in the extent of the bleaching, provided that the competitive reactant does not produce spectral interferences when reacting with $^{\bullet}OH$. Alternatively, the reference compound may react with $^{\bullet}OH$ to form a transient product with a much stronger absorption than the stable reactant. In this case, provided that the product of $^{\bullet}$OH reaction with the competitive reactant does not absorb strongly in the same region, the competition is followed by measurement of the transient absorption.

In such system, the $^{\bullet}$OH radicals react with either reactant in proportion to the products of the concentration multiplied by the rate constant of the respective reactions:

$^{\bullet}OH + C \xrightarrow{k_C}$ absorbing product (R 5-1)

$^{\bullet}OH + S \xrightarrow{k_S}$ non-absorbing product (R 5-2)

Where C is the reference compound and S is the reactant of interest, k_C is the reference rate constant and k_S is the required rate constant.

At a definite reaction time, if A_0 is the absorbance of the absorbing product when the reactant S is absent and A is the absorbance when the reactant S is present in the reaction system, then it follows that:

$$\frac{A_0}{A} = 1 + \frac{k_S[S]}{k_C[C]} \qquad \text{(Eq 5-1)}$$

A plot of A_0/A against the ratio of the reactant concentrations is linear with the slope equal to k_S/k_C. The required rate constant k_S can be derived assuming that the reference rate constant k_C can be measured directly.

A widely used competition kinetics system based on the thiocyanate anion (SCN^-) as a reference reactant was comprehensively explained in the two consecutive studies by Chin and Wine.[308,309] Basically, a dianion $(SCN)_2^{\bullet-}$ is formed in the multistep reaction pathway that is described by the following sequence:

$^{\bullet}OH + SCN^- \rightleftharpoons SCNOH^{\bullet-}$ (R 5-3)

$SCNOH^{\bullet-} \rightleftharpoons SCN^{\bullet} + OH^-$ (R 5-4)

$SCN^{\bullet} + SCN^- \rightleftharpoons (SCN)_2^{\bullet-}$ (R 5-5)

$^{\bullet}$OH + Reactant → products (R 5-6)

The product $(SCN)_2^{\bullet-}$ absorbs strongly in the blue region of the spectrum, with peak absorbance at $\lambda = 475$ nm and extinction coefficient $\varepsilon = 7600\ M^{-1}\ cm^{-1}$.[310,311] Assuming a complete conversion of the initial $^{\bullet}$OH radicals, it can be concluded that the resulting $(SCN)_2^{\bullet-}$ concentration is equal to the initial $[^{\bullet}OH]_0$. Calculations based on available data for the reactivity of intermediate species such as $SCNOH^{\bullet-}$ and $SCN^{\bullet}$ radicals indicate that their possible side reactions do not have influence on the final $(SCN)_2^{\bullet-}$ yield. By the addition of a reactant the yield of $(\mathrm{SCN})_2^{\bullet-}$ is reduced by the fraction of $^\bullet\mathrm{OH}$ consumed by (R 5-6).

Therefore, the yield of $(\mathrm{SCN})_2^{\bullet-}$ can be calculated by (Eq 5-2) and the equations (Eq 5-3) and (Eq 5-4) can be derived.

$$[(\mathrm{SCN})_2^{\bullet-}]_\infty = \frac{k_5[\mathrm{SCN}^\bullet]}{k_2[\mathrm{SCN}^\bullet] + k_5[\mathrm{reactant}]}[^\bullet\mathrm{OH}]_0 \qquad \text{(Eq 5-2)}$$

$$\frac{[^\bullet\mathrm{OH}]_0}{[(\mathrm{SCN})_2^{\bullet-}]_\infty} = 1 + \frac{k_5[\mathrm{reactant}]}{k_2[\mathrm{SCN}^-]} \qquad \text{(Eq 5-3)}$$

or

$$\frac{[(\mathrm{SCN})_2^{\bullet-}]_0}{[(\mathrm{SCN})_2^{\bullet-}]_\infty} = 1 + \frac{k_5[\mathrm{reactant}]}{k_2[\mathrm{SCN}^-]} \qquad \text{(Eq 5-4)}$$

where $[(\mathrm{SCN})_2^{\bullet-}]_0$ represents the maximum concentration of $(\mathrm{SCN})_2^{\bullet-}$ without any additional reactant and $[(\mathrm{SCN})_2^{\bullet-}]_\infty$ corresponds to the maximum concentration of $(\mathrm{SCN})_2^{\bullet-}$ when a reactant is added to the solution. Applying the Lambert-Beer's Law,[312] the absorbance A is proportional to the concentration of $(\mathrm{SCN})_2^{\bullet-}$:

$$A = \log\frac{I_0}{I} = \varepsilon \cdot [(\mathrm{SCN})_2^{\bullet-}] \cdot d \qquad \text{(Eq 5-5)}$$

and correspondingly the concentration $[(\mathrm{SCN})_2^{\bullet-}]$ can be expressed as follows:

$$[(\mathrm{SCN})_2^{\bullet-}] = A / (\varepsilon \cdot d) \qquad \text{(Eq 5-6)}$$

where:

$\varepsilon = 7600\ \mathrm{M^{-1}\ cm^{-1}}$ at $\lambda = 475$ nm [310,311]

d = absorption path length (e.g. 84 cm)

Combining (Eq 5-4) and (Eq 5-6), the ratio of the rate constants k_5 / k_2 is obtained by linear regression of the ratio of the absorbances (A_0 / A) *vs.* the ratio of the concentrations ($[\mathrm{Reactant}] / [\mathrm{SCN}^-]$).

$$\frac{A_0}{A} = 1 + \frac{k_5}{k_2}\frac{[\text{reactant}]}{[\text{SCN}^-]} \qquad \text{(Eq 5-7)}$$

where A_0 is the peak transient absorption of $(SCN)_2^{\bullet-}$, and A is the reduced absorbance when the reactant is present. From the slope of a plot of A_0 / A against [reactant] / [SCN^-], by knowing the reference rate constant (k_2), one can obtain the required second-order rate constant (k_5) for the $^{\bullet}OH$ radical reaction. The reaction system (R 5-3)-(R 5-6) has extensively been studied by Chin and Wine at low SCN^- concentrations. [308,309] Such experiments are sensitive to the reference $^{\bullet}OH + SCN^-$ rate constant.[313–316]

As an example, Table 2 compares the rate constants for the reaction between $^{\bullet}OH$ and 2-propanol in the aqueous phase, obtained with the competition kinetics method **by** employing various reference compounds.

Table 2. The rate constants for the reactions of $^{\bullet}OH$ with 2-propanol in aqueous solution, at 298 K.

Compound	k [l mol^{-1} s^{-1}]	Methods	Technique	References
2-propanol	$1.6 \cdot 10^9$	$^{\bullet}OH + C_6H_5CO_2^-$	PR	317
	$2.4 \cdot 10^9$	$^{\bullet}OH + SCN^-$	PR	318
	$1.9 \cdot 10^9$	$^{\bullet}OH + ABTS^{2-}$	PR	319
	$2.3 \cdot 10^9$	$^{\bullet}OH + [Fe(CN)_6]^{4-}$	PR	320
	$1.9 \cdot 10^9$	$^{\bullet}OH + I^-$	PR	321
	$(2.2 \pm 0.9) \cdot 10^9$	$^{\bullet}OH + SCN^-$	LFP	322

Remarks to the Table: PR = pulse radiolysis; LFP = laser flash photolysis

To study the aqueous phase reactions of $^{\bullet}OH$ radical, Herrmann et al. [323] in their review article suggested an average rate constant, $k = 1.13 \cdot 10^{10}\ M^{-1}\ s^{-1}$ which probably describes best the $^{\bullet}OH + SCN^-$ reaction. For detailed discussion about the reference reaction $^{\bullet}OH + SCN^-$ the readers are referred to the cited review.[323]

The pulse radiolysis is another technique that can be applied to study the $^{\bullet}OH$ reactivity in the aqueous phase. In the pulse radiolysis technique, SCN^- is widely used as the most common reference compound. In addition, ferrocyanide ion is also used as a reference compound.[321,324] This ion is oxidized by $^{\bullet}OH$ rapidly and quantitatively in a one-electron transfer reaction:

$$^{\bullet}OH + [Fe(CN)_6]^{4-} \rightarrow OH^- + [Fe(CN)_6]^{3-} \qquad \text{(R 5-7)}$$

This reaction is almost certainly diffusion-controlled, so that if an intermediate adduct of $^{\bullet}$OH and $[Fe(CN)_6]^{4-}$ is formed it must be very short-lived. Secondary standards are then chosen on the basis that their rate constants can be related directly or indirectly to the observed rate constant for (R 5-7). The product ferricyanide ion is stable and has a characteristic absorption band with maximum at 410 nm (ε = 1000 M^{-1} cm^{-1}).[320] $[Fe(CN)_6]^{4-}$ can be used over the entire range of pH. Although the radicals produced by the reaction of $^{\bullet}$OH with the competitive reactant may in some cases react rapidly with the ferricyanide ion formed in (R 5-7) depending on the concentration of the competitive reactant, such reactions are still too slow to prevent an accurate measurement of the initial values of the absorption.

Another competition kinetics method used to study the $^{\bullet}$OH reactions in the aqueous phase is based on continuous UV photolysis of a mixture of H_2O_2 and two organic compounds, an organic compound of interest and the reference compound. When the reaction with $^{\bullet}$OH radicals is the only sink for the organic compound of interest and for the reference compound, the kinetic system can be described with the equation (Eq 5-1). Compared to the laser flash photolysis system, the disadvantage of using a continuous broadband UV source, is the possibility to photolyze the organic compound of interest.

$$C + h\nu \xrightarrow{J} \text{products} \qquad \text{(R 5-8)}$$

where J is the photolysis frequency of the organic compound.

In this case, when the reaction with $^{\bullet}$OH radicals is the only sink for the reference compound S, but the reactant C is oxidized by $^{\bullet}$OH radicals and photolyzed at the same time, the kinetic system can be described as follows:

$$\frac{1}{t}\ln\left(\frac{[S]_0}{[S]_t}\right) = \frac{k_S}{k_C}\cdot\frac{1}{t}\cdot\ln\left(\frac{[C]_0}{[C]_t}\right) + J \qquad \text{(Eq 5-8)}$$

where $[S]_0$, $[C]_0$, $[S]_t$, $[C]_t$ are the concentrations of the reactant and the reference compound at times 0 and t, respectively. By plotting (1/t) $\ln([S]_0/[S]_t)$ versus (1/t) $\ln([C]_0/[C]_t)$ one obtains a linear curve with a slope of k_S k_C^{-1} and an intercept of J.

This competition kinetics method based on several reference compounds such as ethanol, 1-propanol, methanol, 2-propanol and formaldehyde, was successfully employed by Monod et al [325] to study the reactions of $^{\bullet}$OH radicals with oxygenated organic compounds.

It has to be noted that the competition kinetics method is employed equally in studying aqueous phase reactions and gas-phase reactions, as well. Pulse radiolysis, for instance, is of great importance in understanding gas-phase reactions between $^{\bullet}$OH radical and organic compounds [326].

5.2 Kinetics of formation and reactivity of $^{\bullet}$OH radicals in surface waters

The formation of $^{\bullet}$OH radicals in surface waters is a consequence of the absorption of sunlight by photoactive molecules called photosensitizers. The main $^{\bullet}$OH-producing photosensitizers in surface waters are chromophoric dissolved organic matter (CDOM), the ions nitrite and nitrate, and Fe (hydr)oxides and complexes.[327] The pathways of $^{\bullet}$OH photochemical generation are known in full detail for nitrate and nitrite alone, which produce hydroxyl radicals by direct photolysis upon absorption of UV radiation:[328]

$$NO_3^- + h\nu + H^+ \rightarrow {}^{\bullet}OH + {}^{\bullet}NO_2 \qquad \text{(R 5-9)}$$

$$NO_2^- + h\nu + H^+ \rightarrow {}^{\bullet}OH + {}^{\bullet}NO \qquad \text{(R 5-10)}$$

In the case of nitrate, a further pathway is the photoisomerization to peroxynitrite, which at $pH < 7$ would mainly be present as peroxynitrous acid (HOONO). In solution, HOONO quickly decomposes into either NO_3^- + H^+, or $^{\bullet}OH$ + $^{\bullet}NO_2$.[329] The latter reaction probably accounts for the higher $^{\bullet}$OH photoproduction by NO_3^- at acidic pH.[330]

$$NO_3^- + h\nu \rightarrow ONOO^- \qquad \text{(R 5-11)}$$

$$HOONO \leftrightarrows ONOO^- + H^+ \qquad \text{(R 5-12)}$$

$$HOONO \rightarrow NO_3^- + H^+ \qquad \text{(R 5-13)}$$

$$HOONO \rightarrow {}^{\bullet}OH + {}^{\bullet}NO_2 \qquad \text{(R 5-14)}$$

The issue of the photoproduction of $^{\bullet}$OH by CDOM is much more complex and it is still not completely understood. It is very likely that the process involves at some level the excited triplet states, ^{3}CDOM*, which could take part to two alternative pathways. The triplet states of aromatic carbonyls and quinones, which are representative of the photoactive moieties of CDOM, have usually an oxidizing character and could abstract electrons or hydrogen atoms from oxidizable solutes (S-H).[331,332] In aerated solution the reduced CDOM species could react with dissolved O_2 to produce $HO_2^{\bullet}/O_2^{\bullet-}$, which are then able to disproportionate to H_2O_2. Hydrogen peroxide can yield $^{\bullet}OH$ by photolysis or through the Fenton reaction,[333] and the latter process could link the photochemistry of Fe with that of CDOM. Note that in reaction (R 5-15), ISC = inter-system crossing.

$$\mathrm{CDOM} + h\nu \xrightarrow{\text{(ISC)}} {}^{3}\mathrm{CDOM}^{*} \qquad \text{(R 5-15)}$$

$${}^{3}\mathrm{CDOM}^{*} + \mathrm{S\text{-}H} \rightarrow \mathrm{CDOM}^{\circ-} + \mathrm{S\text{-}H}^{\bullet+} \qquad \text{(R 5-16)}$$

$${}^{3}\mathrm{CDOM}^{*} + \mathrm{S\text{-}H} \rightarrow \mathrm{CDOM\text{-}H}^{\bullet} + \mathrm{S}^{\bullet} \qquad \text{(R 5-17)}$$

$$\mathrm{CDOM}^{\bullet-} + \mathrm{O_2} \rightarrow \mathrm{CDOM} + \mathrm{O_2}^{\bullet-} \qquad \text{(R 5-18)}$$

$$\mathrm{CDOM\text{-}H}^{\bullet} + \mathrm{O_2} \rightarrow \mathrm{CDOM} + \mathrm{HO_2}^{\bullet} \qquad \text{(R 5-19)}$$

$$\mathrm{HO_2}^{\bullet} \leftrightarrows \mathrm{O_2}^{\bullet-} + \mathrm{H}^{+} \qquad \text{(R 5-20)}$$

$$\mathrm{HO_2}^{\bullet} + \mathrm{O_2}^{\bullet-} + \mathrm{H}^{+} \rightarrow \mathrm{H_2O_2} + \mathrm{O_2} \qquad \text{(R 5-21)}$$

$$\mathrm{H_2O_2} + h\nu \rightarrow 2\ {}^{\bullet}\mathrm{OH} \qquad \text{(R 5-22)}$$

$$\mathrm{Fe}^{2+} + \mathrm{H_2O_2} \rightarrow \mathrm{FeOH}^{2+} + {}^{\bullet}\mathrm{OH} \qquad \text{(R 5-23)}$$

It has recently been shown that the H_2O_2 pathway is not the only one that is involved into the photochemical production of $^{\bullet}OH$ by CDOM.[334] Among the possible alternatives, the oxidation of H_2O or OH^- by $^{3}CDOM^{*}$ might be a reasonable possibility.

$${}^{3}\mathrm{CDOM}^{*} + \mathrm{H_2O} \rightarrow \mathrm{CDOM\text{-}H}^{\bullet} + {}^{\bullet}\mathrm{OH} \qquad \text{(R 5-24)}$$

$${}^{3}\mathrm{CDOM}^{*} + \mathrm{OH}^{-} \rightarrow \mathrm{CDOM}^{\bullet-} + {}^{\bullet}\mathrm{OH} \qquad \text{(R 5-25)}$$

While it is well known that many excited triplet states have an hydroxylating power that has nothing to do with the actual $^{\bullet}OH$ generation,[335,336] it has recently been found that the excited triplet state of 1-nitronaphthalene (1NN) is able to oxidize OH^- (presumably to $^{\bullet}OH$), and at the same time that 1NN under irradiation really produces $^{\bullet}OH$.[337,338] Note that the reduction potential of $^{3}1NN^{*}$ is around 2 V, thus the oxidation of OH^- to $^{\bullet}OH$ would be allowed and that of H_2O would depend on pH conditions. However, even with a reaction potential $E = -0.2$ V for the oxidation of water by $^{3}1NN^{*}$ at pH 6.5, which corresponds to an equilibrium constant as low as 0.03, one would obtain a production rate of $^{\bullet}OH$ that is compatible with the observed values.[338] As an alternative, the production of $^{\bullet}$OH by irradiated CDOM could involve the photolysis of -OH containing functional groups (as in the case of e.g. organic peroxides).[323]

As far as Fe is concerned, unfortunately its speciation in surface waters is insufficiently known or understood, which prevents a clear assessment of the role of Fe (hydr)oxides and complexes (with OH^-, including $FeOH^{2+}$, or with organic ligands) to the photochemical $^{\bullet}$OH production. However, there is some evidence that Fe species can be substantial $^{\bullet}$OH sources in Fe-rich waters, where the Fenton reaction can be important, [339] and under acidic conditions.[340,341] The latter are relevant to water bodies that are strongly affected by acidic atmospheric depositions or acidic mine drainage.

At the present state of knowledge it is possible to model the $^{\bullet}$OH production by CDOM, nitrite and nitrate, which depends on the photon flux absorbed by these species. The compounds would compete for sunlight irradiance, with CDOM being by far the main absorber in the UVB and UVA regions. In a mixture made up of CDOM, nitrate and nitrite, the quantities that are easiest to be determined with a simple Lambert-Beer approach are the total absorbance at the wavelength λ, $A_{tot}(\lambda)$, and the corresponding total absorbed spectral photon flux density, $p_a^{tot}(\lambda)$:

$$A_{tot}(\lambda) = A_{CDOM}(\lambda) + \varepsilon_{NO3^-}(\lambda)\, d\, [NO_3^-] + \varepsilon_{NO2^-}(\lambda)\, d\, [NO_2^-] \qquad \text{(Eq 5-9)}$$

$$p_a^{tot}(\lambda) = p°(\lambda)[1 - 10^{-A_{tot}(\lambda)}] \qquad \text{(Eq 5-10)}$$

where d is the optical path length (which can be approximated as the water column depth) and $p°(\lambda)$ is the sunlight spectral photon flux density. If the quantity $A_{CDOM}(\lambda)$ is not known, it is possible to obtain an approximate assessment on the basis of the dissolved organic carbon (DOC) content of water, as follows:[342]

$$\mathrm{A}_{CDOM}(\lambda) = (0.45 \pm 0.04) \cdot d \cdot DOC \cdot \mathrm{e}^{-(0.015 \pm 0.002)\cdot\lambda} \qquad \text{(Eq 5-11)}$$

In a mixture of absorbing compounds under the Lambert-Beer law, the absorbance of each species i ($A_i(\lambda)$) does not vary compared to the absorbance that the same species i has when it is alone in solution. In contrast, the absorbed spectral photon flux density ($p_a^i(\lambda)$) is lower in the mixture. However, the ratio between $p_a^i(\lambda)$ and the total spectral photon flux density absorbed by the solution, $p_a^{tot}(\lambda)$, is equal to the ratio of the respective absorbances:[343]

$$p_a^i(\lambda)\,[p_a^{tot}(\lambda)]^{-1} = A_i(\lambda)\,[A_{tot}(\lambda)]^{-1} \quad \Rightarrow \quad p_a^i(\lambda) = p_a^{tot}(\lambda)\; A_i(\lambda)\,[A_{tot}(\lambda)]^{-1} \qquad \text{(Eq 5-12)}$$

The difference is that $p_a^i(\lambda)$ varies from 0 to $p°(\lambda)$, while $A_i(\lambda)$ could vary, at least theoretically, from 0 to infinity. Equation (Eq 5-12) holds with i = CDOM, NO_3^- or NO_2^-. The photon flux absorbed by i (P_a^i) is:

$$P_a^i = \int_\lambda p_a^i(\lambda)\, d\lambda \qquad \text{(Eq 5-13)}$$

Assume $\Phi_{OH}^i(\lambda)$ as the quantum yield of $^\bullet$OH photoproduction by the species i at the wavelength λ. The $^\bullet$OH formation rate by i is thus:

$$R_{OH}^i = \int_\lambda \Phi_{OH}^i(\lambda)\; p_a^i(\lambda)\; d\lambda = \int_\lambda \Phi_{OH}^i(\lambda)\; p_a^{tot}(\lambda)\;\; A_i(\lambda)\,[A_{tot}(\lambda)]^{-1}\, d\lambda \qquad \text{(Eq 5-14)}$$

However, the values of $\Phi_{OH}^i(\lambda)$ are generally not known, particularly if i = CDOM. A more common approach is that of assuming $R_{OH}^i = \eta_{OH}^i\, P_a^i$, where the values of η_{OH}^i are measured under simulated sunlight. It has been found that:[341,342,344]

$$\eta_{OH}^{CDOM} = (3.0 \pm 0.4)\cdot 10^{-5} \qquad \text{(Eq 5-15)}$$

$$\eta_{OH}^{NO2-} = (7.2 \pm 0.3)\cdot 10^{-2} \qquad \text{(Eq 5-16)}$$

$$\eta_{OH}^{NO3-} = (4.3 \pm 0.2)\cdot 10^{-2} \cdot \frac{[DIC] + 0.0075}{2.25\,[DIC] + 0.0075} \qquad \text{(Eq 5-17)}$$

where [DIC] = $[H_2CO_3] + [HCO_3^-] + [CO_3^{2-}]$ is the total amount of dissolved inorganic carbon. Therefore, the formation rate of $^\bullet$OH by the species i can be expressed as follows:

$$R_{OH}^i = \eta_{OH}^i \cdot \int_\lambda p°(\lambda)\cdot[1 - 10^{-A_{tot}(\lambda)}]\cdot A_i(\lambda)\;[A_{tot}(\lambda)]^{-1}\, d\lambda \qquad \text{(Eq 5-18)}$$

where η_{OH}^i is expressed by equations (Eq 5-15 – Eq 5-17) (with i = CDOM, NO_3^- or NO_2^-) and $A_{tot}(\lambda)$ is described by equation (Eq 5-9). Furthermore, $A_{NO2-}(\lambda) = \varepsilon_{NO2-}(\lambda)\; d\; [NO_2^-]$, $A_{NO3-}(\lambda) = \varepsilon_{NO3-}(\lambda)\; d\; [NO_3^-]$, and $A_{CDOM}(\lambda)$ is expressed by equation (Eq 5-11) or it is otherwise known. At the present state of knowledge there is no reason to believe that the $^\bullet$OH photoproduction rates by CDOM, nitrate and nitrite may be interdependent. By treating them as independent quantities one obtains $R_{OH}^{tot} = \sum_i R_{OH}^i$. After formation, $^\bullet$OH radicals would quickly react in surface waters with the main scavengers (DOM, carbonate, bicarbonate and, to a far lesser extent, nitrite). In saltwater, the main $^\bullet$OH scavenger is bromide. The $^\bullet$OH scavenging rate constant [s^{-1}] can be expressed as follows:[327]

$$k_{OH} = \sum_j k_{j,OH} \cdot C_j \qquad \text{(Eq 5-19)}$$

where C_j is the concentration of the scavenger species j and $k_{j,OH}$ **is** the second-order reaction rate constant between $^{\bullet}$OH and j. It is $k_{j,OH} = 8.5 \cdot 10^6$ M^{-1} s^{-1} for bicarbonate, $3.9 \cdot 10^8$ M^{-1} s^{-1} for carbonate, $1.0 \cdot 10^{10}$ M^{-1} s^{-1} for nitrite, and $1.1 \cdot 10^{10}$ M^{-1} s^{-1} for bromide.[285] In the case of DOM, which can be quantified as DOC (Dissolved Organic Carbon, expressed in mg C L^{-1}), the value of $k_{j,OH}$ has been found to vary between $2 \cdot 10^4$ and $5 \cdot 10^4$ L (mg C)$^{-1}$ s^{-1}.[342,345]

The steady-state $[^{\bullet}OH] = R_{OH}^{tot}\,(k_{OH})^{-1}$, thus one obtains the following equation:

$$[^{\bullet}OH] = \frac{\sum_i \left\{ \eta_{OH}^{i} \cdot \int_{\lambda} p°(\lambda) \cdot [1-10^{-A_{tot}(\lambda)}] \cdot A_i(\lambda)\, [A_{tot}(\lambda)]^{-1}\, d\lambda \right\}}{\sum_j k_{j,OH} \cdot C_j} \qquad \text{(Eq 5-20)}$$

Figure 5 reports as an example the steady-state [$^{\bullet}$OH] as a function of the concentration values of nitrite and DOM (expressed as NPOC, which is a measure of DOC), assuming constant values of nitrate, bicarbonate and carbonate and with $d = 1$ m. Note that [$^{\bullet}$OH] increases with increasing NPOC at low nitrite (where CDOM is practically the only $^{\bullet}$OH source) and that it decreases with NPOC for higher nitrite values (where organic matter plays a more important role as $^{\bullet}$OH sink than as source). The increase of [$^{\bullet}$OH] with nitrite concentration is more important at low NPOC, where organic compounds have a lower impact on either the production or the consumption of $^{\bullet}$OH.

Insert Figure 5

In surface waters, the hydroxyl radicals contribute to the photochemical degradation of pollutants. In the presence of a solute S with a second-order reaction rate constant $k_{S,OH}$ with $^{\bullet}$OH, the pseudo-first order degradation rate constant of S induced by $^{\bullet}$OH is $k_S = k_{S,OH}\,[^{\bullet}OH]$. A major issue is that the described approach is straightforward only for a constant spectral photon flux density of sunlight, $p°(\lambda)$, which produces a constant [$^{\bullet}$OH]. This is obviously not the case for the natural environment, where sunlight irradiance changes. Therefore, conversion strategies between constant irradiation and the actual outdoor days have to be found.[280] After doing this, a good agreement can be obtained between the calculated rates of pollutant phototransformation and the reaction kinetics that are actually observed in the field.[346–349]

6. Reaction mechanisms of the hydroxyl radical in aqueous solution and in the gas phase

6.1. Reaction mechanisms in aqueous solution

The hydroxyl radical is one of the most reactive transients in aqueous solution. It is a very strong oxidant ($E^o_{^\bullet OH/OH^-}$ = 1.90 V; $E^o_{^\bullet OH+H^+/H_2O}$ = 2.73 V) [350] and, additionally, it can take part in a variety of reaction pathways with organic and inorganic molecules.[285]

It is interesting to compare the reduction potential and the reactivity of $^\bullet$OH with those of another very reactive radical species, the sulfate radical $SO_4^{-\bullet}$ ($E^o_{SO_4^{-\bullet}/SO_4^{2-}}$ = 2.43 V). [350] In comparison to $E^o_{SO_4^{-\bullet}/SO_4^{2-}}$, the reduction potential of $^\bullet$OH is strongly pH-dependent. Therefore, $SO_4^{-\bullet}$ can oxidize OH^- and, depending on the pH conditions, it oxidizes water as well:[351]

$$SO_4^{-\bullet} + OH^- \rightarrow SO_4^{2-} + {}^\bullet OH \qquad \text{(R 6-1)}$$

$$SO_4^{-\bullet} + H_2O \rightarrow SO_4^{2-} + {}^\bullet OH + H^+ \qquad \text{(R 6-2)}$$

In contrast, $^\bullet$OH is able to oxidize HSO_4^- that occurs in aqueous solution at $pH < 2$: [285]

$${}^\bullet OH + HSO_4^- \rightarrow H_2O + SO_4^{-\bullet} \qquad \text{(R 6-3)}$$

The $^\bullet$OH radical can be involved in the following reaction mechanisms in aqueous solution:

(i) One-electron abstraction. This is the only possible pathway for many inorganic ions that react with $^\bullet$OH, but it can also take place in the presence of some easily oxidized organic compounds. In some cases the relevant reactions exhibit very fast, diffusion-controlled kinetics, with second-order reaction rate constants around $2\text{-}3 \cdot 10^{10}$ M^{-1} s^{-1}.[285]

(ii) Hydrogen atom (H) abstraction. This reaction pathway is often slower than the previous one, but it is the only possible route for the oxidation of many saturated hydrocarbons.[313] It is probably the less likely type of reactions to show diffusion-controlled kinetics. Interestingly, $^\bullet$OH reacts by H-abstraction much faster compared with other oxidizing radicals such as $SO_4^{-\bullet}$ and $CO_3^{-\bullet}$.[285,351]

(iii) Addition to double bonds or aromatic rings. [285] This pathway obviously involves organic molecules and it can be very fast, sometimes controlled by the diffusion. It ensures rapid $^\bullet$OH reactions also in the presence of kinetic limitations toward one-electron oxidation or H transfer. Together with H abstraction, the addition

processes may explain why ${}^{\bullet}OH$ reacts faster with many organic compounds compared with other strong oxidants of comparable reduction potential, such as $SO_4^{\bullet-}$.[285,351,352]

The following sections introduce the main reaction pathways between ${}^{\bullet}OH$ and water-dissolved compounds. Considerations concerning the ${}^{\bullet}OH$ reaction kinetics will be given at the end of the chapter.

6.1.1. Electron-transfer reactions with inorganic ions

One-electron transfer reactions can take place between ${}^{\bullet}OH$ and some oxidizable inorganic anions such as chloride, bromide, carbonate and nitrite. These processes have a non-negligible importance in surface waters and in technological systems, because they produce radical species that are themselves reactive. The radicals $Cl_2^{\bullet-}$, $Br_2^{\bullet-}$, $CO_3^{\bullet-}$ and ${}^{\bullet}NO_2$ that are formed by oxidation of the anions can be involved in monoelectronic oxidation, but they can also be chlorinating ($Cl_2^{\bullet-}$),[353] brominating ($Br_2^{\bullet-}$)[354] or nitrating (${}^{\bullet}NO_2$) [355] agents. Interestingly, the reaction between Cl^- and ${}^{\bullet}OH$ involves a pre-equilibrium and requires an acidic solution to finally produce $Cl^{\bullet}/Cl_2^{\bullet-}$.[285] For this reason, the generation of chlorine and dichlorine radicals from chloride and ${}^{\bullet}OH$ can be of higher importance in atmospheric waters and in some technological systems than in surface waters. Bromide is the main ${}^{\bullet}OH$ scavenger in seawater (R 2-2), differently from freshwater where the main scavenger of ${}^{\bullet}OH$ is the dissolved organic matter.[356]

${}^{\bullet}OH + Cl^- \leftrightarrows HOCl^{\bullet-}$ (R 6-4)

$HOCl^{\bullet-} + H^+ \leftrightarrows H_2O + Cl^{\bullet}$ (R 6-5)

$Cl^{\bullet} + Cl^- \leftrightarrows Cl_2^{\bullet-}$ (R 6-6)

${}^{\bullet}OH + Br^- \rightarrow OH^- + Br^{\bullet}$ (R 6-7)

$Br^{\bullet} + Br^- \leftrightarrows Br_2^{\bullet-}$ (R 6-8)

${}^{\bullet}OH + CO_3^{2-} \rightarrow OH^- + CO_3^{\bullet-}$ (R 6-9)

${}^{\bullet}OH + NO_2^- \rightarrow OH^- + {}^{\bullet}NO_2$ (R 6-10)

The hydroxyl radical can also react with inorganic cations: the oxidation of Fe^{2+} to Fe(III) can be important in Fenton systems and it may explain (together with the cost of Fe^{2+}) why the catalytic Fenton reagent ($[Fe^{2+}]_o <$

$[H_2O_2]_o$) is preferred over the stoichiometric one ($[Fe^{2+}]_o = [H_2O_2]_o$): in the latter case, Fe^{2+} can become a non-negligible $^{\bullet}OH$ scavenger and decrease the degradation kinetics of pollutants.[357]

6.1.2. Hydrogen abstraction reactions with inorganic ions

This is a first demonstration of the remarkable versatility of the $^{\bullet}OH$ chemistry. For instance, $^{\bullet}OH$ can abstract a hydrogen atom from HSO_4^- (which is the prevailing sulfate form at $pH < 2$) to produce the sulfate radical (R 6-3), while it is not reactive with the sulfate ion *via* electron abstraction (moreover, at sufficiently elevated pH, the latter process would be thermodynamically forbidden).[285,350] A similar H-transfer reaction takes place with bicarbonate, but it is about 20 times slower than the electron abstraction from carbonate. [285]

The possibility for $^{\bullet}OH$ to react through multiple pathways means that it is usually possible to find at least a kinetically favored reaction route for the vast majority of dissolved molecules.

6.1.3. Electron-transfer reactions with organic compounds

Organic molecules are usually not the most likely substrates to undergo one-electron oxidation processes, but such reactions have been shown to take place with $^{\bullet}OH$ in some particular cases. Examples are disulphides, sulphide anions and organic cations such as methylene blue, promazine and promethazine.[285] Electron transfer mechanism also occurs during the reaction of $^{\bullet}OH$ radicals with oxalate, which is not the case regarding the formate anion that proceeds through the hydrogen abstraction mechanism. A major issue is that the abstraction of one electron from an organic compound yields a radical cation that often has to undergo a deprotonation step in aqueous solution to reach a more stable form (R 6-11).[358,359] In contrast, H abstraction directly yields the more stable unprotonated radical (R 6-12). Therefore, the activation energy barrier of (R 6-12) can be lower compared to (R 6-11).

$$\text{R-H} + {}^{\bullet}OH \xrightarrow{e^-\ transfer} \text{R-H}^{\bullet+} + OH^- \rightarrow R^{\bullet} + H_2O \qquad \text{(R 6-11)}$$

$$\text{R-H} + {}^{\bullet}OH \xrightarrow{H\ transfer} R^{\bullet} + H_2O \qquad \text{(R 6-12)}$$

The further reaction of $R^{\bullet}$ oxidation could be induced by a second $^{\bullet}OH$, but other species such as dissolved oxygen are more likely to be involved. Indeed, $R^{\bullet}$ radicals often have relatively low activation energy barriers for reaction with O_2 and, as a consequence, they show quite elevated reaction rate constants. In these cases, because the steady-state [$^{\bullet}$OH] is much lower than the concentration of dissolved oxygen, the hydroxyl radical cannot be a competitive reactant. The situation is completely different for stable molecules. Organic compounds (see R-H above) usually have singlet ground states that are hardly reactive with the triplet ground state of molecular oxygen.[360] Therefore, R-H would not react with O_2 while $R^{\bullet}$ does.

The following Scheme 8 shows some examples of electron-transfer reactions of $^{\bullet}$OH with organic compounds.[285] The case of formate, which could react either by electron or H transfer but where the latter process prevails, is also shown.

Scheme 8. Electron-transfer pathways involving $^{\bullet}$OH and organic compounds. In the case of formate the main pathway (H abstraction) is indicated by the solid arrows, the minor one (e^- transfer) is dashed.

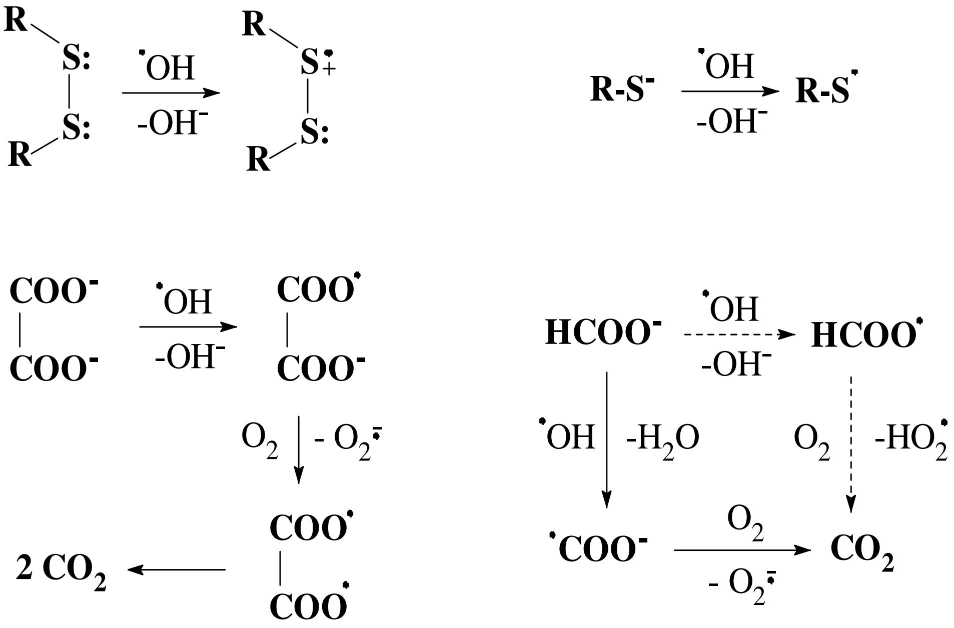

6.1.4. Hydrogen abstraction reactions with organic compounds

Most aliphatic compounds without double C=C bonds react with $^{\bullet}OH$ upon hydrogen abstraction, including carboxylic acids and carboxylates where applicable (an exception is oxalate that has no H atoms). The case of acetate is quite indicative: $^{\bullet}OH$ could in theory abstract an electron from the carboxylate, or a H atom from the methyl group, and the latter process prevails. It is also interesting to consider the H-abstraction reactions when different hydrogen atoms might take part to the process.[314] For instance, acetic and formic acids undergo abstraction of the H atoms linked to carbon, and not the abstraction of the carboxylic ones: [285]

$CH_3COOH + {}^{\bullet}OH \rightarrow CH_2{}^{\bullet}COOH + H_2O$ (R 6-13)

$HCOOH + {}^{\bullet}OH \rightarrow {}^{\bullet}COOH + H_2O$ (R 6-14)

Scheme 9 shows the reaction percentages for H abstraction by $^{\bullet}OH$ on the alcohols 1-propanol, 2-propanol and methanol.

Scheme 9. Importance of the abstraction by $^{\bullet}OH$ of different H atoms for methanol, 1-propanol and 2-propanol.

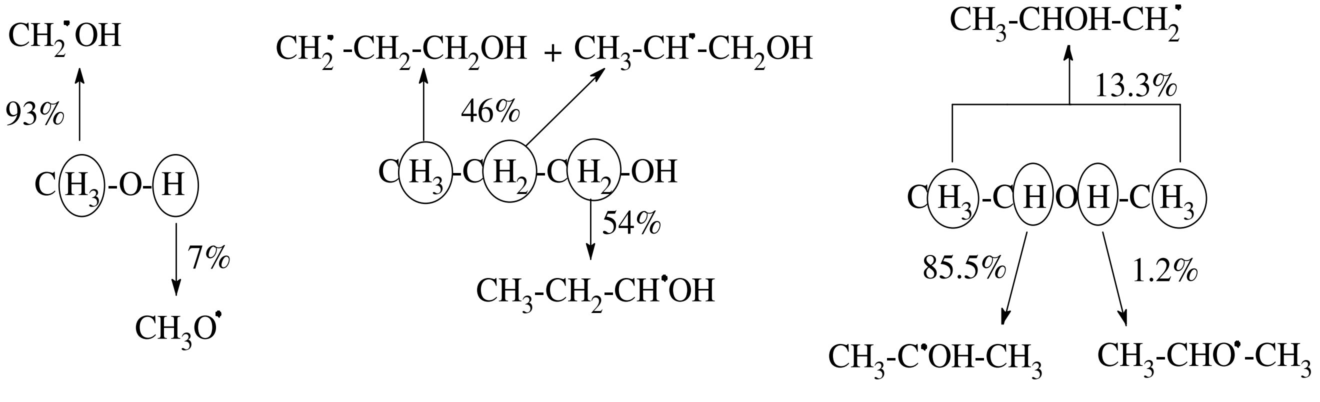

Interestingly, the most reactive hydrogens are those bound to the C atoms bearing the alcoholic function, while the alcoholic hydrogens are the least reactive. A similar issue is also observed with ethanol ($CH_3^{\alpha} - CH_2^{\beta}OH^{\gamma}$): 84.3% of abstraction occurs on the β hydrogens, 13.2% on the α and only 2.5% on the γ one. [285]

The presence of heteroatom-containing groups in aliphatic compounds introduces competition for H abstraction between different functionalities. Interestingly, reaction with hydrogen atoms bound to nitrogen is usually disfavored compared to the H atoms bound to carbon, while HS- groups are usually the first to react. [285]

$^{\bullet}OH + H_2N\text{-}CH_2\text{-}CH_2\text{-}NH_2 \rightarrow H_2O + H_2N\text{-}{}^{\bullet}CH\text{-}CH_2\text{-}NH_2$ (R 6-15)

$^{\bullet}OH + H_2N\text{-}CH_2\text{-}CO\text{-}NH_2 \rightarrow H_2O + H_2N\text{-}{}^{\bullet}CH\text{-}CO\text{-}NH_2$ (R 6-16)

$^{\bullet}OH + H_2N\text{-}CH_2\text{-}COO^- \rightarrow H_2O + H_2N\text{-}{}^{\bullet}CH\text{-}COO^-$ (R 6-17)

$^{\bullet}OH + HS\text{-}CH_2\text{-}CH_2OH \rightarrow H_2O + {}^{\bullet}S\text{-}CH_2\text{-}CH_2OH$ (R 6-18)

$^{\bullet}OH + HS\text{-}CH_2\text{-}CH_2\text{-}COO^- \rightarrow H_2O + {}^{\bullet}S\text{-}CH_2\text{-}CH_2\text{-}COO^-$ (R 6-19)

$^{\bullet}OH + HS\text{-}CH_2\text{-}CH(NH_3^+)COO^- \rightarrow H_2O + {}^{\bullet}S\text{-}CH_2\text{-}CH(NH_3^+)COO^-$ (R 6-20)

Finally, in the case of alkenes and aromatic compounds, $^{\bullet}OH$ addition to the double bond (see section 6.1.5) or to the aromatic ring usually prevails over H abstraction when competition is possible. In the case of toluene, combination of experimental data and quantum mechanical calculations enabled the understanding of the energetics of the reaction pathways in solution and the assessment of their relative importance (Scheme 10).[344] Scheme 10 shows that ring addition of $^{\bullet}OH$ (more than 90% of the total process) strongly prevails over hydrogen abstraction from the methyl group (less than 10% of the process). Note that abstraction of H from the aromatic ring is always a very minor reaction pathway.

Hydrogen abstraction is more likely in the presence of positively charged substituents. For instance, while aniline only undergoes ring addition of $^{\bullet}OH$, the anilinium ion can also react by H abstraction at the level of the $-NH_3^+$ group: [285]

$$^{\bullet}OH + C_6H_5NH_2 \rightarrow HO^{\bullet}C_6H_5NH_2 \qquad \text{(R 6-21)}$$

$$^{\bullet}OH + C_6H_5NH_3^+ - \begin{cases} \rightarrow HO^{\bullet}C_6H_5NH_2 \\ \rightarrow H_2O + C_6H_5N^{\bullet}H_2^+ \end{cases} \qquad \text{(R 6-22)}$$

Scheme 10. Branching ratios of the early reaction pathways between toluene and ${}^{\bullet}OH$, leading to the depicted transformation intermediates.

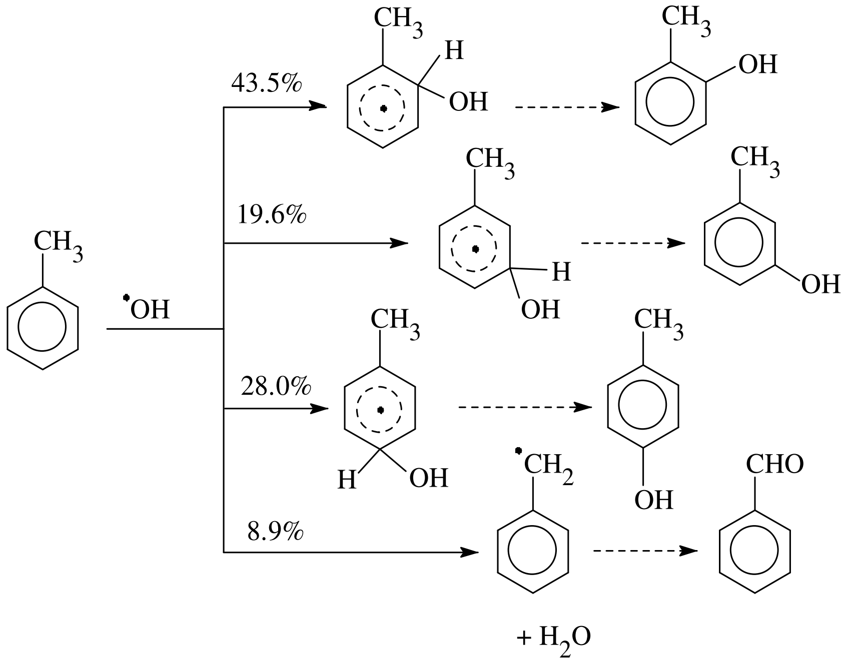

6.1.5. Addition reactions to double bonds and aromatic rings

As already anticipated, addition is the main process taking place with ${}^{\bullet}OH$ in the presence of alkenes and aromatic compounds. Ring addition prevails over H abstraction also in the case of phenols, although hydrogen abstraction from the phenolic group could yield the rather stable phenoxy radicals. After ${}^{\bullet}OH$ addition to the unsaturated system, possible evolutions of the resulting radical intermediate are: *(i)* reaction with O_2 to produce $HO_2^{\bullet}$ and an unsaturated hydroxyderivative (substitution product); *(ii)* addition of O_2 with the final formation of a saturated dihydroxylated compound (addition product), or *(iii)* a reduction pathway to give a saturated monohydroxylated molecule (another addition product). The substitution pathway (addition-elimination) is very common in the case of aromatic rings. [285] The cited processes are depicted in Scheme 11, and a typical pathway for the hydroxylation of an aromatic compound is also shown (here *ortho* addition is reported for simplicity, but *meta* and *para* additions are also very common). Although ${}^{\bullet}OH$ shows some electrophilic character,[361] it follows the typical orientation patterns to a far lesser extent than the actual electrophiles. For instance, while it is practically not possible to form 3-nitrophenol upon phenol nitration, such a compound is an important product of nitrobenzene hydroxylation that yields the three nitrophenol isomers in comparable amount.[362]

Scheme 11. Early and subsequent possible pathways of $^{\bullet}$OH addition to unsaturated hydrocarbons. The reaction marked by (*) can only take place if one of the substituents is H.

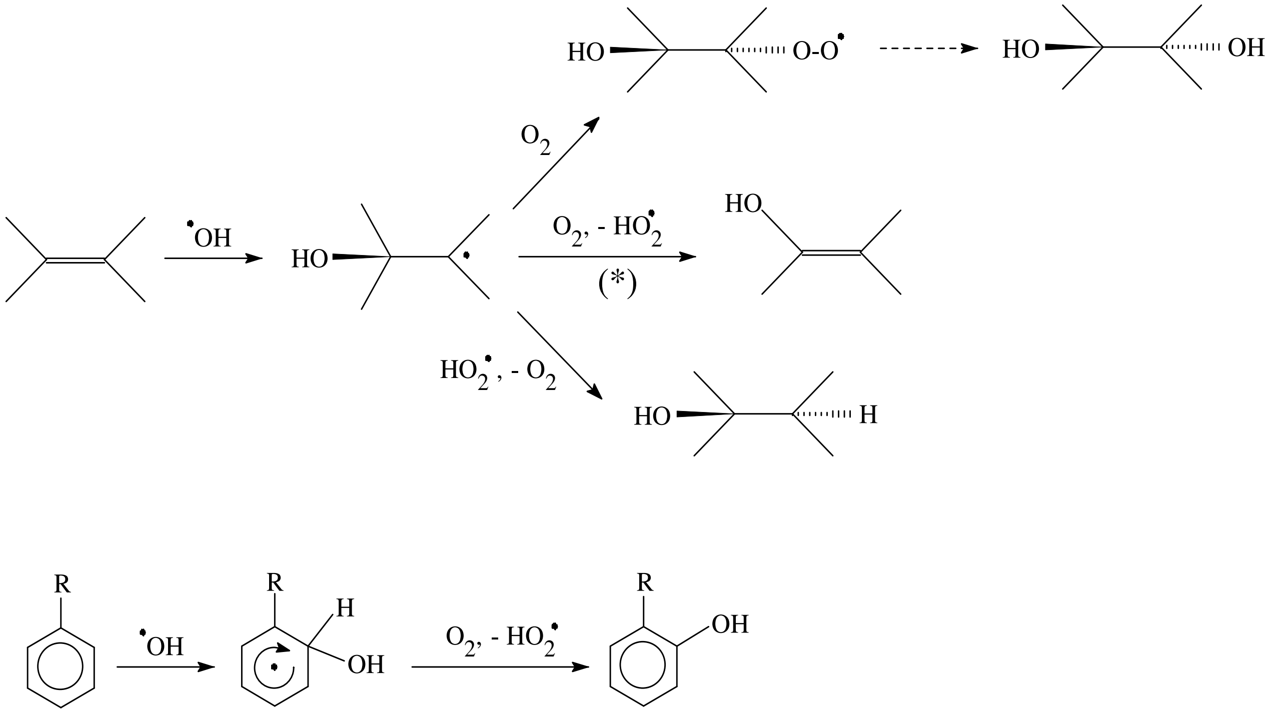

6.1.6. Reaction kinetics as a function of the type of substituents

Substituents can increase or decrease the electron density at particular reactive sites of molecules, thereby modulating the reaction rate constants. The substituent effects can be important in the presence of significant activation energy barriers, but they are minor if a class of reactions is under diffusive control. The latter means that the activation energy is so low that the reaction rate merely depends on the ability of the reactants to diffuse through the solvent until they come in contact and react.

In the case of the hydroxyl radicals, the effects of substituents can be highlighted if the relevant reaction rate constants are sufficiently far from the diffusion control. For aromatic compounds, these effects can be in the form of a significant correlation of the reaction rate constants with the Hammett σ values.[363] It has also been possible to predict several second-order reaction rate constants between dissolved compounds and $^{\bullet}$OH by using a group contribution method. Here the rate constant is expressed as the sum of the contribution of the different parts (*e.g.* aromatic rings, double bonds, primary, secondary and tertiary carbons, heteroatoms) that make up the relevant molecule.[364]

The situation changes radically if the reaction rate constants approach the diffusive control limit. Figure 6 plots the second-order reaction rate constants with $^{\bullet}OH$ and $SO_4^{-\bullet}$ (base-10 logarithms) for benzoates and anisoles, as a function of the ring-substituents' Hammet σ.[365] Significant correlation can be found for $SO_4^{-\bullet}$, for which the one-electron oxidation reactions are favored over competitive reaction pathways.[351] In this case, electron abstraction by $SO_4^{-\bullet}$ is easier if the substituents have an electron-donating character, and more difficult if the substituents withdraw electron density from the aromatic ring. The situation is completely different in the case of $^{\bullet}OH$, for which no correlation is highlighted. For the benzoates one could assume that the hydroxyl radical is more reactive than $SO_4^{-\bullet}$, and that the reaction rate constants with electron-rich compounds cannot increase above the diffusion limit. The possible correlation would, therefore, be lost. Moreover, $^{\bullet}OH$ reacts with aromatics by ring substitution that could depend on substituent effects less than one-electron oxidation. Indeed, when Hammett correlation is observed for $^{\bullet}OH$, the relevant line slopes are much lower than for $SO_4^{-\bullet}$.[363,366] In the case of anisoles the Hammett trend of $^{\bullet}OH$ is opposite of expected, although without significant correlation. In this case the diffusion control cannot be the only explanation, and possibly the steric hindrance of substituents may be more important than the electronic effects.

Insert Figure 6

The involvement of different mechanisms with different compounds, which is very likely in the case of $^{\bullet}OH$, may also account for the lack of correlation. The reactions between $^{\bullet}OH$ and many inorganic anions proceed by one-electron oxidation, but H abstraction or addition (*e.g.* in the case of chloride) are also possible. Monoelectronic oxidation ($X^- \rightarrow X^{\bullet} + e^-$) should be easier if the radical/anion couple has low reduction potential. However, Figure 7 shows a complete lack of correlation between the second-order reaction rate constants of $^{\bullet}OH$ with inorganic anions ($^{\bullet}OH + X^-$) and the corresponding monoelectronic reduction potentials, $E^o(X^{\bullet}/X^-)$.[285,350] On the one side, diffusive control would make it difficult for the rate constants of easily oxidized anions to be much higher than those of more refractory species. On the other hand, different reaction pathways with different anions could completely mask any correlation between reactivity and reduction potential. They could also explain why the rate constants between $^{\bullet}OH$ and hardly oxidized species (e.g. Cl^-) are not so far from the diffusive control.

Insert Figure 7

6.2. Reaction mechanisms of the hydroxyl radical in the gas phase

The mechanisms of $^{\bullet}$OH radical reactions in the gas-phase, or subsets of these reactions, have been reviewed and evaluated previously. [367,368] Therefore, only brief description of the $^{\bullet}$OH reaction mechanism in the gas-phase is given here. The initial reaction of $^{\bullet}$OH radicals with alkanes proceeds by initial H-atom abstraction, and the consequent reactions in the troposphere are shown in Scheme 12.

Scheme 12: Simplified illustration of the reaction mechanism between $^{\bullet}$OH radical and volatile organic compounds (VOCs) in the atmosphere

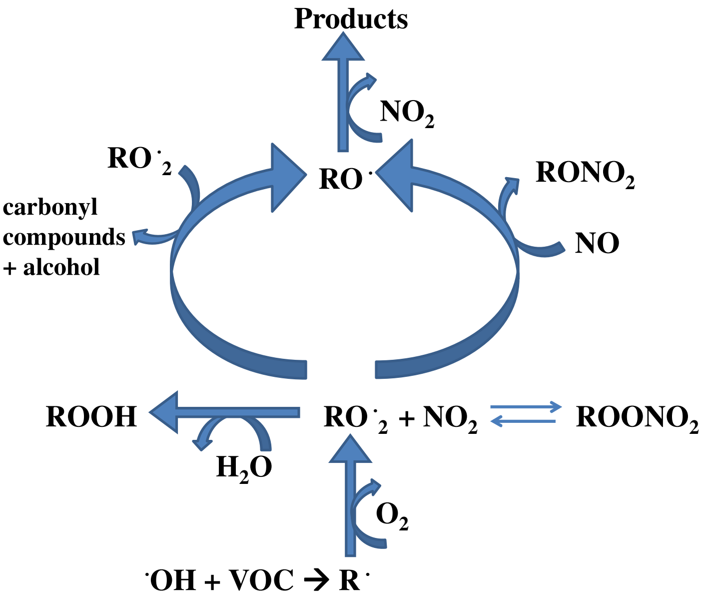

$^{\bullet}$OH radicals react with alcohols by a H-atom abstraction mechanism either from the C–H bonds of the CH_3–, –CH_2–, and >CH– groups in the alkyl chain or from the –OH group. The oxidation of ethers, polyethers, and cyclic ethers in the troposphere is predominantly governed by gas-phase reaction with $^{\bullet}$OH radicals. The reaction of $^{\bullet}$OH radicals with aliphatic ethers proceeds via abstraction of a hydrogen atom from CH_3, –CH_2–, or >CH– groups in the alkyl chain.[367] The available kinetic data set for the reaction of $^{\bullet}$OH radicals with aliphatic ethers shows that ethers are considerably more reactive than the corresponding alkanes. The reactions between $^{\bullet}OH$ radicals and the cyclic esters proceed through H-abstraction mechanism.

The available kinetic and mechanistic data suggest that the reaction of $^{\bullet}OH$ radicals with aldehydes proceeds predominantly by overall H-atom abstraction from the -C(O)H group [369] to form an acyl radical and water, as follows:

$RC(O)H + {}^{\bullet}OH \rightarrow RC^{\bullet}(O) + H_2O$ (R 6-23)

The reactions of $^{\bullet}OH$ with carboxylic acids proceed through an overall H-abstraction mechanism. For example:

$^{\bullet}OH + CH_3COOH \rightarrow {}^{\bullet}CH_2COOH + H_2O$ (R 6-24)

However, the near-zero temperature dependence study by Dagault et al [370] have indicated that this reaction proceeds initially by $^{\bullet}OH$ radical addition to form a complex which then presumably decomposes to products.

With respect to the ketones the description of the reaction mechanism is more complex. In general it is assumed that the reaction of $^{\bullet}OH$ radicals with ketones proceeds by H-atom abstraction mechanism. Reaction (R 6-25) represents an example for the reaction of $^{\bullet}OH$ radical with acetone which leads to the formation of the $^{\bullet}CH_3C(O)CH_2$ radical:

$^{\bullet}OH + CH_3(CO)CH_3 \rightarrow {}^{\bullet}CH_2(CO)CH_3 + H_2O$ (R 6-25)

However, some studies suggested that the reaction of $^{\bullet}OH$ with acetone proceeds through the addition of $^{\bullet}OH$ to the carbonyl group, followed by methyl radical elimination which efficiently leads to the formation of acetic acid [371]. On the other hand, Talukdar et al. [372] have provided compelling evidence that the reaction of $^{\bullet}OH$ with acetone occurs through a hydrogen-bonded complex that leads almost exclusively to ketyl radical and water, independent of temperature between 242 and 350 K. The channel leading to acetic acid has been shown to be negligible at temperatures of atmospheric relevance. Wollenhaupt et al.[238] suggested the formation of an association complex by electrophilic addition of $^{\bullet}OH$ to the carbonyl C atom. The association complex can decompose by C-C bond fission to yield acetic acid, or it can go back to reactants.

It has to be noted, however, that the reactions of $^{\bullet}OH$ with the ketones proceed with rate constants that vary slightly with the temperature, and significantly less compared to reaction with the analogous alkanes, which provides support for the idea that these reactions proceed through different mechanisms.

The products studies with respect to the $^{\bullet}$OH reactions with the esters have demonstrated that these reactions proceed through the H-atom abstraction.[368] Finally, the reactions of $^{\bullet}$OH with unsaturated organic compounds and aromatic compounds proceed through the $^{\bullet}$OH addition to the double bond (>C=C<) or the aromatic ring.[368] In the chapter below, the comparison between the reactions of $^{\bullet}$OH radical in the aqueous phase and in the gas phase, proceeding through the H-abstraction mechanism, is undertaken.

6.3 The comparison between aqueous phase and gas phase reactivity of $^{\bullet}$OH radical

The development of a gas/solution phase reactivity correlation allows one to predict the rates of reaction in one phase from those measured in the other and greatly simplifies the task of estimating atmospheric residence times for trace organics. This in turn helps to remove many of the measurement uncertainties associated with both gas phase and solution phase rate constant studies. Since many compounds with low volatility are often highly soluble (and, conversely, compounds with low solubility are often highly volatile), the use of a gas/solution phase reactivity correlation can circumvent many of the experimental difficulties encountered in conducting gas phase studies with compounds of low volatility and solution phase studies with compounds of low solubility.

Therefore, in Figure 8 the gas phase rate constants from Table 3 are plotted versus the aqueous phase values for the same organic compounds.

Table 3. Comparison between the observed rate constants for the •OH reactions in aqueous solution and in the gas phase

N^{o}	**Compound**	**$k_{\mathrm{Aq.phase}}$ $[\mathrm{l\ mol^{-1}\ s^{-1}}]$**	**Ref.**	**$k_{\mathrm{gas\ phase}}$ $[\mathrm{l\ mol^{-1}\ s^{-1}}]$**	**Ref.**
1	acetone	$(2.1 \pm 0.6) \cdot 10^{8}$	373	$(5.3 \pm 0.8) \cdot 10^{8}$	374
2	acetonylacetone	$(7.6 \pm 1.1) \cdot 10^{8}$	314	$8.8 \cdot 10^{8}$	375
3	methyl ethyl ketone	$(1.5 \pm 0.7) \cdot 10^{9}$	314	$2.0 \cdot 10^{9}$	376
4	diacetyl	$(2.8 \pm 0.6) \cdot 10^{8}$	314	$1.5 \cdot 10^{8}$	375
5	2-pentanone	$2.1 \cdot 10^{9}$	377	$(2.8 \pm 0.18) \cdot 10^{9}$	378
6	3-pentanone	$1.5 \cdot 10^{9}$	377	$(1.2 \pm 0.09) \cdot 10^{9}$	379
7	methyl isobutyl ketone	$2.5 \cdot 10^{9}$	380	$8.5 \cdot 10^{9}$	326
8	tert-butanol	$(5.0 \pm 0.6) \cdot 10^{8}$	373	$(4.9 \pm 1.0) \cdot 10^{8}$	381
9	ethanol	$(2.1 \pm 0.1) \cdot 10^{9}$	373	$(2.3 \pm 0.2) \cdot 10^{9}$	382
10	1-propanol	$(3.2 \pm 0.2) \cdot 10^{9}$	373	$(3.4 \pm 0.3) \cdot 10^{9}$	383
11	1-butanol	$(4.1 \pm 0.8) \cdot 10^{9}$	384	$9.4 \cdot 10^{9}$	383
12	2-propanol	$(2.1 \pm 0.9) \cdot 10^{9}$	373	$(3.3 \pm 0.3) \cdot 10^{9}$	382
13	2-butanol	$(3.5 \pm 0.4) \cdot 10^{9}$	384	$(4.9 \pm 1.2) \cdot 10^{9}$	385
14	acetaldehyde	$2.4 \cdot 10^{9}$	386	$(1.0 \pm 0.2) \cdot 10^{10}$	387
15	propionaldehyde	$(2.8 \pm 0.3) \cdot 10^{9}$	388	$1.2 \cdot 10^{10}$	326
16	butyraldehyde	$(3.9 \pm 1.0) \cdot 10^{9}$	389	$(1.4 \pm 0.1) \cdot 10^{10}$	390
17	isobutyraldehyde	$(2.9 \pm 1.0) \cdot 10^{9}$	314	$(1.1 \pm 0.2) \cdot 10^{10}$	391
18	2,2-dimethylpropanal	$3.2 \cdot 10^{9}$	392	$(1.6 \pm 0.1) \cdot 10^{10}$	390
19	isovaleraldehyde	$2.9 \cdot 10^{9}$	393	$1.8 \cdot 10^{10}$	394
20	n-hexanal	$2.5 \cdot 10^{9}$	393	$(1.7 \pm 0.1) \cdot 10^{10}$	390
21	glyoxal	$(1.1 \pm 0.04) \cdot 10^{9}$	395	$5.3 \cdot 10^{9}$	396
22	methylglyoxal	$(1.1 \pm 0.2) \cdot 10^{9}$	380	$7.1 \cdot 10^{9}$	397
23	2-methybutanal	$3.1 \cdot 10^{9}$	393	$2.0 \cdot 10^{10}$	390
24	pentanal	$3.9 \cdot 10^{9}$	380	$(1.6 \pm 0.1) \cdot 10^{10}$	390
25	Pyruvic acid	$(1.2 \pm 0.4) \cdot 10^{8}$	373	$7.4 \cdot 10^{7}$	398
26	Formic acid	$1.3 \cdot 10^{8}$	285	$2.7 \cdot 10^{8}$	399
27	Propionic acid	$6.2 \cdot 10^{8}$	400	$7.2 \cdot 10^{8}$	401
28	Butyric acid	$2.2 \cdot 10^{9}$	400	$(1.1 \pm 0.1) \cdot 10^{9}$	402
29	ethyl formate	$(3.3 \pm 0.8) \cdot 10^{8}$	314	$5.3 \cdot 10^{8}$	403
30	Ethyl acetate	$4.1 \cdot 10^{8}$	377	$9.0 \cdot 10^{8}$	404
31	Methyl acetate	$2.2 \cdot 10^{8}$	377	$2.1 \cdot 10^{8}$	405,

For a series of alcohols, ketones, esters, acids and aldehydes there is essentially a correlation between the rates in the two phases, as expected for reactions proceeding via a hydrogen abstraction mechanism (Figure 8)

Insert Figure 8

The solid line represents the regression line which corresponds to the following equation:

$$\lg (k_{gas}/M^{-1}s^{-1}) = (2.54 \pm 2.19) + (1.31 \pm 0.24) \cdot \lg (k_{aq}/M^{-1}s^{-1}) \qquad \text{(Eq 6-1)}$$

with $n = 31$; $r = 0.90$

This empirical relationship can be used together with mechanistic information to estimate the $^{\bullet}OH$ reactivity in one phase from the measured rate constant in the other. The dashed line in Figure 8 represents the 1:1 reactivity correlation. As can be seen, the fit according to equation (Eq 6-1) represents a line nearly parallel to the 1:1 reactivity line. The comparison suggests that the order of magnitude of the rate constants in both phases are comparable, demonstrating that the reaction mechanism is the same. However, the rate constants in the gas phase are slightly faster than in the aqueous phase. A possible explanation comes from the solvation effects on the reactants and the activated complex. It has to be noted that the $^{\bullet}OH$ rate constants for many organics in the gas-phase follow non-Arrhenius behavior which implies that the reaction mechanism can differ at other temperatures than 298 K, as was discussed in the chapter above.

Concerning the aqueous tropospheric phase, Herrmann and co-workers have compiled large kinetic data set.[240,323] Further extension of both data bases to compounds covering wider ranges of reactivity will improve such correlations. For the Table 3 the recommended values were chosen or the data from the more recent studies.

7. Concluding remarks and outlook

Hydroxyl radicals dominate the daytime chemistry in the troposphere and (at a definitely lesser extent) in natural waters. Due to its high oxidative capacity, $^{\bullet}OH$ radical is called a "detergent of the atmosphere". High reactivity of hydroxyl radicals with respect to other oxidative species leads to oxidation and chemical conversion of most tropospheric trace compounds or pollutants. The chemistry of $^{\bullet}OH$ radical in the atmospheric gas phase and aqueous phase were recently discussed by Mellouki et al.[406] and Herrmann et al.[407] respectively, in the special issue "Chemistry in Climate" published in Chemical Reviews. The $^{\bullet}OH$ radical also plays an important role in surface waters, although its importance in that compartment is limited by the contemporary presence of other reactive species such as $CO_3^{-\bullet}$, $^1O_2$ and ^{3}CDOM*. We provide an extensive view on the role of hydroxyl radical in different environmental compartments and in laboratory systems, with the aim of drawing more attention to this emerging issue. Further research on processes related to the hydroxyl radical chemistry in the environmental compartments is highly demanded. A comprehensive understanding of the sources and sinks of $^{\bullet}OH$ radicals including their implications in the natural waters and in the atmosphere is of crucial importance, including the way irradiated CDOM in surface waters yields $^{\bullet}OH$ through the H_2O_2-independent pathway, and the assessment of the relative importance of gas-phase vs. aqueous-phase reactions of $^{\bullet}OH$ with many atmospheric components. Moreover, to date, the advanced oxidation processes were characterized based on their ability to produce $^{\bullet}OH$. Despite this, the exact role of $^{\bullet}OH$ in several AOPs is still an object of investigation because different oxidants can be produced at the same time. This complication is crucial in heterogeneous processes (*e.g.* the heterogeneous photocatalysis) and most notably in the first $^{\bullet}OH$-involving reaction that was studied, the Fenton process. Here the controversy about the reactive species involved is particularly significant at pH values around neutrality, as in most Fenton applications proposed recently. Therefore, there is still wide room for fundamental studies on this old reaction.

A particular attention should be paid to the chemical processes involving hydroxyl radicals within indoor environments. This is extremely important considering that people in Western societies spend on average 80-90% of their life indoors and that the indoor environment has recently been demonstrated by Gligorovski and his coworkers [57] to be an active reaction chamber as far as $^\bullet$OH occurrence is concerned, a fact which consequences remain to be explored hereafter [66,72,408]

References

(1) Haber, F.; Weiss, J. The Catalytic Decomposition of Hydrogen Peroxide by Iron Salts. *Proc. R. Soc. Lond. Ser. Math. Phys. Sci.* **1934**, *147* (861), 332–351.

(2) Fenton, H. J. H. LXXIII.—Oxidation of Tartaric Acid in Presence of Iron. *J. Chem. Soc. Trans.* **1894**, *65* (0), 899–910.

(3) Herrmann, H. On the Photolysis of Simple Anions and Neutral Molecules as Sources of O^-/OH, SO_x^- and Cl in Aqueous Solution. *Phys. Chem. Chem. Phys.* **2007**, *9* (30), 3935–3964.

(4) Zafiriou, O. C.; True, M. B. Nitrite Photolysis in Seawater by Sunlight. *Mar. Chem.* **1979**, *8* (1), 9–32.

(5) Moffett, J. W.; Zika, R. G. Reaction Kinetics of Hydrogen Peroxide with Copper and Iron in Seawater. *Environ. Sci. Technol.* **1987**, *21* (8), 804–810.

(6) Zepp, R. G.; Faust, B. C.; Hoigne, J. Hydroxyl Radical Formation in Aqueous Reactions (pH 3-8) of iron(II) with Hydrogen Peroxide: The Photo-Fenton Reaction. *Environ. Sci. Technol.* **1992**, *26* (2), 313–319.

(7) Zellner, R.; Exner, M.; Herrmann, H. Absolute OH Quantum Yields in the Laser Photolysis of Nitrate, Nitrite and Dissolved H_2O_2 at 308 and 351 Nm in the Temperature Range 278–353 K. *J. Atmospheric Chem.* **1990**, *10* (4), 411–425.

(8) Zhou, X.; Mopper, K. Determination of Photochemically Produced Hydroxyl Radicals in Seawater and Freshwater. *Mar. Chem.* **1990**, *30*, 71–88.

(9) De Laurentiis, E.; Minella, M.; Sarakha, M.; Marrese, A.; Minero, C.; Mailhot, G.; Brigante, M.; Vione, D. Photochemical Processes Involving the UV Absorber Benzophenone-4 (2-Hydroxy-4-Methoxybenzophenone-5-Sulphonic Acid) in Aqueous Solution: Reaction Pathways and Implications for Surface Waters. *Water Res.* **2013**, *47* (15), 5943–5953.

(10) Clifford, D.; Donaldson, D. J.; Brigante, M.; D'Anna, B.; George, C. Reactive Uptake of Ozone by Chlorophyll at Aqueous Surfaces. *Environ. Sci. Technol.* **2008**, *42* (4), 1138–1143.

(11) Reeser, D. I.; George, C.; Donaldson, D. J. Photooxidation of Halides by Chlorophyll at the Air−Salt Water Interface. *J. Phys. Chem. A* **2009**, *113* (30), 8591–8595.

(12) True, M. B.; Zafirou, O. C. In *Photochemistry of Environmental Aquatic Systems*; ACS Symposium Series 327; R.G. Zika and W.J. Cooper: Washington, 1987.

(13) Levy, H. Normal Atmosphere: Large Radical and Formaldehyde Concentrations Predicted. *Science* **1971**, *173* (3992), 141–143.

(14) Stone, D.; Whalley, L. K.; Heard, D. E. Tropospheric OH and HO_2 Radicals: Field Measurements and Model Comparisons. *Chem. Soc. Rev.* **2012**, *41* (19), 6348–6404.

(15) Wennberg, P. O. Atmospheric Chemistry: Radicals Follow the Sun. *Nature* **2006**, *442* (7099), 145–146.

(16) Logan, J. A.; Prather, M. J.; Wofsy, S. C.; McElroy, M. B. Tropospheric Chemistry: A Global Perspective. *J. Geophys. Res. Oceans* **1981**, *86* (C8), 7210–7254.

(17) Rohrer, F.; Berresheim, H. Strong Correlation between Levels of Tropospheric Hydroxyl Radicals and Solar Ultraviolet Radiation. *Nature* **2006**, *442* (7099), 184–187.

(18) Ravishankara, A. R.; Hancock, G.; Kawasaki, M.; Matsumi, Y. Photochemistry of Ozone: Surprises and Recent Lessons. *Science* **1998**, *280* (5360), 60–61.

(19) Carr, S.; Heard, D. E.; Blitz, M. A. Comment on "Atmospheric Hydroxyl Radical Production from Electronically Excited NO_2 and H_2O." *Science* **2009**, *324* (5925), 336–336.

(20) Paulson, S. E.; Orlando, J. J. The Reactions of Ozone with Alkenes: An Important Source of HOx in the Boundary Layer. *Geophys. Res. Lett.* **1996**, *23* (25), 3727–3730.

(21) Collins, W. J.; Stevenson, D. S.; Johnson, C. E.; Derwent, R. G. Role of Convection in Determining the Budget of Odd Hydrogen in the Upper Troposphere. *J. Geophys. Res. Atmospheres* **1999**, *104* (D21), 26927–26941.

(22) Jaeglé, L.; Jacob, D. J.; Brune, W. H.; Wennberg, P. O. Chemistry of HO_x Radicals in the Upper Troposphere. *Atmos. Environ.* **2001**, *35* (3), 469–489.

(23) Müller, J.-F.; Brasseur, G. Sources of Upper Tropospheric HO_X : A Three-Dimensional Study. *J. Geophys. Res. Atmospheres* **1999**, *104* (D1), 1705–1715.

(24) Singh, H. B.; Salas, L. J.; Chatfield, R. B.; Czech, E.; Fried, A.; Walega, J.; Evans, M. J.; Field, B. D.; Jacob, D. J.; Blake, D.; et al. Analysis of the Atmospheric Distribution, Sources, and Sinks of Oxygenated Volatile Organic Chemicals Based on Measurements over the Pacific during TRACE-P. *J. Geophys. Res. Atmospheres* **2004**, *109* (D15), D15S07.

(25) Tie, X.; Guenther, A.; Holland, E. Biogenic Methanol and Its Impacts on Tropospheric Oxidants. *Geophys. Res. Lett.* **2003**, *30* (17), 1881.

(26) Harris, G. W.; Carter, W. P. L.; Winer, A. M.; Pitts, J. N.; Platt, U.; Perner, D. Observations of Nitrous Acid in the Los Angeles Atmosphere and Implications for Predictions of Ozone-Precursor Relationships. *Environ. Sci. Technol.* **1982**, *16* (7), 414–419.

(27) Stutz, J.; Kim, E. S.; Platt, U.; Bruno, P.; Perrino, C.; Febo, A. UV-Visible Absorption Cross Sections of Nitrous Acid. *J. Geophys. Res. Atmospheres* **2000**, *105* (D11), 14585–14592.

(28) Bohn, B.; Zetzsch, C. Rate Constants of HO_2 + NO Covering Atmospheric Conditions. 1. HO_2 Formed by OH + H_2O_2. *J. Phys. Chem. A* **1997**, *101* (8), 1488–1493.

(29) Alicke, B.; Geyer, A.; Hofzumahaus, A.; Holland, F.; Konrad, S.; Pätz, H. W.; Schäfer, J.; Stutz, J.; Volz-Thomas, A.; Platt, U. OH Formation by HONO Photolysis during the BERLIOZ Experiment. *J. Geophys. Res. Atmospheres* **2003**, *108* (D4), 8247.

(30) Aumont, B.; Chervier, F.; Laval, S. Contribution of HONO Sources to the $NO_x/HO_x/O_3$ Chemistry in the Polluted Boundary Layer. *Atmos. Environ.* **2003**, *37* (4), 487–498.

(31) Kleffmann, J.; Gavriloaiei, T.; Hofzumahaus, A.; Holland, F.; Koppmann, R.; Rupp, L.; Schlosser, E.; Siese, M.; Wahner, A. Daytime Formation of Nitrous Acid: A Major Source of OH Radicals in a Forest. *Geophys. Res. Lett.* **2005**, *32* (5), L05818.

(32) Ren, X.; Harder, H.; Martinez, M.; Lesher, R. L.; Oliger, A.; Simpas, J. B.; Brune, W. H.; Schwab, J. J.; Demerjian, K. L.; He, Y.; et al. OH and HO_2 Chemistry in the Urban Atmosphere of New York City. *Atmos. Environ.* **2003**, *37* (26), 3639–3651.

(33) Vogel, B.; Vogel, H.; Kleffmann, J.; Kurtenbach, R. Measured and Simulated Vertical Profiles of Nitrous acid—Part II. Model Simulations and Indications for a Photolytic Source. *Atmos. Environ.* **2003**, *37* (21), 2957–2966.

(34) Zhou, X.; Civerolo, K.; Dai, H.; Huang, G.; Schwab, J.; Demerjian, K. Summertime Nitrous Acid Chemistry in the Atmospheric Boundary Layer at a Rural Site in New York State. *J. Geophys. Res. Atmospheres* **2002**, *107* (D21), 4590.

(35) Sörgel, M.; Regelin, E.; Bozem, H.; Diesch, J.-M.; Drewnick, F.; Fischer, H.; Harder, H.; Held, A.; Hosaynali-Beygi, Z.; Martinez, M.; et al. Quantification of the Unknown HONO Daytime Source and Its Relation to NO_2. *Atmos Chem Phys* **2011**, *11* (20), 10433–10447.

(36) Elshorbany, Y. F.; Kurtenbach, R.; Wiesen, P.; Lissi, E.; Rubio, M.; Villena, G.; Gramsch, E.; Rickard, A. R.; Pilling, M. J.; Kleffmann, J. Oxidation Capacity of the City Air of Santiago, Chile. *Atmos Chem Phys* **2009**, *9* (6), 2257–2273.

(37) Elshorbany, Y. F.; Kleffmann, J.; Kurtenbach, R.; Lissi, E.; Rubio, M.; Villena, G.; Gramsch, E.; Rickard, A. R.; Pilling, M. J.; Wiesen, P. Seasonal Dependence of the Oxidation Capacity of the City of Santiago de Chile. *Atmos. Environ.* **2010**, *44* (40), 5383–5394.

(38) Taraborrelli, D.; Lawrence, M. G.; Crowley, J. N.; Dillon, T. J.; Gromov, S.; Groß, C. B. M.; Vereecken, L.; Lelieveld, J. Hydroxyl Radical Buffered by Isoprene Oxidation over Tropical Forests. *Nat. Geosci.* **2012**, *5* (3), 190–193.

(39) Fuchs, H.; Hofzumahaus, A.; Rohrer, F.; Bohn, B.; Brauers, T.; Dorn, H.-P.; Häseler, R.; Holland, F.; Kaminski, M.; Li, X.; et al. Experimental Evidence for Efficient Hydroxyl Radical Regeneration in Isoprene Oxidation. *Nat. Geosci.* **2013**, *6* (12), 1023–1026.

(40) Lelieveld, J.; Butler, T. M.; Crowley, J. N.; Dillon, T. J.; Fischer, H.; Ganzeveld, L.; Harder, H.; Lawrence, M. G.; Martinez, M.; Taraborrelli, D.; et al. Atmospheric Oxidation Capacity Sustained by a Tropical Forest. *Nature* **2008**, *452* (7188), 737–740.

(41) Stone, D.; Evans, M. J.; Edwards, P. M.; Commane, R.; Ingham, T.; Rickard, A. R.; Brookes, D. M.; Hopkins, J.; Leigh, R. J.; Lewis, A. C.; et al. Isoprene Oxidation Mechanisms: Measurements and Modelling of OH and HO_2 over a South-East Asian Tropical Rainforest during the OP3 Field Campaign. *Atmos Chem Phys* **2011**, *11* (13), 6749–6771.

(42) Whalley, L. K.; Edwards, P. M.; Furneaux, K. L.; Goddard, A.; Ingham, T.; Evans, M. J.; Stone, D.; Hopkins, J. R.; Jones, C. E.; Karunaharan, A.; et al. Quantifying the Magnitude of a Missing Hydroxyl Radical Source in a Tropical Rainforest. *Atmos Chem Phys* **2011**, *11* (14), 7223–7233.

(43) Peeters, J.; Müller, J.-F.; Stavrakou, T.; Nguyen, V. S. Hydroxyl Radical Recycling in Isoprene Oxidation Driven by Hydrogen Bonding and Hydrogen Tunneling: The Upgraded LIM1 Mechanism. *J. Phys. Chem. A* **2014**, *118* (38), 8625–8643.

(44) Montzka, S. A.; Krol, M.; Dlugokencky, E.; Hall, B.; Jöckel, P.; Lelieveld, J. Small Interannual Variability of Global Atmospheric Hydroxyl. *Science* **2011**, *331* (6013), 67–69.

(45) Patra, P. K.; Krol, M. C.; Montzka, S. A.; Arnold, T.; Atlas, E. L.; Lintner, B. R.; Stephens, B. B.; Xiang, B.; Elkins, J. W.; Fraser, P. J.; et al. Observational Evidence for Interhemispheric Hydroxyl-Radical Parity. *Nature* **2014**, *513* (7517), 219–223.

(46) Manning, M. R.; Lowe, D. C.; Moss, R. C.; Bodeker, G. E.; Allan, W. Short-Term Variations in the Oxidizing Power of the Atmosphere. *Nature* **2005**, *436* (7053), 1001–1004.

(47) Heard, D. E.; Pilling, M. J. Measurement of OH and HO_2 in the Troposphere. *Chem. Rev.* **2003**, *103* (12), 5163–5198.

(48) Nazaroff, W. W.; Cass, G. R. Mathematical Modeling of Chemically Reactive Pollutants in Indoor Air. *Environ. Sci. Technol.* **1986**, *20* (9), 924–934.

(49) Weschler, C. J.; Shields, H. C. Production of the Hydroxyl Radical in Indoor Air. *Environ. Sci. Technol.* **1996**, *30* (11), 3250–3258.

(50) Weschler, C. J.; Shields, H. C. Measurements of the Hydroxyl Radical in a Manipulated but Realistic Indoor Environment. *Environ. Sci. Technol.* **1997**, *31* (12), 3719–3722.

(51) Sarwar, G.; Corsi, R.; Kimura, Y.; Allen, D.; Weschler, C. J. Hydroxyl Radicals in Indoor Environments. *Atmos. Environ.* **2002**, *36* (24), 3973–3988.

(52) Carslaw, N. A New Detailed Chemical Model for Indoor Air Pollution. *Atmos. Environ.* **2007**, *41* (6), 1164–1179.

(53) White, I. R.; Martin, D.; Muñoz, M. P.; Petersson, F. K.; Henshaw, S. J.; Nickless, G.; Lloyd-Jones, G. C.; Clemitshaw, K. C.; Shallcross, D. E. Use of Reactive Tracers To Determine Ambient OH Radical Concentrations: Application within the Indoor Environment. *Environ. Sci. Technol.* **2010**, *44* (16), 6269–6274.

(54) Alvarez, E. G.; Amedro, D.; Afif, C.; Gligorovski, S.; Schoemaecker, C.; Fittschen, C.; Doussin, J.-F.; Wortham, H. Unexpectedly High Indoor Hydroxyl Radical Concentrations Associated with Nitrous Acid. *Proc. Natl. Acad. Sci.* **2013**, *110* (33), 13294–13299.

(55) Bartolomei, V.; Gomez Alvarez, E.; Wittmer, J.; Tlili, S.; Strekowski, R.; Temime-Roussel, B.; Quivet, E.; Wortham, H.; Zetzsch, C.; Kleffmann, J.; et al. Combustion Processes as a Source of High Levels of Indoor Hydroxyl Radicals through the Photolysis of Nitrous Acid. *Environ. Sci. Technol.* **2015**.

(56) Bartolomei, V.; Sörgel, M.; Gligorovski, S.; Alvarez, E. G.; Gandolfo, A.; Strekowski, R.; Quivet, E.; Held, A.; Zetzsch, C.; Wortham, H. Formation of Indoor Nitrous Acid (HONO) by Light-Induced NO2 Heterogeneous Reactions with White Wall Paint. *Environ. Sci. Pollut. Res.* **2014**, *21* (15), 9259–9269.

(57) Alvarez, E. G.; Amedro, D.; Afif, C.; Gligorovski, S.; Schoemaecker, C.; Fittschen, C.; Doussin, J.-F.; Wortham, H. Unexpectedly High Indoor Hydroxyl Radical Concentrations Associated with Nitrous Acid. *Proc. Natl. Acad. Sci.* **2013**, *110* (33), 13294–13299.

(58) Brauer, M.; Ryan, P. B.; Suh, H. H.; Koutrakis, P.; Spengler, J. D.; Leslie, N. P.; Billick, I. H. Measurements of Nitrous Acid inside Two Research Houses. *Environ. Sci. Technol.* **1990**, *24* (10), 1521–1527.

(59) Finlayson-Pitts, B. J.; Wingen, L. M.; Sumner, A. L.; Syomin, D.; Ramazan, K. A. The Heterogeneous Hydrolysis of NO_2 in Laboratory Systems and in Outdoor and Indoor Atmospheres: An Integrated Mechanism. *Phys. Chem. Chem. Phys.* **2003**, *5* (2), 223–242.

(60) Bartolomei, V.; Sörgel, M.; Gligorovski, S.; Alvarez, E. G.; Gandolfo, A.; Strekowski, R.; Quivet, E.; Held, A.; Zetzsch, C.; Wortham, H. Formation of Indoor Nitrous Acid (HONO) by Light-Induced NO_2 Heterogeneous Reactions with White Wall Paint. *Environ. Sci. Pollut. Res.* **2014**, *21* (15), 9259–9269.

(61) Gómez Alvarez, E.; Sörgel, M.; Gligorovski, S.; Bassil, S.; Bartolomei, V.; Coulomb, B.; Zetzsch, C.; Wortham, H. Light-Induced Nitrous Acid (HONO) Production from NO_2 Heterogeneous Reactions on Household Chemicals. *Atmos. Environ.* **2014**, *95*, 391–399.

(62) Jammoul, A.; Gligorovski, S.; George, C.; D'Anna, B. Photosensitized Heterogeneous Chemistry of Ozone on Organic Films. *J. Phys. Chem. A* **2008**, *112* (6), 1268–1276.

(63) Stemmler, K.; Ammann, M.; Donders, C.; Kleffmann, J.; George, C. Photosensitized Reduction of Nitrogen Dioxide on Humic Acid as a Source of Nitrous Acid. *Nature* **2006**, *440* (7081), 195–198.

(64) Gandolfo, A.; Bartolomei, V.; Gomez Alvarez, E.; Tlili, S.; Gligorovski, S.; Kleffmann, J.; Wortham, H. The Effectiveness of Indoor Photocatalytic Paints on NO_x and HONO Levels. *Appl. Catal. B Environ.* **2015**, *166–167*, 84–90.

(65) Gandolfo, A.; Bartolomei, V.; Gomez Alvarez, E.; Tlili, S.; Gligorovski, S.; Kleffmann, J.; Wortham, H. The Effectiveness of Indoor Photocatalytic Paints on NO_x and HONO Levels. *Appl. Catal. B Environ.* **2015**, *166–167*, 84–90.

(66) Gligorovski, S. Nitrous Acid (HONO): An Emerging Indoor Pollutant. *J. Photochem. Photobiol. Chem.*

(67) Jenkin, M. E.; Saunders, S. M.; Wagner, V.; Pilling, M. J. Protocol for the Development of the Master Chemical Mechanism, MCM v3 (Part B): Tropospheric Degradation of Aromatic Volatile Organic Compounds. *Atmos Chem Phys* **2003**, *3* (1), 181–193.

(68) Saunders, S. M.; Jenkin, M. E.; Derwent, R. G.; Pilling, M. J. Protocol for the Development of the Master Chemical Mechanism, MCM v3 (Part A): Tropospheric Degradation of Non-Aromatic Volatile Organic Compounds. *Atmos Chem Phys* **2003**, *3* (1), 161–180.

(69) Elshorbany, Y.; Barnes, I.; Becker, K. H.; Kleffmann, J.; Wiesen, P. Sources and Cycling of Tropospheric Hydroxyl Radicals – An Overview. *Z. Für Phys. Chem. Int. J. Res. Phys. Chem. Chem. Phys.* **2010**, *224* (7-8), 967–987.

(70) Kylling, A.; Webb, A. R.; Bais, A. F.; Blumthaler, M.; Schmitt, R.; Thiel, S.; Kazantzidis, A.; Kift, R.; Misslbeck, M.; Schallhart, B.; et al. Actinic Flux Determination from Measurements of Irradiance. *J. Geophys. Res. Atmospheres* **2003**, *108* (D16), 4506.

(71) Brown, S. K.; Sim, M. R.; Abramson, M. J.; Gray, C. N. Concentrations of Volatile Organic Compounds in Indoor Air – A Review. *Indoor Air* **1994**, *4* (2), 123–134.

(72) Gligorovski, S.; Weschler, C. J. The Oxidative Capacity of Indoor Atmospheres. *Environ. Sci. Technol.* **2013**, *47* (24), 13905–13906.

(73) Montoya, J. F.; Salvador, P. The Influence of Surface Fluorination in the Photocatalytic Behaviour of TiO_2 Aqueous Dispersions: An Analysis in the Light of the Direct–indirect Kinetic Model. *Appl. Catal. B Environ.* **2010**, *94* (1–2), 97–107.

(74) Montoya, J. F.; Ivanova, I.; Dillert, R.; Bahnemann, D. W.; Salvador, P.; Peral, J. Catalytic Role of Surface Oxygens in TiO_2 Photooxidation Reactions: Aqueous Benzene Photooxidation with $Ti^{18}O_2$ under Anaerobic Conditions. *J. Phys. Chem. Lett.* **2013**, *4* (9), 1415–1422.

(75) Abramović, B.; Kler, S.; Šojić, D.; Laušević, M.; Radović, T.; Vione, D. Photocatalytic Degradation of Metoprolol Tartrate in Suspensions of Two TiO_2-Based Photocatalysts with Different Surface Area. Identification of Intermediates and Proposal of Degradation Pathways. *J. Hazard. Mater.* **2011**, *198*, 123–132.

(76) Qu, Y.; Duan, X. Progress, Challenge and Perspective of Heterogeneous Photocatalysts. *Chem. Soc. Rev.* **2013**, *42* (7), 2568–2580.

(77) Lang, X.; Chen, X.; Zhao, J. Heterogeneous Visible Light Photocatalysis for Selective Organic Transformations. *Chem. Soc. Rev.* **2013**, *43* (1), 473–486.

(78) Herrmann, H. On the Photolysis of Simple Anions and Neutral Molecules as Sources of O^-/OH, SO_x^- and Cl in Aqueous Solution. *Phys. Chem. Chem. Phys.* **2007**, *9* (30), 3935–3964.

(79) Botti, H.; Trujillo, M.; Batthyány, C.; Rubbo, H.; Ferrer-Sueta, G.; Radi, R. Homolytic Pathways Drive Peroxynitrite-Dependent Trolox C Oxidation. *Chem. Res. Toxicol.* **2004**, *17* (10), 1377–1384.

(80) Vione, D.; Minella, M.; Maurino, V.; Minero, C. Indirect Photochemistry in Sunlit Surface Waters: Photoinduced Production of Reactive Transient Species. *Chem. – Eur. J.* **2014**, *20* (34), 10590–10606.

(81) Fischer, M.; Warneck, P. Photodecomposition of Nitrite and Undissociated Nitrous Acid in Aqueous Solution. *J. Phys. Chem.* **1996**, *100* (48), 18749–18756.

(82) Hong, A. C.; Wren, S. N.; Donaldson, D. J. Enhanced Surface Partitioning of Nitrate Anion in Aqueous Bromide Solutions. *J. Phys. Chem. Lett.* **2013**, *4* (17), 2994–2998.

(83) Goldstein, S.; Rabani, J. Mechanism of Nitrite Formation by Nitrate Photolysis in Aqueous Solutions: The Role of Peroxynitrite, Nitrogen Dioxide, and Hydroxyl Radical. *J. Am. Chem. Soc.* **2007**, *129* (34), 10597–10601.

(84) Warneck, P.; Wurzinger, C. Product Quantum Yields for the 305-nm Photodecomposition of Nitrate in Aqueous Solution. *J. Phys. Chem.* **1988**, *92* (22), 6278–6283.

(85) Kleffmann, J.; Lörzer, J. C.; Wiesen, P.; Kern, C.; Trick, S.; Volkamer, R.; Rodenas, M.; Wirtz, K. Intercomparison of the DOAS and LOPAP Techniques for the Detection of Nitrous Acid (HONO). *Atmos. Environ.* **2006**, *40* (20), 3640–3652.

(86) Das, R.; Dutta, B. K.; Maurino, V.; Vione, D.; Minero, C. Suppression of Inhibition of Substrate Photodegradation by Scavengers of Hydroxyl Radicals: The Solvent-Cage Effect of Bromide on Nitrate Photolysis. *Environ. Chem. Lett.* **2009**, *7* (4), 337–342.

(87) Vione, D.; Sur, B.; Dutta, B. K.; Maurino, V.; Minero, C. On the Effect of 2-Propanol on Phenol Photonitration upon Nitrate Photolysis. *J. Photochem. Photobiol. Chem.* **2011**, *224* (1), 68–70.

(88) Chiron, S.; Barbati, S.; Khanra, S.; Dutta, B. K.; Minella, M.; Minero, C.; Maurino, V.; Pelizzetti, E.; Vione, D. Bicarbonate-Enhanced Transformation of Phenol upon Irradiation of Hematite, Nitrate, and Nitrite. *Photochem. Photobiol. Sci.* **2009**, *8* (1), 91–100.

(89) Loegager, T.; Sehested, K. Formation and Decay of Peroxynitrous Acid: A Pulse Radiolysis Study. *J. Phys. Chem.* **1993**, *97* (25), 6664–6669.

(90) Machado, F.; Boule, P. Photonitration and Photonitrosation of Phenolic Derivatives Induced in Aqueous Solution by Excitation of Nitrite and Nitrate Ions. *J. Photochem. Photobiol. Chem.* **1995**, *86* (1–3), 73–80.

(91) Dzengel, J.; Theurich, J.; Bahnemann, D. W. Formation of Nitroaromatic Compounds in Advanced Oxidation Processes: Photolysis versus Photocatalysis. *Environ. Sci. Technol.* **1998**, *33* (2), 294–300.

(92) Minero, C.; Bono, F.; Rubertelli, F.; Pavino, D.; Maurino, V.; Pelizzetti, E.; Vione, D. On the Effect of pH in Aromatic Photonitration upon Nitrate Photolysis. *Chemosphere* **2007**, *66* (4), 650–656.

(93) Zheng, A.; Dzombak, D. A.; Zheng, R. G. Effects of Nitrosation on the Formation of Cyanide in Publicly Owned Treatment Works Secondary Effluent. *Water Environ. Res.* **2004**, *76* (3), 197–204.

(94) Vione, D.; Maurino, V.; Minero, C.; Pelizzetti, E. Aqueous Atmospheric Chemistry: Formation of 2,4-Dinitrophenol upon Nitration of 2-Nitrophenol and 4-Nitrophenol in Solution. *Environ. Sci. Technol.* **2005**, *39* (20), 7921–7931.

(95) Arakaki, T.; Miyake, T.; Hirakawa, T.; Sakugawa, H. pH Dependent Photoformation of Hydroxyl Radical and Absorbance of Aqueous-Phase N(III) (HNO_2 and NO_2^-). *Environ. Sci. Technol.* **1999**, *33* (15), 2561–2565.

(96) Vione, D.; Maurino, V.; Minero, C.; Pelizzetti, E. Nitration and Photonitration of Naphthalene in Aqueous Systems. *Environ. Sci. Technol.* **2005**, *39* (4), 1101–1110.

(97) Carlos, L.; Fabbri, D.; Capparelli, A. L.; Prevot, A. B.; Pramauro, E.; Einschlag, F. S. G. Intermediate Distributions and Primary Yields of Phenolic Products in Nitrobenzene Degradation by Fenton's Reagent. *Chemosphere* **2008**, *72* (6), 952–958.

(98) Beitz, T.; Bechmann, W.; Mitzner, R. Investigation on the Photoreactions of Nitrate and Nitrite Ions with Selected Azaarenes in Water. *Chemosphere* **1999**, *38* (2), 351–361.

(99) Kwon, B. G.; Kwon, J.-H. Measurement of the Hydroxyl Radical Formation from H_2O_2, NO_3^-, and Fe(III) Using a Continuous Flow Injection Analysis. *J. Ind. Eng. Chem.* **2010**, *16* (2), 193–199.

(100) Buxton, G. V.; Greenstock, C. L.; Helman, W. P.; Ross, A. B. Critical Review of Rate Constants for Reactions of Hydrated Electrons, Hydrogen Atoms and Hydroxyl Radicals ($^\bullet OH/^\bullet O^-$ in Aqueous Solution. *J. Phys. Chem. Ref. Data* **1988**, *17* (2), 513–886.

(101) Li, C.; Gao, N.; Li, W. Photochemical Degradation of Typical Herbicides Simazine by UV/H_2O_2 in Aqueous Solution. *Desalination Water Treat.* **2011**, *36* (1-3), 197–202.

(102) Olmez-Hanci, T.; Arslan-Alaton, I.; Basar, G. Multivariate Analysis of Anionic, Cationic and Nonionic Textile Surfactant Degradation with the H_2O_2/UV-C Process by Using the Capabilities of Response Surface Methodology. *J. Hazard. Mater.* **2011**, *185* (1), 193–203.

(103) Vaghjiani, G. L.; Ravishankara, A. R. Photodissociation of H_2O_2 and CH_3OOH at 248 Nm and 298 K: Quantum Yields for OH, O(3P) and H(2S). *J. Chem. Phys.* **1990**, *92* (2), 996–1003.

(104) Olmez-Hanci, T.; Kabdaşlı, I.; Tünay, O.; Ecer, ç.; Aydın, B. A Statistical Experimental Design Approach for Mineralization and Detoxification of Diethyl Phthalate by H_2O_2 /UV-C Process. *Water Sci. Technol.* **2013**, *68* (4), 856.

(105) Braslavsky, S. E.; Braun, A. M.; Cassano, A. E.; Emeline, A. V.; Litter, M. I.; Palmisano, L.; Parmon, V. N.; Serpone, N. Glossary of Terms Used in Photocatalysis and Radiation Catalysis (IUPAC Recommendations 2011). *Pure Appl. Chem.* **2011**, *83* (4), 931–1014.

(106) Naumczyk, J.; Bogacki, J.; Marcinowski, P.; Kowalik, P. Cosmetic Wastewater Treatment by Coagulation and Advanced Oxidation Processes. *Environ. Technol.* **2014**, *35* (5), 541–548.

(107) Ayoub, K.; van Hullebusch, E. D.; Cassir, M.; Bermond, A. Application of Advanced Oxidation Processes for TNT Removal: A Review. *J. Hazard. Mater.* **2010**, *178* (1–3), 10–28.

(108) Vione, D.; Bagnus, D.; Maurino, V.; Minero, C. Quantification of Singlet Oxygen and Hydroxyl Radicals upon UV Irradiation of Surface Water. *Environ. Chem. Lett.* **2010**, *8* (2), 193–198.

(109) Pereira, M. C.; Oliveira, L. C. A.; Murad, E. Iron Oxide Catalysts: Fenton and Fenton-like Reactions - a Review. *Clay Miner.* **2012**, *47* (3), 285–302.

(110) Feng, Y.; Wu, D.; Ma, L. Iron Oxide Catalyzed Fenton-Like Reaction. *Prog. Chem.* **2013**, *25* (07), 1219–1228.

(111) Nidheesh, P. V.; Gandhimathi, R.; Ramesh, S. T. Degradation of Dyes from Aqueous Solution by Fenton Processes: A Review. *Environ. Sci. Pollut. Res.* **2013**, *20* (4), 2099–2132.

(112) Giri, A. S.; Golder, A. K. Ciprofloxacin Degradation from Aqueous Solution by Fenton Oxidation: Reaction Kinetics and Degradation Mechanisms. *RSC Adv.* **2014**, *4* (13), 6738–6745.

(113) Torrades, F.; García-Montaño, J. Using Central Composite Experimental Design to Optimize the Degradation of Real Dye Wastewater by Fenton and Photo-Fenton Reactions. *Dyes Pigments* **2014**, *100*, 184–189.

(114) Mitsika, E. E.; Christophoridis, C.; Fytianos, K. Fenton and Fenton-like Oxidation of Pesticide Acetamiprid in Water Samples: Kinetic Study of the Degradation and Optimization Using Response Surface Methodology. *Chemosphere* **2013**, *93* (9), 1818–1825.

(115) Zanta, C. L. P. S.; Friedrich, L. C.; Machulek Jr., A.; Higa, K. M.; Quina, F. H. Surfactant Degradation by a Catechol-Driven Fenton Reaction. *J. Hazard. Mater.* **2010**, *178* (1–3), 258–263.

(116) Gomis, J.; Bianco Prevot, A.; Montoneri, E.; González, M. C.; Amat, A. M.; Mártire, D. O.; Arques, A.; Carlos, L. Waste Sourced Bio-Based Substances for Solar-Driven Wastewater Remediation: Photodegradation of Emerging Pollutants. *Chem. Eng. J.* **2014**, *235*, 236–243.

(117) Zhao, J.; Yang, J.; Ma, J. Mn(II)-Enhanced Oxidation of Benzoic Acid by Fe(III)/H_2O_2 System. *Chem. Eng. J.* **2014**, *239*, 171–177.

(118) Bataineh, H.; Pestovsky, O.; Bakac, A. pH-Induced Mechanistic Changeover from Hydroxyl Radicals to iron(IV) in the Fenton Reaction. *Chem. Sci.* **2012**, *3* (5), 1594–1599.

(119) Minero, C.; Lucchiari, M.; Maurino, V.; Vione, D. A Quantitative Assessment of the Production of $^{\cdot}OH$ and Additional Oxidants in the Dark Fenton Reaction: Fenton Degradation of Aromatic Amines. *RSC Adv.* **2013**, *3* (48), 26443–26450.

(120) Vermilyea, A. W.; Voelker, B. M. Photo-Fenton Reaction at Near Neutral pH. *Environ. Sci. Technol.* **2009**, *43* (18), 6927–6933.

(121) Barbusiński, K. Fenton Reaction - Controversy Concerning the Chemistry. *Ecol Chem Eng S* **2009**, *16* (3), 347–358.

(122) Freinbichler, W.; Colivicchi, M. A.; Stefanini, C.; Bianchi, L.; Ballini, C.; Misini, B.; Weinberger, P.; Linert, W.; Varešlija, D.; Tipton, K. F.; et al. Highly Reactive Oxygen Species: Detection, Formation, and Possible Functions. *Cell. Mol. Life Sci.* **2011**, *68* (12), 2067–2079.

(123) Trovó, A. G.; Pupo Nogueira, R. F.; Agüera, A.; Fernandez-Alba, A. R.; Malato, S. Paracetamol Degradation Intermediates and Toxicity during Photo-Fenton Treatment Using Different Iron Species. *Water Res.* **2012**, *46* (16), 5374–5380.

(124) Wang, Z.; Song, W.; Ma, W.; Zhao, J. Environmental Photochemistry of Iron Complexes and Their Involvement in Environmental Chemical Processes. *Prog. Chem.* **2012**, *24*, 423–432.

(125) Durán, A.; Monteagudo, J. M.; Sanmartín, I.; Carrasco, A. Solar Photo-Fenton Mineralization of Antipyrine in Aqueous Solution. *J. Environ. Manage.* **2013**, *130*, 64–71.

(126) Nissenson, P.; Dabdub, D.; Das, R.; Maurino, V.; Minero, C.; Vione, D. Evidence of the Water-Cage Effect on the Photolysis of and $FeOH^{2+}$. Implications of This Effect and of H_2O_2 Surface Accumulation on Photochemistry at the Air–water Interface of Atmospheric Droplets. *Atmos. Environ.* **2010**, *44* (38), 4859–4866.

(127) Huang, W.; Brigante, M.; Wu, F.; Mousty, C.; Hanna, K.; Mailhot, G. Assessment of the Fe(III)–EDDS Complex in Fenton-Like Processes: From the Radical Formation to the Degradation of Bisphenol A. *Environ. Sci. Technol.* **2013**, *47* (4), 1952–1959.

(128) Li, J.; Mailhot, G.; Wu, F.; Deng, N. Photodegradation of E2 in the Presence of Natural Montmorillonite and the Iron Complexing Agent Ethylenediamine-N,N'-Disuccinic Acid. *Photochem. Photobiol. Sci. Off. J. Eur. Photochem. Assoc. Eur. Soc. Photobiol.* **2012**, *11* (12), 1880–1885.

(129) Weller, C.; Horn, S.; Herrmann, H. Photolysis of Fe(III) Carboxylato Complexes: Fe(II) Quantum Yields and Reaction Mechanisms. *J. Photochem. Photobiol. Chem.* **2013**, *268*, 24–36.

(130) Iurascu, B.; Siminiceanu, I.; Vione, D.; Vicente, M. A.; Gil, A. Phenol Degradation in Water through a Heterogeneous Photo-Fenton Process Catalyzed by Fe-Treated Laponite. *Water Res.* **2009**, *43* (5), 1313–1322.

(131) Nidheesh, P. V.; Gandhimathi, R. Trends in Electro-Fenton Process for Water and Wastewater Treatment: An Overview. *Desalination* **2012**, *299*, 1–15.

(132) Oonnittan, A.; E.T. Sillanpaa, M. Water Treatment by Electro-Fenton Process. *Curr. Org. Chem.* **2012**, *16* (18), 2060–2072.

(133) Sirés, I.; Brillas, E. Remediation of Water Pollution Caused by Pharmaceutical Residues Based on Electrochemical Separation and Degradation Technologies: A Review. *Environ. Int.* **2012**, *40*, 212–229.

(134) Isarain-Chávez, E.; Arias, C.; Cabot, P. L.; Centellas, F.; Rodríguez, R. M.; Garrido, J. A.; Brillas, E. Mineralization of the Drug B-Blocker Atenolol by Electro-Fenton and Photoelectro-Fenton Using an Air-Diffusion Cathode for H_2O_2 Electrogeneration Combined with a Carbon-Felt Cathode for Fe^{2+} Regeneration. *Appl. Catal. B Environ.* **2010**, *96* (3–4), 361–369.

(135) Feng, L.; van Hullebusch, E. D.; Rodrigo, M. A.; Esposito, G.; Oturan, M. A. Removal of Residual Anti-Inflammatory and Analgesic Pharmaceuticals from Aqueous Systems by Electrochemical Advanced Oxidation Processes. A Review. *Chem. Eng. J.* **2013**, *228*, 944–964.

(136) Loaiza-Ambuludi, S.; Panizza, M.; Oturan, N.; Özcan, A.; Oturan, M. A. Electro-Fenton Degradation of Anti-Inflammatory Drug Ibuprofen in Hydroorganic Medium. *J. Electroanal. Chem.* **2013**, *702*, 31–36.

(137) Martínez, S. S.; Bahena, C. L. Chlorbromuron Urea Herbicide Removal by Electro-Fenton Reaction in Aqueous Effluents. *Water Res.* **2009**, *43* (1), 33–40.

(138) Nachiappan, S.; Muthukumar, K. Intensification of Textile Effluent Chemical Oxygen Demand Reduction by Innovative Hybrid Methods. *Chem. Eng. J.* **2010**, *163* (3), 344–354.

(139) Eren, Z. Ultrasound as a Basic and Auxiliary Process for Dye Remediation: A Review. *J. Environ. Manage.* **2012**, *104*, 127–141.

(140) Özdemir, C.; Öden, M. K.; Şahinkaya, S.; Kalipçi, E. Color Removal from Synthetic Textile Wastewater by Sono-Fenton Process. *CLEAN – Soil Air Water* **2011**, *39* (1), 60–67.

(141) Bhasarkar, J. B.; Chakma, S.; Moholkar, V. S. Mechanistic Features of Oxidative Desulfurization Using Sono-Fenton–Peracetic Acid (Ultrasound/Fe^{2+}–CH_3COOH–H_2O_2) System. *Ind. Eng. Chem. Res.* **2013**, *52* (26), 9038–9047.

(142) Le, C.; Liang, J.; Wu, J.; Li, P.; Wang, X.; Zhu, N.; Wu, P.; Yang, B. Effective Degradation of *para* -Chloronitrobenzene through a Sequential Treatment Using Zero-Valent Iron Reduction and Fenton Oxidation. *Water Sci. Technol.* **2011**, *64* (10), 2126.

(143) Ruhl, A. S.; Ünal, N.; Jekel, M. Evaluation of Two-Component Fe(0) Fixed Bed Filters with Porous Materials for Reductive Dechlorination. *Chem. Eng. J.* **2012**, *209*, 401–406.

(144) Raychoudhury, T.; Scheytt, T. Potential of Zerovalent Iron Nanoparticles for Remediation of Environmental Organic Contaminants in Water: A Review. *Water Sci. Technol.* **2013**, *68* (7), 1425.

(145) Segura, Y.; Martínez, F.; Melero, J. A. Effective Pharmaceutical Wastewater Degradation by Fenton Oxidation with Zero-Valent Iron. *Appl. Catal. B Environ.* **2013**, *136–137*, 64–69.

(146) Cao, M.; Wang, L.; Wang, L.; Chen, J.; Lu, X. Remediation of DDTs Contaminated Soil in a Novel Fenton-like System with Zero-Valent Iron. *Chemosphere* **2013**, *90* (8), 2303–2308.

(147) Kang, S.-H.; Choi, W. Oxidative Degradation of Organic Compounds Using Zero-Valent Iron in the Presence of Natural Organic Matter Serving as an Electron Shuttle. *Environ. Sci. Technol.* **2008**, *43* (3), 878–883.

(148) Shimizu, A.; Tokumura, M.; Nakajima, K.; Kawase, Y. Phenol Removal Using Zero-Valent Iron Powder in the Presence of Dissolved Oxygen: Roles of Decomposition by the Fenton Reaction and Adsorption/precipitation. *J. Hazard. Mater.* **2012**, *201–202*, 60–67.

(149) Kuo, J.; Chan, T.-F. Disinfection and Antimicrobial Processes. *Water Environ. Res.* **2012**, *84* (10), 1286–1309.

(150) Deborde, M.; von Gunten, U. Reactions of Chlorine with Inorganic and Organic Compounds during Water treatment—Kinetics and Mechanisms: A Critical Review. *Water Res.* **2008**, *42* (1–2), 13–51.

(151) Heeb, M. B.; Criquet, J.; Zimmermann-Steffens, S. G.; von Gunten, U. Oxidative Treatment of Bromide-Containing Waters: Formation of Bromine and Its Reactions with Inorganic and Organic Compounds--a Critical Review. *Water Res.* **2014**, *48*, 15–42.

(152) Krasner, S. W.; Mitch, W. A.; McCurry, D. L.; Hanigan, D.; Westerhoff, P. Formation, Precursors, Control, and Occurrence of Nitrosamines in Drinking Water: A Review. *Water Res.* **2013**, *47* (13), 4433–4450.

(153) Geering, F. Ozone Applications The State-of-the-Art in Switzerland. *Ozone Sci. Eng.* **1999**, *21* (2), 187–200.

(154) Long, B. W.; Hulsey, R. A.; Hoehn, R. C. Complementary Uses of Chlorine Dioxide and Ozone for Drinking Water Treatment. *Ozone Sci. Eng.* **1999**, *21* (5), 465–476.

(155) Gerrity, D.; Snyder, S. Review of Ozone for Water Reuse Applications: Toxicity, Regulations, and Trace Organic Contaminant Oxidation. *Ozone Sci. Eng.* **2011**, *33* (4), 253–266.

(156) Sharma, V. K. Oxidative Transformations of Environmental Pharmaceuticals by Cl_2, ClO_2, O_3, and Fe(VI): Kinetics Assessment. *Chemosphere* **2008**, *73* (9), 1379–1386.

(157) Wang, J. L.; Xu, L. J. Advanced Oxidation Processes for Wastewater Treatment: Formation of Hydroxyl Radical and Application. *Crit. Rev. Environ. Sci. Technol.* **2012**, *42* (3), 251–325.

(158) Gardoni, D.; Vailati, A.; Canziani, R. Decay of Ozone in Water: A Review. *Ozone Sci. Eng.* **2012**, *34* (4), 233–242.

(159) Barndõk, H.; Hermosilla, D.; Cortijo, L.; Negro, C.; Blanco, Á. Assessing the Effect of Inorganic Anions on TiO_2-Photocatalysis and Ozone Oxidation Treatment Efficiencies. *J. Adv. Oxid. Technol.* **2012**, *15* (1), 125–132.

(160) Umar, M.; Roddick, F.; Fan, L.; Aziz, H. A. Application of Ozone for the Removal of Bisphenol A from Water and Wastewater – A Review. *Chemosphere* **2013**, *90* (8), 2197–2207.

(161) Rosal, R.; Rodríguez, A.; Perdigón-Melón, J. A.; Petre, A.; García-Calvo, E. Oxidation of Dissolved Organic Matter in the Effluent of a Sewage Treatment Plant Using Ozone Combined with Hydrogen Peroxide (O_3/H_2O_2). *Chem. Eng. J.* **2009**, *149* (1–3), 311–318.

(162) Von Gunten, U.; Salhi, E.; Schmidt, C. K.; Arnold, W. A. Kinetics and Mechanisms of N-Nitrosodimethylamine Formation upon Ozonation of N,N-Dimethylsulfamide-Containing Waters: Bromide Catalysis. *Environ. Sci. Technol.* **2010**, *44* (15), 5762–5768.

(163) Khan, M. H.; Jung, H.-S.; Lee, W.; Jung, J.-Y. Chlortetracycline Degradation by Photocatalytic Ozonation in the Aqueous Phase: Mineralization and the Effects on Biodegradability. *Environ. Technol.* **2013**, *34* (1-4), 495–502.

(164) Von Sonntag, C. Advanced Oxidation Processes: Mechanistic Aspects. *Water Sci. Technol.* **2008**, *58* (5), 1015.

(165) Azbar, N.; Yonar, T.; Kestioglu, K. Comparison of Various Advanced Oxidation Processes and Chemical Treatment Methods for COD and Color Removal from a Polyester and Acetate Fiber Dyeing Effluent. *Chemosphere* **2004**, *55* (1), 35–43.

(166) Bremner, D. H.; Burgess, A. E.; Chand, R. The Chemistry of Ultrasonic Degradation of Organic Compounds. *Curr. Org. Chem.* **2011**, 168.

(167) Mahamuni, N. N.; Adewuyi, Y. G. Advanced Oxidation Processes (AOPs) Involving Ultrasound for Waste Water Treatment: A Review with Emphasis on Cost Estimation. *Ultrason. Sonochem.* **2010**, *17* (6), 990–1003.

(168) González-García, J.; Sáez, V.; Tudela, I.; Díez-Garcia, M. I.; Deseada Esclapez, M.; Louisnard, O. Sonochemical Treatment of Water Polluted by Chlorinated Organocompounds. A Review. *Water* **2010**, *2* (1), 28–74.

(169) Moumeni, O.; Hamdaoui, O.; Pétrier, C. Sonochemical Degradation of Malachite Green in Water. *Chem. Eng. Process. Process Intensif.* **2012**, *62*, 47–53.

(170) Merouani, S.; Hamdaoui, O.; Saoudi, F.; Chiha, M.; Pétrier, C. Influence of Bicarbonate and Carbonate Ions on Sonochemical Degradation of Rhodamine B in Aqueous Phase. *J. Hazard. Mater.* **2010**, *175* (1–3), 593–599.

(171) Adewuyi, Y. G. Sonochemistry in Environmental Remediation. 1. Combinative and Hybrid Sonophotochemical Oxidation Processes for the Treatment of Pollutants in Water. *Environ. Sci. Technol.* **2005**, *39* (10), 3409–3420.

(172) Singla, R.; Grieser, F.; Ashokkumar, M. The Mechanism of Sonochemical Degradation of a Cationic Surfactant in Aqueous Solution. *Ultrason. Sonochem.* **2011**, *18* (2), 484–488.

(173) Kumar, P.; Khanna, S.; Moholkar, V. S. Flow Regime Maps and Optimization Thereby of Hydrodynamic Cavitation Reactors. *AIChE J.* **2012**, *58* (12), 3858–3866.

(174) Gogate, P. R.; Bhosale, G. S. Comparison of Effectiveness of Acoustic and Hydrodynamic Cavitation in Combined Treatment Schemes for Degradation of Dye Wastewaters. *Chem. Eng. Process. Process Intensif.* **2013**, *71*, 59–69.

(175) Minero, C.; Pellizzari, P.; Maurino, V.; Pelizzetti, E.; Vione, D. Enhancement of Dye Sonochemical Degradation by Some Inorganic Anions Present in Natural Waters. *Appl. Catal. B Environ.* **2008**, *77* (3–4), 308–316.

(176) De Laurentiis, E.; Minella, M.; Maurino, V.; Minero, C.; Mailhot, G.; Sarakha, M.; Brigante, M.; Vione, D. Assessing the Occurrence of the Dibromide Radical (Br_2^-) in Natural Waters: Measures of Triplet-Sensitised Formation, Reactivity, and Modelling. *Sci. Total Environ.* **2012**, *439*, 299–306.

(177) Saraswathy, P.; Sunanda, K.; Aparna, S.; Raja Sekhar, B. N. Photoabsorption Spectra of Ammonia in 1050 to 2250 Å Region. *Spectrosc. Lett.* **2010**, *43* (4), 290–297.

(178) Salvermoser, M.; Murnick, D. E.; Kogelschatz, U. Influence of Water Vapor on Photochemical Ozone Generation with Efficient 172 Nm Xenon Excimer Lamps. *Ozone Sci. Eng.* **2008**, *30* (3), 228–237.

(179) Duca, C.; Imoberdorf, G.; Mohseni, M. Novel Collimated Beam Setup to Study the Kinetics of VUV-Induced Reactions. *Photochem. Photobiol.* **2014**, *90* (1), 238–240.

(180) Ung, A.-M.; Back, R. The Photolysis of Water Vapor and Reactions of Hydroxyl Radicals. *Can. J. Chem.* **1964**, *42* (4), 753–763.

(181) Dainton, F.; Fowles, P. The Photolysis of Aqueous Systems at 1849 Å. I. Solutions Containing Nitrous Oxide. *Proc. R. Soc. Lond. Ser. Math. Phys. Sci.* **1965**, *287* (1410), 295–311.

(182) Black, G.; Porter, G. Vacuum Ultra-Violet Flash Photolysis of Water Vapour. *Proc. R. Soc. Lond. Ser. Math. Phys. Sci.* **1962**, *266* (1325), 185–197.

(183) Baxendale, J. The Flash Photolysis of Water and Aqueous Solutions. *Radiat. Res.* **1962**, *17* (3), 312–326.

(184) Porter, G. Flash Photolysis and Spectroscopy. A New Method for the Study of Free Radical Reactions. *Proc. R. Soc. Lond. Ser. Math. Phys. Sci.* **1950**, *200* (1061), 284–300.

(185) McGrath, W. D.; Norrish, R. G. W. The Flash Photolysis of Ozone. *Proc. R. Soc. Lond. Ser. Math. Phys. Sci.* **1957**, *242* (1230), 265–276.

(186) McGrath, W.; Norrish, R. Studies of the Reactions of Excited Oxygen Atoms and Molecules Produced in the Flash Photolysis of Ozone. *Proc. R. Soc. Lond. Ser. Math. Phys. Sci.* **1960**, *254* (1278), 317–326.

(187) Birch, D.; Imhof, R. Coaxial Nanosecond Flashlamp. *Rev. Sci. Instrum.* **1981**, *52* (8), 1206–1212.

(188) Matafonova, G.; Batoev, V. Recent Progress on Application of UV Excilamps for Degradation of Organic Pollutants and Microbial Inactivation. *Chemosphere* **2012**, *89* (6), 637–647.

(189) Oppenländer, T. Mercury-Free Sources of VUV/UV Radiation: Application of Modern Excimer Lamps (excilamps) for Water and Air Treatment. *J. Environ. Eng. Sci.* **2007**, *6* (3), 253–264.

(190) Tarasenko, V.; Avdeev, S.; M. Erofeev; M. Lomaev; Sosnin, E.; Skakun, V.; Shitz, D. High Power UV and VUV Excilamps and Their Applications. *ACTA Phys. Pol. A* **2009**, *116* (4), 576–578.

(191) Robl, S.; Wörner, M.; Maier, D.; Braun, A. M. Formation of Hydrogen Peroxide by VUV-Photolysis of Water and Aqueous Solutions with Methanol. *Photochem. Photobiol. Sci.* **2012**, *11* (6), 1041–1050.

(192) Tarasov, V. V.; Barancova, G. S.; Zaitsev, N. K.; Dongxiang, Z. Photochemical Kinetics of Organic Dye Oxidation in Water. *Process Saf. Environ. Prot.* **2003**, *81* (4), 243–249.

(193) Horikoshi, S.; Tsuchida, A.; Sakai, H.; Abe, M.; Serpone, N. Microwave Discharge Electrodeless Lamps (MDELs). VI. Performance Evaluation of a Novel Microwave Discharge Granulated Electrodeless Lamp (MDGEL)—Photoassisted Defluorination of Perfluoroalkoxy Acids in Aqueous Media. *J. Photochem. Photobiol. Chem.* **2011**, *222* (1), 97–104.

(194) Nieuwenhuijsen, M. J.; Martinez, D.; Grellier, J.; Bennett, J.; Best, N.; Iszatt, N.; Vrijheid, M.; Toledano, M. Chlorination Disinfection By-Products in Drinking Water and Congenital Anomalies: Review and Meta-Analyses. *Environ. Health Perspect.* **2009**, *117* (10), 1486–1493.

(195) Von Sonntag, C. The Basics of Oxidants in Water Treatment. Part A: OH Radical Reactions. *Water Sci. Technol.* **2007**, *55* (12), 19–23.

(196) Ikehata, K.; Gamal El-Din, M. Aqueous Pesticide Degradation by Ozonation and Ozone-Based Advanced Oxidation Processes: A Review (Part II). *Ozone Sci. Eng.* **2005**, *27* (3), 173–202.

(197) Carra, I.; García Sánchez, J. L.; Casas López, J. L.; Malato, S.; Sánchez Pérez, J. A. Phenomenological Study and Application of the Combined Influence of Iron Concentration and Irradiance on the Photo-Fenton Process to Remove Micropollutants. *Sci. Total Environ.* **2014**, *478*, 123–132.

(198) Miralles-Cuevas, S.; Oller, I.; Ruiz Aguirre, A.; Sánchez Pérez, J. A.; Malato Rodríguez, S. Removal of Pharmaceuticals at μg L^{-1} by Combined Nanofiltration and Mild Solar Photo-Fenton. *Chem. Eng. J.* **2014**, *239*, 68–74.

(199) Ortega-Gómez, E.; Ballesteros Martín, M. M.; Esteban García, B.; Sánchez Pérez, J. A.; Fernández Ibáñez, P. Solar Photo-Fenton for Water Disinfection: An Investigation of the Competitive Role of Model Organic Matter for Oxidative Species. *Appl. Catal. B Environ.* **2014**, *148–149*, 484–489.

(200) McGuigan, K. G.; Conroy, R. M.; Mosler, H.-J.; Preez, M. du; Ubomba-Jaswa, E.; Fernandez-Ibañez, P. Solar Water Disinfection (SODIS): A Review from Bench-Top to Roof-Top. *J. Hazard. Mater.* **2012**, *235–236*, 29–46.

(201) Ndounla, J.; Spuhler, D.; Kenfack, S.; Wéthé, J.; Pulgarin, C. Inactivation by Solar Photo-Fenton in Pet Bottles of Wild Enteric Bacteria of Natural Well Water: Absence of Re-Growth after One Week of Subsequent Storage. *Appl. Catal. B Environ.* **2013**, *129*, 309–317.

(202) Sciacca, F.; Rengifo-Herrera, J. A.; Wéthé, J.; Pulgarin, C. Dramatic Enhancement of Solar Disinfection (SODIS) of Wild Salmonella Sp. in PET Bottles by H_2O_2 Addition on Natural Water of Burkina Faso Containing Dissolved Iron. *Chemosphere* **2010**, *78* (9), 1186–1191.

(203) Ochiai, T.; Fujishima, A. Photoelectrochemical Properties of TiO_2 Photocatalyst and Its Applications for Environmental Purification. *J. Photochem. Photobiol. C Photochem. Rev.* **2012**, *13* (4), 247–262.

(204) Pelaez, M.; Nolan, N. T.; Pillai, S. C.; Seery, M. K.; Falaras, P.; Kontos, A. G.; Dunlop, P. S. M.; Hamilton, J. W. J.; Byrne, J. A.; O'Shea, K.; et al. A Review on the Visible Light Active Titanium Dioxide Photocatalysts for Environmental Applications. *Appl. Catal. B Environ.* **2012**, *125*, 331–349.

(205) Salvador, P. On the Nature of Photogenerated Radical Species Active in the Oxidative Degradation of Dissolved Pollutants with TiO_2 Aqueous Suspensions: A Revision in the Light of the Electronic Structure of Adsorbed Water. *J. Phys. Chem. C* **2007**, *111* (45), 17038–17043.

(206) Du, Y.; Rabani, J. The Measure of TiO_2 Photocatalytic Efficiency and the Comparison of Different Photocatalytic Titania. *J. Phys. Chem. B* **2003**, *107* (43), 11970–11978.

(207) Zhang, L.; Mohamed, H. H.; Dillert, R.; Bahnemann, D. Kinetics and Mechanisms of Charge Transfer Processes in Photocatalytic Systems: A Review. *J. Photochem. Photobiol. C Photochem. Rev.* **2012**, *13* (4), 263–276.

(208) Sun, H.; Wang, S.; Ang, H. M.; Tadé, M. O.; Li, Q. Halogen Element Modified Titanium Dioxide for Visible Light Photocatalysis. *Chem. Eng. J.* **2010**, *162* (2), 437–447.

(209) Imoberdorf, G.; Mohseni, M. Degradation of Natural Organic Matter in Surface Water Using Vacuum-UV Irradiation. *J. Hazard. Mater.* **2011**, *186* (1), 240–246.

(210) Augugliaro, V.; Litter, M.; Palmisano, L.; Soria, J. The Combination of Heterogeneous Photocatalysis with Chemical and Physical Operations: A Tool for Improving the Photoprocess Performance. *J. Photochem. Photobiol. C Photochem. Rev.* **2006**, *7* (4), 127–144.

(211) Joseph, C. G.; Li Puma, G.; Bono, A.; Krishnaiah, D. Sonophotocatalysis in Advanced Oxidation Process: A Short Review. *Ultrason. Sonochem.* **2009**, *16* (5), 583–589.

(212) Zoschke, K.; Börnick, H.; Worch, E. Vacuum-UV Radiation at 185 nm in Water Treatment – A Review. *Water Res.* **2014**, *52*, 131–145.

(213) Paulson, S. E.; Flagan, R. C.; Seinfeld, J. H. Atmospheric Photooxidation of Isoprene Part II: The Ozone-Isoprene Reaction. *Int. J. Chem. Kinet.* **1992**, *24* (1), 103–125.

(214) Paulson, S. E.; Seinfeld, J. Atmospheric Photochemical Oxidation of 1-Octene: OH, O_3, and O(3P) Reactions. *Environ. Sci. Technol.* **1992**, *26* (6), 1165–1173.

(215) Atkinson, R.; Aschmann, S. M.; Arey, J.; Shorees, B. Formation of OH Radicals in the Gas Phase Reactions of O_3 with a Series of Terpenes. *J. Geophys. Res. Atmospheres* **1992**, *97* (D5), 6065–6073.

(216) Atkinson, R.; Tuazon, E. C.; Aschmann, S. M. Products of the Gas-Phase Reactions of O_3 with Alkenes. *Environ. Sci. Technol.* **1995**, *29* (7), 1860–1866.

(217) Hard, T. M.; George, L. A.; O'Brien, R. J. An Absolute Calibration for Gas-Phase Hydroxyl Measurements. *Environ. Sci. Technol.* **2002**, *36* (8), 1783–1790.

(218) Atkinson, R.; Baulch, D. L.; Cox, R. A.; Crowley, J. N.; Hampson, R. F.; Hynes, R. G.; Jenkin, M. E.; Rossi, M. J.; Troe, J. Evaluated Kinetic and Photochemical Data for Atmospheric Chemistry: Volume I - Gas Phase Reactions of O_x, HO_x, NO_x and SO_x Species. *Atmos Chem Phys* **2004**, *4* (6), 1461–1738.

(219) Atkinson, R.; Aschmann, S. M. Hydroxyl Radical Production from the Gas-Phase Reactions of Ozone with a Series of Alkenes under Atmospheric Conditions. *Environ. Sci. Technol.* **1993**, *27* (7), 1357–1363.

(220) Carr, S. A.; Glowacki, D. R.; Liang, C.-H.; Baeza-Romero, M. T.; Blitz, M. A.; Pilling, M. J.; Seakins, P. W. Experimental and Modeling Studies of the Pressure and Temperature Dependences of the Kinetics and the OH Yields in the Acetyl + O_2 Reaction. *J. Phys. Chem. A* **2011**, *115* (6), 1069–1085.

(221) Rohrer, F.; Bohn, B.; Brauers, T.; Brüning, D.; Johnen, F.-J.; Wahner, A.; Kleffmann, J. Characterisation of the Photolytic HONO-Source in the Atmosphere Simulation Chamber SAPHIR. *Atmos Chem Phys* **2005**, *5* (8), 2189–2201.

(222) Rohrer, F.; Bohn, B.; Brauers, T.; Brüning, D.; Johnen, F.-J.; Wahner, A.; Kleffmann, J. Characterisation of the Photolytic HONO-Source in the Atmosphere Simulation Chamber SAPHIR. *Atmos Chem Phys* **2005**, *5* (8), 2189–2201.

(223) Sakamaki, F.; Akimoto, H. HONO Formation as Unknown Radical Source in Photochemical Smog Chamber. *Int. J. Chem. Kinet.* **1988**, *20* (2), 111–116.

(224) Glasson, W. A.; Dunker, A. M. Investigation of Background Radical Sources in a Teflon-Film Irradiation Chamber. *Environ. Sci. Technol.* **1989**, *23* (8), 970–978.

(225) Killus, J. P.; Whitten, G. Z. Background Reactivity in Smog Chambers. *Int. J. Chem. Kinet.* **1990**, *22* (6), 547–575.

(226) Akimoto, H.; Takagi, H.; Sakamaki, F. Photoenhancement of the Nitrous Acid Formation in the Surface Reaction of Nitrogen Dioxide and Water Vapor: Extra Radical Source in Smog Chamber Experiments. *Int. J. Chem. Kinet.* **1987**, *19* (6), 539–551.

(227) Carter, W. P. L.; Atkinson, R.; Winer, A. M.; Pitts, J. N. Evidence for Chamber-Dependent Radical Sources: Impact on Kinetic Computer Models for Air Pollution. *Int. J. Chem. Kinet.* **1981**, *13* (8), 735–740.

(228) Carter, W. P. L.; Atkinson, R.; Winer, A. M.; Pitts, J. N. Experimental Investigation of Chamber-Dependent Radical Sources. *Int. J. Chem. Kinet.* **1982**, *14* (10), 1071–1103.

(229) Finlayson-Pitts, B. J.; Wingen, L. M.; Sumner, A. L.; Syomin, D.; Ramazan, K. A. The Heterogeneous Hydrolysis of NO2 in Laboratory Systems and in Outdoor and Indoor Atmospheres: An Integrated Mechanism. *Phys. Chem. Chem. Phys.* **2003**, *5* (2), 223–242.

(230) Svensson, R.; Ljungström, E.; Lindqvist, O. Kinetics of the Reaction between Nitrogen Dioxide and Water Vapour. *Atmospheric Environ. 1967* **1987**, *21* (7), 1529–1539.

(231) Kleffmann, J.; Becker, K. H.; Wiesen, P. Heterogeneous NO_2 Conversion Processes on Acid Surfaces: Possible Atmospheric Implications. *Atmos. Environ.* **1998**, *32* (16), 2721–2729.

(232) Pitts, J. N.; Sanhueza, E.; Atkinson, R.; Carter, W. P. L.; Winer, A. M.; Harris, G. W.; Plum, C. N. An Investigation of the Dark Formation of Nitrous Acid in Environmental Chambers. *Int. J. Chem. Kinet.* **1984**, *16* (7), 919–939.

(233) William H. Glaze; Kang, J.-W. Advanced Oxidation Processes for Treating Groundwater Contaminated With TCE and PCE: Laboratory Studies (PDF). *J. Am. Water Works Assoc.* **1988**, *80* (5), 57–63.

(234) Eisele, F. L.; Tanner, D. J. Ion-Assisted Tropospheric OH Measurements. *J. Geophys. Res. Atmospheres* **1991**, *96* (D5), 9295–9308.

(235) Kukui, A.; Ancellet, G.; Bras, G. L. Chemical Ionisation Mass Spectrometer for Measurements of OH and Peroxy Radical Concentrations in Moderately Polluted Atmospheres. *J. Atmospheric Chem.* **2009**, *61* (2), 133–154.

(236) Kukui, A.; Legrand, M. R.; Ancellet, G.; Gros, V.; Bekki, S.; Sarda-Estève, R.; Loisil, R.; Preunkert, S. Measurements of OH and RO_2 Radicals at the Coastal Antarctic Site of Dumont d'Urville (East Antarctica) in Summer 2010-2011. *J. Geophys. Res. Atmospheres* **2012**, *117*, D12310.

(237) Vaghjiani, G. L.; Ravishankara, A. R. New Measurement of the Rate Coefficient for the Reaction of OH with Methane. *Nature* **1991**, *350* (6317), 406–409.

(238) Wollenhaupt, M.; Carl, S. A.; Horowitz, A.; Crowley, J. N. Rate Coefficients for Reaction of OH with Acetone between 202 and 395 K. *J. Phys. Chem. A* **2000**, *104* (12), 2695–2705.

(239) Talukdar, R.; Mellouki, A.; Gierczak, T.; Burkholder, J. B.; McKeen, S. A.; Ravishankara, A. R. Atmospheric Fate of Difluoromethane, 1,1,1-Trifloroethane, Pentafluoroethane, and 1,1-Dichloro-1-Fluoroethane: Rate Coefficients for Reactions with Hydroxyl and UV Absorption Cross Sections of 1,1-Dichloro-1-Fluoroethane. *J. Phys. Chem.* **1991**, *95* (15), 5815–5821.

(240) Herrmann, H. Kinetics of Aqueous Phase Reactions Relevant for Atmospheric Chemistry. *Chem. Rev.* **2003**, *103* (12), 4691–4716.

(241) Atherton, N. M. *Electron Spin Resonance*; Wiley: New York, 1973.

(242) Weil, J. A.; Bolton, J. R. *Electron Paramagnetic Resonance: Elementary Theory and Practical Applications*; John Wiley & Sons, 2007.

(243) Perkins, M. J. Spin Trapping. In *Advances in Physical Organic Chemistry*; Bethell, V. G. and D., Ed.; Academic Press, 1981; Vol. 17, pp 1–64.

(244) Tordo, P. Spin-Trapping: Recent Developments and Applications. In *Electron Paramagnetic Resonance*; Specialist Periodical Reports; The Royal Society of Chemistry, 1998; Vol. 16, pp 116–144.

(245) Clément, J.-L.; Tordo, P. Advances in Spin Trapping. In *Electron Paramagnetic Resonance*; The Royal Society of Chemistry: Cambridge, UK, 2007; Vol. 20, pp 29–49.

(246) Goldstein, S.; Rosen, G. M.; Russo, A.; Samuni, A. Kinetics of Spin Trapping Superoxide, Hydroxyl, and Aliphatic Radicals by Cyclic Nitrones. *J. Phys. Chem. A* **2004**, *108* (32), 6679–6685.

(247) Villamena, F. A.; Hadad, C. M.; Zweier, J. L. Kinetic Study and Theoretical Analysis of Hydroxyl Radical Trapping and Spin Adduct Decay of Alkoxycarbonyl and Dialkoxyphosphoryl Nitrones in Aqueous Media. *J. Phys. Chem. A* **2003**, *107* (22), 4407–4414.

(248) Li, L.; Abe, Y.; Mashino, T.; Mochizuki, M.; Miyata, N. Signal Enhancement in ESR Spin-Trapping for Hydroxyl Radicals. *Anal. Sci.* **2003**, *19* (7), 1083–1084.

(249) Contreras, D.; Rodríguez, J.; Freer, J.; Schwederski, B.; Kaim, W. Enhanced Hydroxyl Radical Production by Dihydroxybenzene-Driven Fenton Reactions: Implications for Wood Biodegradation. *JBIC J. Biol. Inorg. Chem.* **2007**, *12* (7), 1055–1061.

(250) Buettner, G. R. Spin Trapping: ESR Parameters of Spin Adducts 1474 1528V. *Free Radic. Biol. Med.* **1987**, *3* (4), 259–303.

(251) Eberson, L. Inverted Spin Trapping. Part III. Further Studies on the Chemical and Photochemical Oxidation of Spin Traps in the Presence of Nucleophiles. *J. Chem. Soc. Perkin Trans. 2* **1994**, No. 2, 171–176.

(252) Chignell, C. F.; Motten, A. G.; Sik, R. H.; Parker, C. E.; Reszka, K. A Spin Trapping Study of the Photochemistry of 5,5-Dimethyl-1-Pyrroline N-Oxide (DMPO). *Photochem. Photobiol.* **1994**, *59* (1), 5–11.

(253) Finkelstein, E.; Rosen, G. M.; Rauckman, E. J. Spin Trapping of Superoxide and Hydroxyl Radical: Practical Aspects. *Arch. Biochem. Biophys.* **1980**, *200* (1), 1–16.

(254) Jaeger, C. D.; Bard, A. J. Spin Trapping and Electron Spin Resonance Detection of Radical Intermediates in the Photodecomposition of Water at Titanium Dioxide Particulate Systems. *J. Phys. Chem.* **1979**, *83* (24), 3146–3152.

(255) Kochany, J.; Bolton, J. R. Mechanism of Photodegradation of Aqueous Organic Pollutants. 1. EPR Spin-Trapping Technique for the Determination of Hydroxyl Radical Rate Constants in the Photooxidation of Chlorophenols Following the Photolysis of Hydrogen Peroxide. *J. Phys. Chem.* **1991**, *95* (13), 5116–5120.

(256) Brezova, V.; Stasko, A.; Biskupic, S.; Blazkova, A.; Havlinova, B. Kinetics of Hydroxyl Radical Spin Trapping in Photoactivated Homogeneous (H_2O_2) and Heterogeneous (TiO_2, O_2) Aqueous Systems. *J. Phys. Chem.* **1994**, *98* (36), 8977–8984.

(257) Zalomaeva, O. V.; Trukhan, N. N.; Ivanchikova, I. D.; Panchenko, A. A.; Roduner, E.; Talsi, E. P.; Sorokin, A. B.; Rogov, V. A.; Kholdeeva, O. A. EPR Study on the Mechanism of H_2O_2-Based Oxidation of Alkylphenols over Titanium Single-Site Catalysts. *J. Mol. Catal. Chem.* **2007**, *277* (1–2), 185–192.

(258) Brezova, V.; Stasko, A. Spin Trap Study of Hydroxyl Radicals Formed in the Photocatalytic System TiO_2-Water-P-Cresol-Oxygen. *J. Catal.* **1994**, *147* (1), 156–162.

(259) Lloyd, R. V.; Hanna, P. M.; Mason, R. P. The Origin of the Hydroxyl Radical Oxygen in the Fenton Reaction. *Free Radic. Biol. Med.* **1997**, *22* (5), 885–888.

(260) Bachir, S.; Barbati, S.; Ambrosio, M.; Tordo, P. Kinetics and Mechanism of Wet-Air Oxidation of Nuclear-Fuel-Chelating Compounds. *Ind. Eng. Chem. Res.* **2001**, *40* (8), 1798–1804.

(261) Robert, R.; Barbati, S.; Ricq, N.; Ambrosio, M. Intermediates in Wet Oxidation of Cellulose: Identification of Hydroxyl Radical and Characterization of Hydrogen Peroxide. *Water Res.* **2002**, *36* (19), 4821–4829.

(262) Floyd, R. A.; Watson, J. J.; Wong, P. K. Sensitive Assay of Hydroxyl Free Radical Formation Utilizing High Pressure Liquid Chromatography with Electrochemical Detection of Phenol and Salicylate Hydroxylation Products. *J. Biochem. Biophys. Methods* **1984**, *10* (3–4), 221–235.

(263) Coudray, C.; Talla, M.; Martin, S.; Fatome, M.; Favier, A. High-Performance Liquid Chromatography-Electrochemical Determination of Salicylate Hydroxylation Products as an in Vivo Marker of Oxidative Stress. *Anal. Biochem.* **1995**, *227* (1), 101–111.

(264) Ai, S.; Wang, Q.; Li, H.; Jin, L. Study on Production of Free Hydroxyl Radical and Its Reaction with Salicylic Acid at Lead Dioxide Electrode. *J. Electroanal. Chem.* **2005**, *578* (2), 223–229.

(265) Cheng, H.; Cao, Y. Determination of Hydroxyl Radical in $CuSO_4$-Vitamin C Reaction System Using Capillary Electrophoresis with Electrochemical Detection and Its Application in the Determination of the Scavenging Activities of Chrysanthemum. *Chin. J. Chromatogr.* **2007**, *25* (5), 681–685.

(266) Wang, Q.; Ding, F.; Zhu, N.; Li, H.; He, P.; Fang, Y. Determination of Hydroxyl Radical by Capillary Zone Electrophoresis with Amperometric Detection. *J. Chromatogr. A* **2003**, *1016* (1), 123–128.

(267) Coolen, S. A. J.; Huf, F. A.; Reijenga, J. C. Determination of Free Radical Reaction Products and Metabolites of Salicylic Acid Using Capillary Electrophoresis and Micellar Electrokinetic Chromatography. *J. Chromatogr. B. Biomed. Sci. App.* **1998**, *717* (1–2), 119–124.

(268) Stein, G.; Weiss, J. Detection of Free Hydroxyl Radicals by Hydroxylation of Aromatic Compounds. *Nature* **1950**, *166* (4235), 1104–1105.

(269) Oturan, M. A.; Pinson, J. Hydroxylation by Electrochemically Generated $^{\bullet}OH$ Radicals. Mono- and Polyhydroxylation of Benzoic Acid: Products and Isomer Distribution. *J. Phys. Chem.* **1995**, *99* (38), 13948–13954.

(270) Liu, B.; Wang, H. Determination of Atmospheric Hydroxyl Radical by HPLC Coupled with Electrochemical Detection. *J. Environ. Sci.* **2008**, *20* (1), 28–32.

(271) Jen, J.-F.; Leu, M.-F.; Yang, T. C. Determination of Hydroxyl Radicals in an Advanced Oxidation Process with Salicylic Acid Trapping and Liquid Chromatography. *J. Chromatogr. A* **1998**, *796* (2), 283–288.

(272) Karnik, B. S.; Davies, S. H.; Baumann, M. J.; Masten, S. J. Use of Salicylic Acid as a Model Compound to Investigate Hydroxyl Radical Reaction in an Ozonation–Membrane Filtration Hybrid Process. *Environ. Eng. Sci.* **2007**, *24* (6), 852–860.

(273) Coudray, C.; Talla, M.; Martin, S.; Fatome, M.; Favier, A. High-Performance Liquid Chromatography-Electrochemical Determination of Salicylate Hydroxylation Products as an in Vivo Marker of Oxidative Stress. *Anal. Biochem.* **1995**, *227* (1), 101–111.

(274) Cheng, H.; Cao, Y. Determination of Hydroxyl Radical in $CuSO_4$-Vitamin C Reaction System Using Capillary Electrophoresis with Electrochemical Detection and Its Application in the Determination of the Scavenging Activities of Chrysanthemum. *Chin. J. Chromatogr.* **2007**, *25* (5), 681–685.

(275) Cho, M.; Chung, H.; Choi, W.; Yoon, J. Linear Correlation between Inactivation of E. Coli and OH Radical Concentration in TiO_2 Photocatalytic Disinfection. *Water Res.* **2004**, *38* (4), 1069–1077.

(276) Tai, C.; Peng, J.-F.; Liu, J.-F.; Jiang, G.-B.; Zou, H. Determination of Hydroxyl Radicals in Advanced Oxidation Processes with Dimethyl Sulfoxide Trapping and Liquid Chromatography. *Anal. Chim. Acta* **2004**, *527* (1), 73–80.

(277) Fang, X.; Mark, G.; von Sonntag, C. OH Radical Formation by Ultrasound in Aqueous Solutions Part I: The Chemistry Underlying the Terephthalate Dosimeter. *Ultrason. Sonochem.* **1996**, *3* (1), 57–63.

(278) Yan, E. B.; Unthank, J. K.; Castillo-Melendez, M.; Miller, S. L.; Langford, S. J.; Walker, D. W. Novel Method for in Vivo Hydroxyl Radical Measurement by Microdialysis in Fetal Sheep Brain in Utero. *J. Appl. Physiol.* **2005**, *98* (6), 2304–2310.

(279) Baj, S.; Krawczyk, T. An Investigation into the Reaction of Hemin-Catalysed Luminol Oxidation by Peroxy Compounds. *J. Photochem. Photobiol. Chem.* **2006**, *183* (1–2), 111–120.

(280) Vione, D.; Falletti, G.; Maurino, V.; Minero, C.; Pelizzetti, E.; Malandrino, M.; Ajassa, R.; Olariu, R.-I.; Arsene, C. Sources and Sinks of Hydroxyl Radicals upon Irradiation of Natural Water Samples. *Environ. Sci. Technol.* **2006**, *40* (12), 3775–3781.

(281) Nakatani, N.; Hashimoto, N.; Shindo, H.; Yamamoto, M.; Kikkawa, M.; Sakugawa, H. Determination of Photoformation Rates and Scavenging Rate Constants of Hydroxyl Radicals in Natural Waters Using an Automatic Light Irradiation and Injection System. *Anal. Chim. Acta* **2007**, *581* (2), 260–267.

(282) Takeda, K.; Takedoi, H.; Yamaji, S.; Ohta, K.; Sakugawa, H. Determination of Hydroxyl Radical Photoproduction Rates in Natural Waters. *Anal. Sci.* **2004**, *20* (1), 153–158.

(283) Kilinc, E. Determination of the Hydroxyl Radical by Its Adduct Formation with Phenol and Liquid Chromatography/electrochemical Detection. *Talanta* **2005**, *65* (4), 876–881.

(284) Lindsey, M. E.; Tarr, M. A. Quantitation of Hydroxyl Radical during Fenton Oxidation Following a Single Addition of Iron and Peroxide. *Chemosphere* **2000**, *41* (3), 409–417.

(285) Buxton, G. V.; Greenstock, C. L.; Helman, W. P.; Ross, A. B. Critical Review of Rate Constants for Reactions of Hydrated Electrons, Hydrogen Atoms and Hydroxyl Radicals ($^•OH/^•O^-$ in Aqueous Solution. *J. Phys. Chem. Ref. Data* **1988**, *17* (2), 513–886.

(286) Babbs, C. F.; Gale, M. J. Colorimetric Assay for Methanesulfinic Acid in Biological Samples. *Anal. Biochem.* **1987**, *163* (1), 67–73.

(287) Grannas, A. M.; Martin, C. B.; Chin, Y.-P.; Platz, M. Hydroxyl Radical Production from Irradiated Arctic Dissolved Organic Matter. *Biogeochemistry* **2006**, *78* (1), 51–66.

(288) Gomes, A.; Fernandes, E.; Lima, J. L. F. C. Fluorescence Probes Used for Detection of Reactive Oxygen Species. *J. Biochem. Biophys. Methods* **2005**, *65* (2–3), 45–80.

(289) Bartosz, G. Use of Spectroscopic Probes for Detection of Reactive Oxygen Species. *Clin. Chim. Acta* **2006**, *368* (1–2), 53–76.

(290) Soh, N. Recent Advances in Fluorescent Probes for the Detection of Reactive Oxygen Species. *Anal. Bioanal. Chem.* **2006**, *386* (3), 532–543.

(291) Setsukinai, K.; Urano, Y.; Kakinuma, K.; Majima, H. J.; Nagano, T. Development of Novel Fluorescence Probes That Can Reliably Detect Reactive Oxygen Species and Distinguish Specific Species. *J. Biol. Chem.* **2003**, *278* (5), 3170–3175.

(292) Ou, B.; Hampsch-Woodill, M.; Flanagan, J.; Deemer, E. K.; Prior, R. L.; Huang, D. Novel Fluorometric Assay for Hydroxyl Radical Prevention Capacity Using Fluorescein as the Probe. *J. Agric. Food Chem.* **2002**, *50* (10), 2772–2777.

(293) Czili, H.; Horváth, A. Applicability of Coumarin for Detecting and Measuring Hydroxyl Radicals Generated by Photoexcitation of TiO_2 Nanoparticles. *Appl. Catal. B Environ.* **2008**, *81* (3–4), 295–302.

(294) Fang, X.; Mark, G.; von Sonntag, C. OH Radical Formation by Ultrasound in Aqueous Solutions Part I: The Chemistry Underlying the Terephthalate Dosimeter. *Ultrason. Sonochem.* **1996**, *3* (1), 57–63.

(295) Linxiang, L.; Abe, Y.; Nagasawa, Y.; Kudo, R.; Usui, N.; Imai, K.; Mashino, T.; Mochizuki, M.; Miyata, N. An HPLC Assay of Hydroxyl Radicals by the Hydroxylation Reaction of Terephthalic Acid. *Biomed. Chromatogr.* **2004**, *18* (7), 470–474.

(296) Tang, B.; Zhang, L.; Geng, Y. Determination of the Antioxidant Capacity of Different Food Natural Products with a New Developed Flow Injection Spectrofluorimetry Detecting Hydroxyl Radicals. *Talanta* **2005**, *65* (3), 769–775.

(297) Manevich, Y.; Held, K. D.; Biaglow, J. E. Coumarin-3-Carboxylic Acid as a Detector for Hydroxyl Radicals Generated Chemically and by Gamma Radiation. *Radiat. Res.* **1997**, *148* (6), 580–591.

(298) Yu, F.; Xu, D.; Lei, R.; Li, N.; Li, K. Free-Radical Scavenging Capacity Using the Fenton Reaction with Rhodamine B as the Spectrophotometric Indicator. *J. Agric. Food Chem.* **2008**, *56* (3), 730–735.

(299) Liang, A.-H.; Zhou, S.-M.; Jiang, Z.-L. A Simple and Sensitive Resonance Scattering Spectral Method for Determination of Hydroxyl Radical in Fenton System Using Rhodamine S and Its Application to Screening the Antioxidant. *Talanta* **2006**, *70* (2), 444–448.

(300) Newton, G. L.; Milligan, J. R. Fluorescence Detection of Hydroxyl Radicals. *Radiat. Phys. Chem.* **2006**, *75* (4), 473–478.

(301) Lu, C.; Song, G.; Lin, J.-M. Reactive Oxygen Species and Their Chemiluminescence-Detection Methods. *TrAC Trends Anal. Chem.* **2006**, *25* (10), 985–995.

(302) White, E. H.; Zafiriou, O.; Kagi, H. H.; Hill, J. H. M. Chemilunimescence of Luminol: The Chemcial Reaction. *J. Am. Chem. Soc.* **1964**, *86* (5), 940–941.

(303) Hu, Y.; Zhang, Z.; Yang, C. Measurement of Hydroxyl Radical Production in Ultrasonic Aqueous Solutions by a Novel Chemiluminescence Method. *Ultrason. Sonochem.* **2008**, *15* (5), 665–672.

(304) Tsai, C.-H.; Stern, A.; Chiou, J.-F.; Chern, C.-L.; Liu, T.-Z. Rapid and Specific Detection of Hydroxyl Radical Using an Ultraweak Chemiluminescence Analyzer and a Low-Level Chemiluminescence Emitter: Application to Hydroxyl Radical-Scavenging Ability of Aqueous Extracts of Food Constituents. *J. Agric. Food Chem.* **2001**, *49* (5), 2137–2141.

(305) Satoh, A. Y.; Trosko, J. E.; Masten, S. J. Methylene Blue Dye Test for Rapid Qualitative Detection of Hydroxyl Radicals Formed in a Fenton's Reaction Aqueous Solution. *Environ. Sci. Technol.* **2007**, *41* (8), 2881–2887.

(306) Cohn, C. A.; Laffers, R.; Schoonen, M. A. A. Using Yeast RNA as a Probe for Generation of Hydroxyl Radicals by Earth Materials. *Environ. Sci. Technol.* **2006**, *40* (8), 2838–2843.

(307) Zellner, R.; Herrmann, H. *Advances in Spectroscopy*, Wiley.; Clark R.J. and Hester R.E.: London, 1995.

(308) Chin, M.; Wine, P. H. A Temperature-Dependent Kinetics Study of the Aqueous Phase Reactions $OH + SCN^- \rightarrow SCNOH^-$ and $SCN + SCN^- \leftrightarrows (SCN)_2^-$. *J. Photochem. Photobiol. Chem.* **1992**, *69* (1), 17–25.

(309) Chin, M.; Wine, P. H. *Aquatic and Surface Photochemistry*, Lewis Publishers.; Helz, G.R.; Zepp, R.G.; Crosby, D.G.: Boca Raton, FL., 1994.

(310) Baxendale, J. H.; Bevan, P. L. T.; Stott, D. A. Pulse Radiolysis of Aqueous Thiocyanate and Iodide Solutions. *Trans. Faraday Soc.* **1968**, *64* (0), 2389–2397.

(311) Schuler, R. H.; Patterson, L. K.; Janata, E. Yield for the Scavenging of Hydroxyl Radicals in the Radiolysis of Nitrous Oxide-Saturated Aqueous Solutions. *J. Phys. Chem.* **1980**, *84* (16), 2088–2089.

(312) Atkins, P. W. *Physical Chemistry*, Oxford University Press.; Oxford, 1986.

(313) Ervens, B.; Gligorovski, S.; Herrmann, H. Temperature-Dependent Rate Constants for Hydroxyl Radical Reactions with Organic Compounds in Aqueous Solutions. *Phys. Chem. Chem. Phys.* **2003**, *5* (9), 1811–1824.

(314) Gligorovski, S.; Herrmann, H. Kinetics of Reactions of OH with Organic Carbonyl Compounds in Aqueous Solution. *Phys. Chem. Chem. Phys.* **2004**, *6* (16), 4118–4126.

(315) Morozov, I.; Gligorovski, S.; Barzaghi, P.; Hoffmann, D.; Lazarou, Y. G.; Vasiliev, E.; Herrmann, H. Hydroxyl Radical Reactions with Halogenated Ethanols in Aqueous Solution: Kinetics and Thermochemistry. *Int. J. Chem. Kinet.* **2008**, *40* (4), 174–188.

(316) Gligorovski, S.; Rousse, D.; George, C. H.; Herrmann, H. Rate Constants for the OH Reactions with Oxygenated Organic Compounds in Aqueous Solution. *Int. J. Chem. Kinet.* **2009**, *41* (5), 309–326.

(317) Motohashi, N.; Saito, Y. Competitive Measurement of Rate Constants for Hydroxyl Radical Reactions Using Radiolytic Hydroxylation of Benzoate. *Chem. Pharm. Bull. (Tokyo)* **1993**, *41* (10), 1842–1845.

(318) Elliot, A. J.; Simsons, A. S. Rate Constants for Reactions of Hydroxyl Radicals as a Function of Temperature. *Radiat. Phys. Chem. 1977* **1984**, *24* (2), 229–231.

(319) Wolfenden, B. S.; Willson, R. L. Radical-Cations as Reference Chromogens in Kinetic Studies of Ono-Electron Transfer Reactions: Pulse Radiolysis Studies of 2,2′-Azinobis-(3-Ethylbenzthiazoline-6-Sulphonate). *J. Chem. Soc. Perkin Trans. 2* **1982**, No. 7, 805–812.

(320) Willson, R. L.; Greenstock, C. L.; Adams, G. E.; Wageman, R.; Dorfman, L. M. The Standardization of Hydroxyl Radical Rate Data from Radiation Chemistry. *Int. J. Radiat. Phys. Chem.* **1971**, *3* (3), 211–220.

(321) Thomas, J. K. Rates of Reaction of the Hydroxyl Radical. *Trans. Faraday Soc.* **1965**, *61* (0), 702–707.

(322) Ervens, B.; Gligorovski, S.; Herrmann, H. Temperature-Dependent Rate Constants for Hydroxyl Radical Reactions with Organic Compounds in Aqueous Solutions. *Phys. Chem. Chem. Phys.* **2003**, *5* (9), 1811–1824.

(323) Herrmann, H.; Hoffmann, D.; Schaefer, T.; Bräuer, P.; Tilgner, A. Tropospheric Aqueous-Phase Free-Radical Chemistry: Radical Sources, Spectra, Reaction Kinetics and Prediction Tools. *ChemPhysChem* **2010**, *11* (18), 3796–3822.

(324) Adams, G. E.; Boag, J. W.; Michael, B. D. Spectroscopic Studies of Reactions of the OH Radical in Aqueous Solutions. Reaction of OH with the Ferrocyanide Ion. *Trans. Faraday Soc.* **1965**, *61* (0), 492–505.

(325) Monod, A.; Poulain, L.; Grubert, S.; Voisin, D.; Wortham, H. Kinetics of OH-Initiated Oxidation of Oxygenated Organic Compounds in the Aqueous Phase: New Rate Constants, Structure–activity Relationships and Atmospheric Implications. *Atmos. Environ.* **2005**, *39* (40), 7667–7688.

(326) Atkinson, R. Kinetics and Mechanisms of the Gas-Phase Reactions of the Hydroxyl Radical with Organic Compounds under Atmospheric Conditions. *Chem. Rev.* **1986**, *86* (1), 69–201.

(327) Hoigné, J.; Morel, F. The Kinetics of Trace Metal Complexation: Implications for Metal Reactivity in Natural Waters. In *Aquatic Chemical Kinetics: Reaction Rates of Processes in Natural Waters*; Stumm, W., Ed.; Wiley: New York, 1990; p 560.

(328) Mack, J.; Bolton, J. R. Photochemistry of Nitrite and Nitrate in Aqueous Solution: A Review. *J. Photochem. Photobiol. Chem.* **1999**, *128* (1–3), 1–13.

(329) Mark, G.; Korth, H.-G.; Schuchmann, H.-P.; von Sonntag, C. The Photochemistry of Aqueous Nitrate Ion Revisited. *J. Photochem. Photobiol. Chem.* **1996**, *101* (2–3), 89–103.

(330) Vione, D.; Khanra, S.; Man, S. C.; Maddigapu, P. R.; Das, R.; Arsene, C.; Olariu, R.-I.; Maurino, V.; Minero, C. Inhibition vs. Enhancement of the Nitrate-Induced Phototransformation of Organic Substrates by the •OH Scavengers Bicarbonate and Carbonate. *Water Res.* **2009**, *43* (18), 4718–4728.

(331) Wenk, J.; von Gunten, U.; Canonica, S. Effect of Dissolved Organic Matter on the Transformation of Contaminants Induced by Excited Triplet States and the Hydroxyl Radical. *Environ. Sci. Technol.* **2011**, *45* (4), 1334–1340.

(332) Maurino, V.; Bedini, A.; Borghesi, D.; Vione, D.; Minero, C. Phenol Transformation Photosensitised by Quinoid Compounds. *Phys. Chem. Chem. Phys. PCCP* **2011**, *13* (23), 11213–11221.

(333) Ikehata, K.; El-Din, M. G. Aqueous Pesticide Degradation by Hydrogen Peroxide/ultraviolet Irradiation and Fenton-Type Advanced Oxidation Processes: A Review. *J Env. Eng Sci* **2006**, *5* (2), 81–135.

(334) Page, S. E.; Arnold, W. A.; McNeill, K. Assessing the Contribution of Free Hydroxyl Radical in Organic Matter-Sensitized Photohydroxylation Reactions. *Environ. Sci. Technol.* **2011**, *45* (7), 2818–2825.

(335) Pochon, A.; Vaughan, P. P.; Gan, D.; Vath, P.; Blough, N. V.; Falvey, D. E. Photochemical Oxidation of Water by 2-Methyl-1,4-Benzoquinone: Evidence against the Formation of Free Hydroxyl Radical. *J. Phys. Chem. A* **2002**, *106* (12), 2889–2894.

(336) Maddigapu, P. R.; Bedini, A.; Minero, C.; Maurino, V.; Vione, D.; Brigante, M.; Mailhot, G.; Sarakha, M. The pH-Dependent Photochemistry of Anthraquinone-2-Sulfonate. *Photochem Photobiol Sci* **2010**, *9* (3), 323–330.

(337) Brigante, M.; Charbouillot, T.; Vione, D.; Mailhot, G. Photochemistry of 1-Nitronaphthalene: A Potential Source of Singlet Oxygen and Radical Species in Atmospheric Waters. *J. Phys. Chem. A* **2010**, *114* (8), 2830–2836.

(338) Sur, B.; Rolle, M.; Minero, C.; Maurino, V.; Vione, D.; Brigante, M.; Mailhot, G. Formation of Hydroxyl Radicals by Irradiated 1-Nitronaphthalene (1NN): Oxidation of Hydroxyl Ions and Water by the 1NN Triplet State. *Photochem Photobiol Sci* **2011**, *10* (11), 1817–1824.

(339) White, E. M.; Vaughan, P. P.; Zepp, R. G. Role of the Photo-Fenton Reaction in the Production of Hydroxyl Radicals and Photobleaching of Colored Dissolved Organic Matter in a Coastal River of the Southeastern United States. *Aquat. Sci.* **2003**, *65* (4), 402–414.

(340) Anesio, A. M.; Granéli, W. Increased Photoreactivity of DOC by Acidification: Implications for the Carbon Cycle in Humic Lakes. *Limnol. Oceanogr.* **2003**, *48* (2), 735–744.

(341) Vione, D.; Lauri, V.; Minero, C.; Maurino, V.; Malandrino, M.; Carlotti, M. E.; Olariu, R.-I.; Arsene, C. Photostability and Photolability of Dissolved Organic Matter upon Irradiation of Natural Water Samples under Simulated Sunlight. *Aquat. Sci.* **2009**, *71* (1), 34–45.

(342) Vione, D.; Das, R.; Rubertelli, F.; Maurino, V.; Minero, C.; Barbati, S.; Chiron, S. Modelling the Occurrence and Reactivity of Hydroxyl Radicals in Surface Waters: Implications for the Fate of Selected Pesticides. *Int. J. Environ. Anal. Chem.* **2010**, *90* (3-6), 260–275.

(343) Braslavsky, S. E. Glossary of Terms Used in Photochemistry, 3rd Edition (IUPAC Recommendations 2006). *Pure Appl. Chem.* **2007**, *79* (3), 293–465.

(344) Hatipoglu, A.; Vione, D.; Yalçın, Y.; Minero, C.; Çınar, Z. Photo-Oxidative Degradation of Toluene in Aqueous Media by Hydroxyl Radicals. *J. Photochem. Photobiol. Chem.* **2010**, *215* (1), 59–68.

(345) Brezonik, P. L.; Fulkerson-Brekken, J. Nitrate-Induced Photolysis in Natural Waters: Controls on Concentrations of Hydroxyl Radical Photo-Intermediates by Natural Scavenging Agents. *Environ. Sci. Technol.* **1998**, *32* (19), 3004–3010.

(346) Vione, D.; Maddigapu, P. R.; De Laurentiis, E.; Minella, M.; Pazzi, M.; Maurino, V.; Minero, C.; Kouras, S.; Richard, C. Modelling the Photochemical Fate of Ibuprofen in Surface Waters. *Water Res.* **2011**, *45* (20), 6725–6736.

(347) Maddigapu, P. R.; Minella, M.; Vione, D.; Maurino, V.; Minero, C. Modeling Phototransformation Reactions in Surface Water Bodies: 2,4-Dichloro-6-Nitrophenol as a Case Study. *Environ. Sci. Technol.* **2011**, *45* (1), 209–214.

(348) De Laurentiis, E.; Chiron, S.; Kouras-Hadef, S.; Richard, C.; Minella, M.; Maurino, V.; Minero, C.; Vione, D. Photochemical Fate of Carbamazepine in Surface Freshwaters: Laboratory Measures and Modeling. *Environ. Sci. Technol.* **2012**, *46* (15), 8164–8173.

(349) Marchetti, G.; Minella, M.; Maurino, V.; Minero, C.; Vione, D. Photochemical Transformation of Atrazine and Formation of Photointermediates under Conditions Relevant to Sunlit Surface Waters: Laboratory Measures and Modelling. *Water Res.* **2013**, *47* (16), 6211–6222.

(350) Wardman, P. Reduction Potentials of One-Electron Couples Involving Free Radicals in Aqueous Solution. *J. Phys. Chem. Ref. Data* **1989**, *18* (4), 1637–1755.

(351) Neta, P.; Huie, R. E.; Ross, A. B. Rate Constants for Reactions of Inorganic Radicals in Aqueous Solution. *J. Phys. Chem. Ref. Data* **1988**, *17* (3), 1027–1284.

(352) Herrmann, H.; Exner, M.; Jacobi, H.-W.; Raabe, G.; Reese, A.; Zellner, R. Laboratory Studies of Atmospheric Aqueous-Phase Free-Radical Chemistry: Kinetic and Spectroscopic Studies of Reactions of NO_3 and SO_4^- Radicals with Aromatic Compounds. *Faraday Discuss.* **1995**, *100* (0), 129–153.

(353) Vione, D.; Maurino, V.; Minero, C.; Calza, P.; Pelizzetti, E. Phenol Chlorination and Photochlorination in the Presence of Chloride Ions in Homogeneous Aqueous Solution. *Environ. Sci. Technol.* **2005**, *39* (13), 5066–5075.

(354) Vione, D.; Maurino, V.; Man, S. C.; Khanra, S.; Arsene, C.; Olariu, R.-I.; Minero, C. Formation of Organobrominated Compounds in the Presence of Bromide under Simulated Atmospheric Aerosol Conditions. *ChemSusChem* **2008**, *1* (3), 197–204.

(355) Chiron, S.; Minero, C.; Vione, D. Occurrence of 2,4-Dichlorophenol and of 2,4-Dichloro-6-Nitrophenol in the Rhône River Delta (Southern France). *Environ. Sci. Technol.* **2007**, *41* (9), 3127–3133.

(356) Bouillon, R.-C.; Miller, W. L. Photodegradation of Dimethyl Sulfide (DMS) in Natural Waters: Laboratory Assessment of the Nitrate-Photolysis-Induced DMS Oxidation. *Environ. Sci. Technol.* **2005**, *39* (24), 9471–9477.

(357) Harimurti, S.; Dutta, B. K.; Ariff, I. F. B. M.; Chakrabarti, S.; Vione, D. Degradation of Monoethanolamine in Aqueous Solution by Fenton's Reagent with Biological Post-Treatment. *Water. Air. Soil Pollut.* **2010**, *211* (1-4), 273–286.

(358) Omura, K. Electron Transfer between Protonated and Unprotonated Phenoxyl Radicals1. *J. Org. Chem.* **2008**, *73* (3), 858–867.

(359) Sultimova, N. B.; Levin, P. P.; Chaikovskaya, O. N. Kinetics of Radical Formation and Decay in Photooxidation of 4-Halophenols Sensitized by 4-Carboxybenzophenone in Aqueous Solutions. *Russ. Chem. Bull.* **2005**, *54* (6), 1439–1444.

(360) Krasnovsky, A. A. Primary Mechanisms of Photoactivation of Molecular Oxygen. History of Development and the Modern Status of Research. *Biochem. Mosc.* **2007**, *72* (10), 1065–1080.

(361) Albarran, G.; Bentley, J.; Schuler, R. H. Substituent Effects in the Reaction of OH Radicals with Aromatics: Toluene. *J. Phys. Chem. A* **2003**, *107* (39), 7770–7774.

(362) Harrison, M. A. J.; Barra, S.; Borghesi, D.; Vione, D.; Arsene, C.; Iulian Olariu, R. Nitrated Phenols in the Atmosphere: A Review. *Atmos. Environ.* **2005**, *39* (2), 231–248.

(363) Peres, J. A.; Domínguez, J. R.; Beltran-Heredia, J. Reaction of Phenolic Acids with Fenton-Generated Hydroxyl Radicals: Hammett Correlation. *Desalination* **2010**, *252* (1–3), 167–171.

(364) Minakata, D.; Li, K.; Westerhoff, P.; Crittenden, J. Development of a Group Contribution Method To Predict Aqueous Phase Hydroxyl Radical ($HO^•$) Reaction Rate Constants. *Environ. Sci. Technol.* **2009**, *43* (16), 6220–6227.

(365) Vione, D.; Maurino, V.; Minero, C.; Pelizzetti, E. An Empirical, Quantitative Approach to Predict the Reactivity of Some Substituted Aromatic Compounds Towards Reactive Radical Species ($Cl_2^{-•}$, $Br_2^{-•}$, $^•NO_2$, $SO_3^{-•}$, $SO_4^{-•}$) in Aqueous Solution. *Environ. Sci. Pollut. Res.* **2006**, *13* (4), 212–214.

(366) Vione, D.; Maurino, V.; Minero, C.; Pelizzetti, E. An Empirical, Quantitative Approach to Predict the Reactivity of Some Substituted Aromatic Compounds Towards Reactive Radical Species ($Cl_2^{-•}$, $Br_2^{-•}$, $^•NO_2$, $SO_3^{-•}$, $SO_4^{-•}$) in Aqueous Solution. *Environ. Sci. Pollut. Res.* **2006**, *13* (4), 212–214.

(367) Atkinson, R.; Arey, J. Atmospheric Degradation of Volatile Organic Compounds. *Chem. Rev.* **2003**, *103* (12), 4605–4638.

(368) Mellouki, A.; Le Bras, G.; Sidebottom, H. Kinetics and Mechanisms of the Oxidation of Oxygenated Organic Compounds in the Gas Phase. *Chem. Rev.* **2003**, *103* (12), 5077–5096.

(369) Tyndall, G. S.; Orlando, J. J.; Wallington, T. J.; Hurley, M. D.; Goto, M.; Kawasaki, M. Mechanism of the Reaction of OH Radicals with Acetone and Acetaldehyde at 251 and 296 K. *Phys Chem Chem Phys* **2002**, *4* (11), 2189–2193.

(370) Dagaut, P.; Wallington, T. J.; Liu, R.; Kurylo, M. J. The Gas Phase Reactions of Hydroxyl Radicals with a Series of Carboxylic Acids over the Temperature Range 240–440 K. *Int. J. Chem. Kinet.* **1988**, *20* (4), 331–338.

(371) Wollenhaupt, M.; Crowley, J. N. Kinetic Studies of the Reactions $CH_3 + NO_2 \rightarrow$ Products, $CH_3O + NO_2 \rightarrow$ Products, and $OH + CH_3C(O)CH_3 \rightarrow CH_3C(O)OH + CH_3$, over a Range of Temperature and Pressure. *J. Phys. Chem. A* **2000**, *104* (27), 6429–6438.

(372) Talukdar, R. K.; Gierczak, T.; McCabe, D. C.; Ravishankara, A. R. Reaction of Hydroxyl Radical with Acetone. 2. Products and Reaction Mechanism. *J. Phys. Chem. A* **2003**, *107* (25), 5021–5032.

(373) Ervens, B.; Gligorovski, S.; Herrmann, H. Temperature-Dependent Rate Constants for Hydroxyl Radical Reactions with Organic Compounds in Aqueous Solutions. *Phys. Chem. Chem. Phys.* **2003**, *5* (9), 1811–1824.

(374) Bott, J. F.; Cohen, N. A Shock Tube Study of the Reaction of Methyl Radicals with Hydroxyl Radicals. *Int. J. Chem. Kinet.* **1991**, *23* (11), 1017–1033.

(375) Dagaut, P.; Wallington, T. J.; Liu, R.; Kurylo, M. J. The Gas Phase Reactions of Hydroxyl Radicals with a Series of Carboxylic Acids over the Temperature Range 240–440 K. *Int. J. Chem. Kinet.* **1988**, *20* (4), 331–338.

(376) Winer, A. M.; Lloyd, A. C.; Darnall, K. R.; Pitts, J. N. Relative Rate Constants for the Reaction of the Hydroxyl Radical with Selected Ketones, Chloroethenes, and Monoterpene Hydrocarbons. *J. Phys. Chem.* **1976**, *80* (14), 1635–1639.

(377) Adams, G. E.; Boag, J. W.; Michael, B. D. Spectroscopic Studies of Reactions of the OH Radical in Aqueous Solutions. Reaction of OH with the Ferrocyanide Ion. *Trans. Faraday Soc.* **1965**, *61* (0), 492–505.

(378) Atkinson, R.; Tuazon, E. C.; Aschmann, S. M. Atmospheric Chemistry of 2-Pentanone and 2-Heptanone. *Environ. Sci. Technol.* **2000**, *34* (4), 623–631.

(379) Atkinson, R.; Aschmann, S. M. Comment on “Flash Photolysis Resonance Fluorescence Investigation of the Gas-Phase Reactions of Hydroxyl Radicals with a Series of Aliphatic Ketones over the Temperature Range 240-440 K.” *J. Phys. Chem.* **1988**, *92* (13), 4008–4008.

(380) Monod, A.; Poulain, L.; Grubert, S.; Voisin, D.; Wortham, H. Kinetics of OH-Initiated Oxidation of Oxygenated Organic Compounds in the Aqueous Phase: New Rate Constants, Structure–activity Relationships and Atmospheric Implications. *Atmos. Environ.* **2005**, *39* (40), 7667–7688.

(381) Saunders, S. M.; Baulch, D. L.; Cooke, K. M.; Pilling, M. J.; Smurthwaite, P. I. Kinetics and Mechanisms of the Reactions of OH with Some Oxygenated Compounds of Importance in Tropospheric Chemistry. *Int. J. Chem. Kinet.* **1994**, *26* (1), 113–130.

(382) Overend, R.; Paraskevopoulos, G. Rates of Hydroxyl Radical Reactions. 4. Reactions with Methanol, Ethanol, 1-Propanol, and 2-Propanol at 296 K. *J. Phys. Chem.* **1978**, *82* (12), 1329–1333.

(383) Nelson, L.; Rattigan, O.; Neavyn, R.; Sidebottom, H.; Treacy, J.; Nielsen, O. J. Absolute and Relative Rate Constants for the Reactions of Hydroxyl Radicals and Chlorine Atoms with a Series of Aliphatic Alcohols and Ethers at 298 K. *Int. J. Chem. Kinet.* **1990**, *22* (11), 1111–1126.

(384) Wolfenden, B. S.; Willson, R. L. Radical-Cations as Reference Chromogens in Kinetic Studies of Ono-Electron Transfer Reactions: Pulse Radiolysis Studies of 2,2′-Azinobis-(3-Ethylbenzthiazoline-6-Sulphonate). *J. Chem. Soc. Perkin Trans. 2* **1982**, No. 7, 805–812.

(385) Baxley, J. S.; Wells, J. R. The Hydroxyl Radical Reaction Rate Constant and Atmospheric Transformation Products of 2-Butanol and 2-Pentanol. *Int. J. Chem. Kinet.* **1998**, *30* (10), 745–752.

(386) Schuchmann, M. N.; Von Sonntag, C. The Rapid Hydration of the Acetyl Radical. A Pulse Radiolysis Study of Acetaldehyde in Aqueous Solution. *J. Am. Chem. Soc.* **1988**, *110* (17), 5698–5701.

(387) Balestra-Garcia, C.; Le Bras, G.; Mac Leod, H. Kinetic Study of the Reactions Hydroxyl + Mono-, Di-, Trichloroacetaldehyde and Acetaldehyde by Laser Photolysis-Resonance Fluorescence at 298 K. *J. Phys. Chem.* **1992**, *96* (8), 3312–3316.

(388) Mezyk, S. P. Rate Constant and Activation Energy Determination for Reaction of E−(aq) and •OH with 2-Butanone and Propanal. *Can. J. Chem.* **1994**, *72* (4), 1116–1119.

(389) Adams, G. E., Boag, J. W., Currant, J., and Michael, B. D. Absolute Rate Constants for the Reaction of the Hydroxyl Radical with Organic Compounds. In *Pulse Radiolysis*; Ebert, M., Keene, J. P., Swallow, A. J., and Baxendale, J. H: New York, 1965; pp 131–143.

(390) D’Anna, B.; Andresen, Ø.; Gefen, Z.; Nielsen, C. J. Kinetic Study of OH and NO3 Radical Reactions with 14 Aliphatic Aldehydes. *Phys. Chem. Chem. Phys.* **2001**, *3* (15), 3057–3063.

(391) Audley, G. J.; Baulch, D. L.; Campbell, I. M. Gas-Phase Reactions of Hydroxyl Radicals with Aldehydes in Flowing H_2O_2+ NO_2+ CO Mixtures. *J. Chem. Soc. Faraday Trans. 1 Phys. Chem. Condens. Phases* **1981**, *77* (10), 2541–2549.

(392) Acero, J. L.; Haderlein, S. B.; Schmidt, T. C.; Suter, M. J.-F.; von Gunten, U. MTBE Oxidation by Conventional Ozonation and the Combination Ozone/Hydrogen Peroxide: Efficiency of the Processes and Bromate Formation. *Environ. Sci. Technol.* **2001**, *35* (21), 4252–4259.

(393) Jürgens, M.; Jacob, F.; Ekici, P.; Friess, A.; Parlar, H. Determination of Direct Photolysis Rate Constants and OH Radical Reactivity of Representative Odour Compounds in Brewery Broth Using a Continuous Flow-Stirred Photoreactor. *Atmos. Environ.* **2007**, *41* (22), 4571–4584.

(394) Jimenez, E.; Lanza, B.; Antinolo, M.; Albaladejo, J. Influence of Temperature on the Chemical Removal of 3-Methylbutanal, Trans-2-Methyl-2-Butenal, and 3-Methyl-2-Butenal by OH Radicals in the Troposphere. *Atmos. Environ.* **2009**, *43* (26), 4043–4049.

(395) Buxton, G. V.; Malone, T. N.; Salmon, G. A. Oxidation of Glyoxal Initiated by OH Inoxygenated Aqueous Solution. *J. Chem. Soc. Faraday Trans.* **1997**, *93* (16), 2889–2891.

(396) Feierabend, K. J.; Zhu, L.; Talukdar, R. K.; Burkholder, J. B. Rate Coefficients for the OH + HC(O)C(O)H (Glyoxal) Reaction between 210 and 390 K. *J. Phys. Chem. A* **2008**, *112* (1), 73–82.

(397) Baeza-Romero, M. T.; Glowacki, D. R.; Blitz, M. A.; Heard, D. E.; Pilling, M. J.; Rickard, A. R.; Seakins, P. W. A Combined Experimental and Theoretical Study of the Reaction between Methylglyoxal and OH/OD Radical: OH Regeneration. *Phys. Chem. Chem. Phys.* **2007**, *9* (31), 4114–4128.

(398) Mellouki, A.; Le Bras, G.; Sidebottom, H. Kinetics and Mechanisms of the Oxidation of Oxygenated Organic Compounds in the Gas Phase. *Chem. Rev.* **2003**, *103* (12), 5077–5096.

(399) Atkinson, R.; Baulch, D. L.; Cox, R. A.; Crowley, J. N.; Hampson, R. F.; Hynes, R. G.; Jenkin, M. E.; Rossi, M. J.; Troe, J. Evaluated Kinetic and Photochemical Data for Atmospheric Chemistry: Volume I - Gas Phase Reactions of O_x, HO_x, NO_x and SO_x Species. *Atmos Chem Phys* **2004**, *4* (6), 1461–1738.

(400) Scholes, G.; Willson, R. L. Γ-Radiolysis of Aqueous Thymine Solutions. Determination of Relative Reaction Rates of OH Radicals. *Trans. Faraday Soc.* **1967**, *63* (0), 2983–2993.

(401) Atkinson, R.; Baulch, D. L.; Cox, R. A.; Crowley, J. N.; Hampson, R. F.; Hynes, R. G.; Jenkin, M. E.; Rossi, M. J.; Troe, J. Evaluated Kinetic and Photochemical Data for Atmospheric Chemistry: Volume I - Gas Phase Reactions of O_x, HO_x, NO_x and SO_x Species. *Atmos Chem Phys* **2004**, *4* (6), 1461–1738.

(402) Zetzsch, C.; Stuhl, F. Rate Constants for Reactions of OH with Carbonic Acids; 1982; Vol. 7624, p 129.

(403) Le Calvé, S.; Le Bras, G.; Mellouki, A. Temperature Dependence for the Rate Coefficients of the Reactions of the OH Radical with a Series of Formates. *J. Phys. Chem. A* **1997**, *101* (30), 5489–5493.

(404) Wallington, T. J.; Dagaut, P.; Liu, R.; Kurylo, M. J. The Gas Phase Reactions of Hydroxyl Radicals with a Series of Esters over the Temperature Range 240–440 K. *Int. J. Chem. Kinet.* **1988**, *20* (2), 177–186.

(405) El Boudali, A.; Le Calvé, S.; Le Bras, G.; Mellouki, A. Kinetic Studies of OH Reactions with a Series of Acetates. *J. Phys. Chem.* **1996**, *100* (30), 12364–12368.

(406) Mellouki, A.; Wallington, T. J.; Chen, J. Atmospheric Chemistry of Oxygenated Volatile Organic Compounds: Impacts on Air Quality and Climate. *Chem. Rev.* **2015**, *115* (10), 3984–4014.

(407) Herrmann, H.; Schaefer, T.; Tilgner, A.; Styler, S. A.; Weller, C.; Teich, M.; Otto, T. Tropospheric Aqueous-Phase Chemistry: Kinetics, Mechanisms, and Its Coupling to a Changing Gas Phase. *Chem. Rev.* **2015**, *115* (10), 4259–4334.

(408) Gligorovski, S.; Wortham, H.; Kleffmann, J. The Hydroxyl Radical (OH) in Indoor Air: Sources and Implications. *Atmos. Environ.* **2014**, *99*, 568–570.

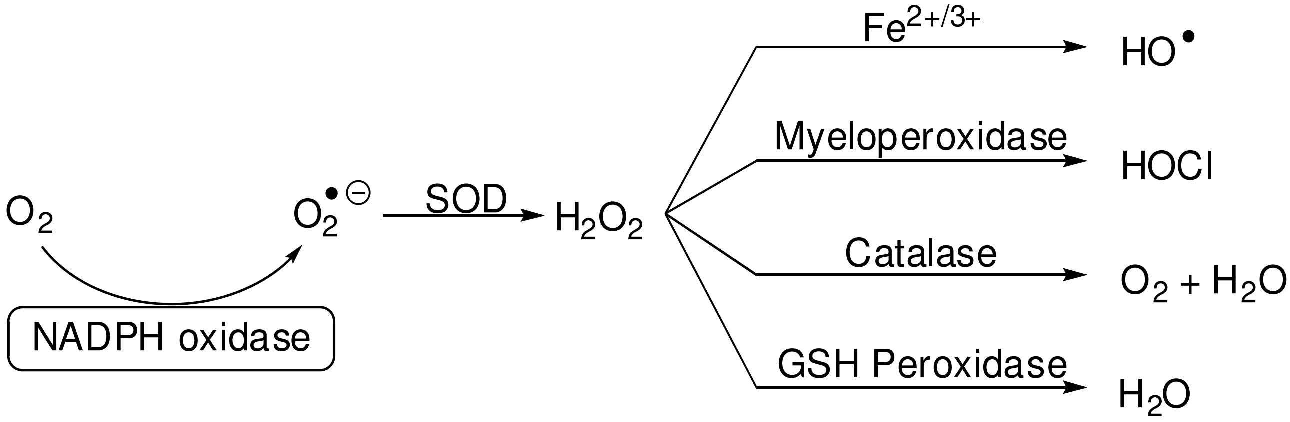

Figure 1: Production of superoxide anion induced by NADPH oxidase/Neutrophil during phagocytosis and possible routes evolution

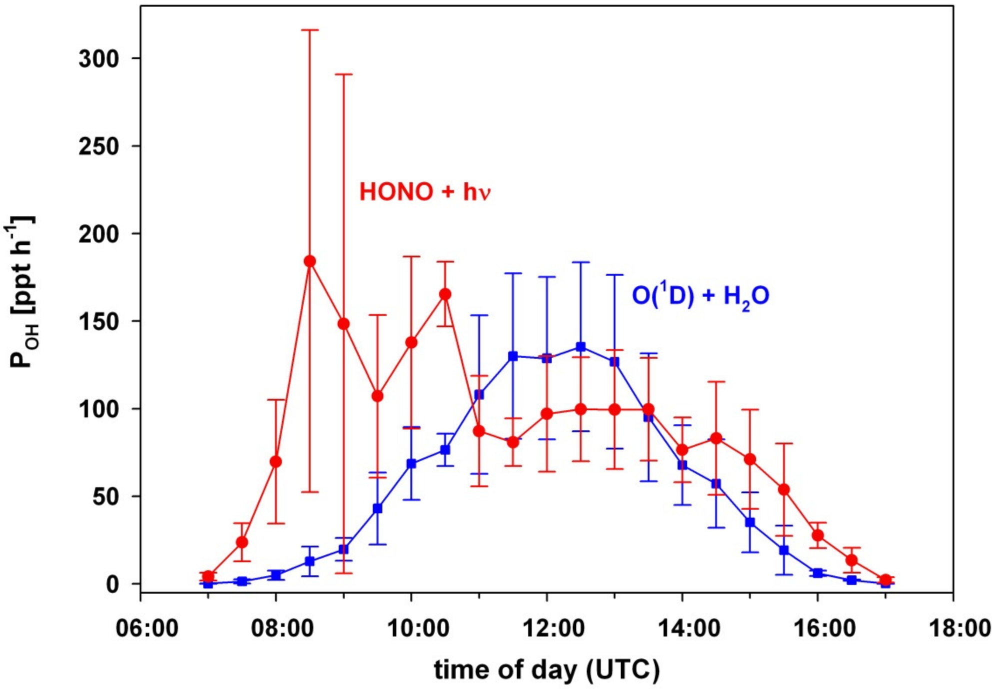

Figure 2: Comparison of the estimated $^\bullet$OH production by HONO and ozone photolysis during the campaign conducted in southwest Spain, 4 meters above the forest canopy for the seven clear days of the campaign.

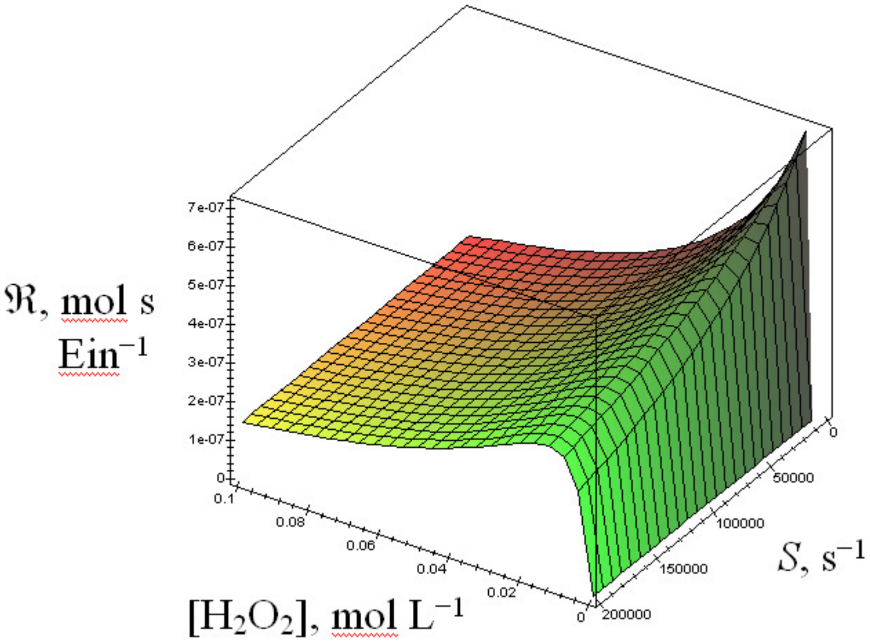

Figure 3: Plot of $\Re = [^{\bullet}OH]\,[p°(\lambda)]^{-1}$, as a function of H_2O_2 concentration ($[H_2O_2]$) and of the first-order rate constant of $^{\bullet}OH$ scavenging, S. The trend of $\Re$ is described by equation (3-3), with the numerical values given in the text.

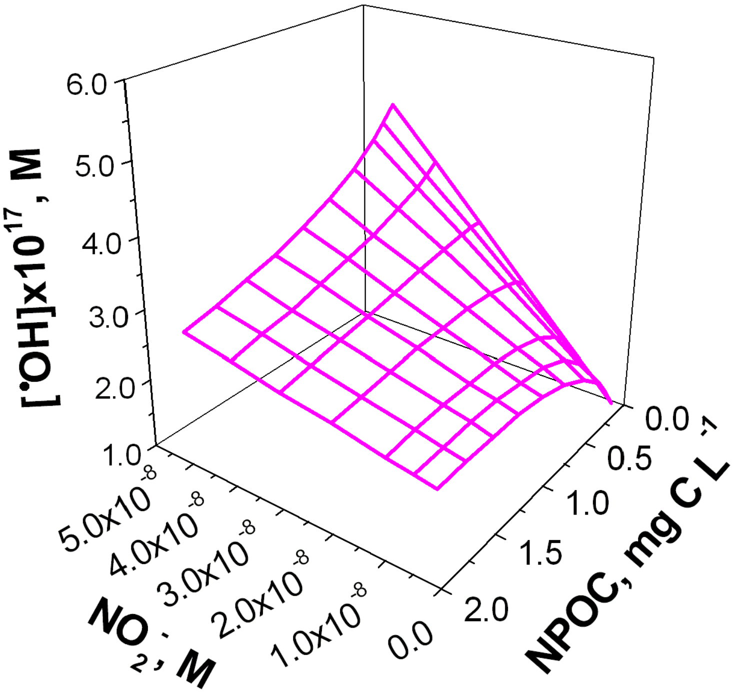

Figure 4. Steady-state [·OH] as a function of nitrite and NPOC (nonpurgeable organic carbon), which is a measure of DOC (dissolved organic carbon). Other conditions: 1 μM nitrate, 2.1 mM bicarbonate, 26 μM carbonate, d = 1 m, and 22 W m−2 sunlight UV irradiance

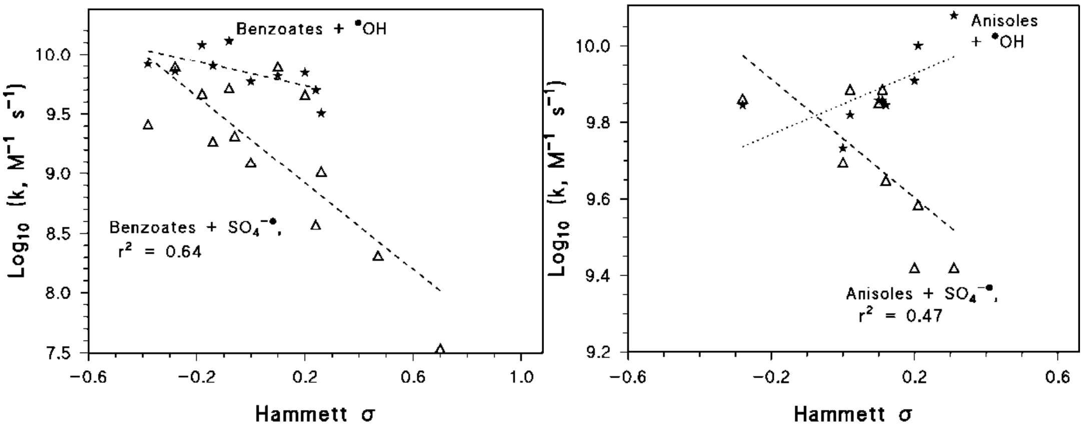

Figure 5. Correlation between second-order reaction rate constants of benzoates and anisoles with $^\bullet$OH and $SO_4^{-\bullet}$, and the corresponding σ values of the ring substituents.[365]

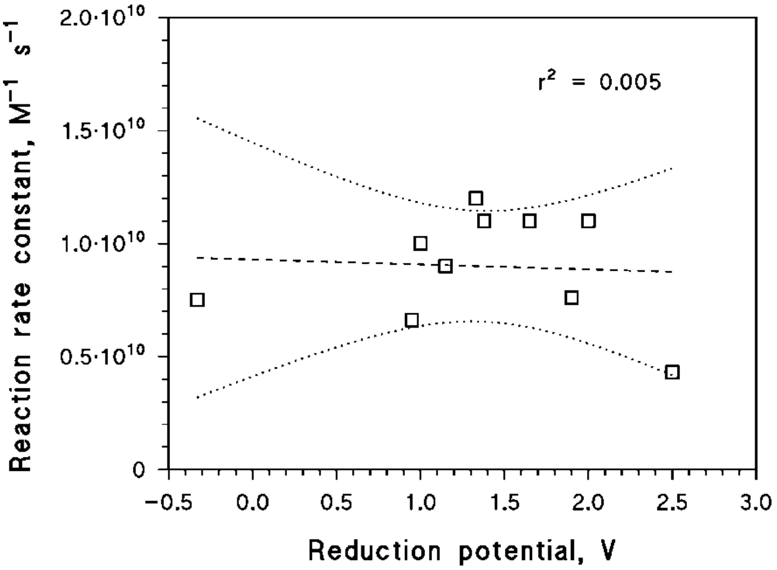

Figure 6. Reaction rate constants between $^{\bullet}$OH and inorganic anions ($^{\bullet}OH + X^{-} \rightarrow OH^{-} + X^{\bullet}$) as a function of the reduction potentials $E^{o}(X^{\bullet}/X^{-})$.[100,350]

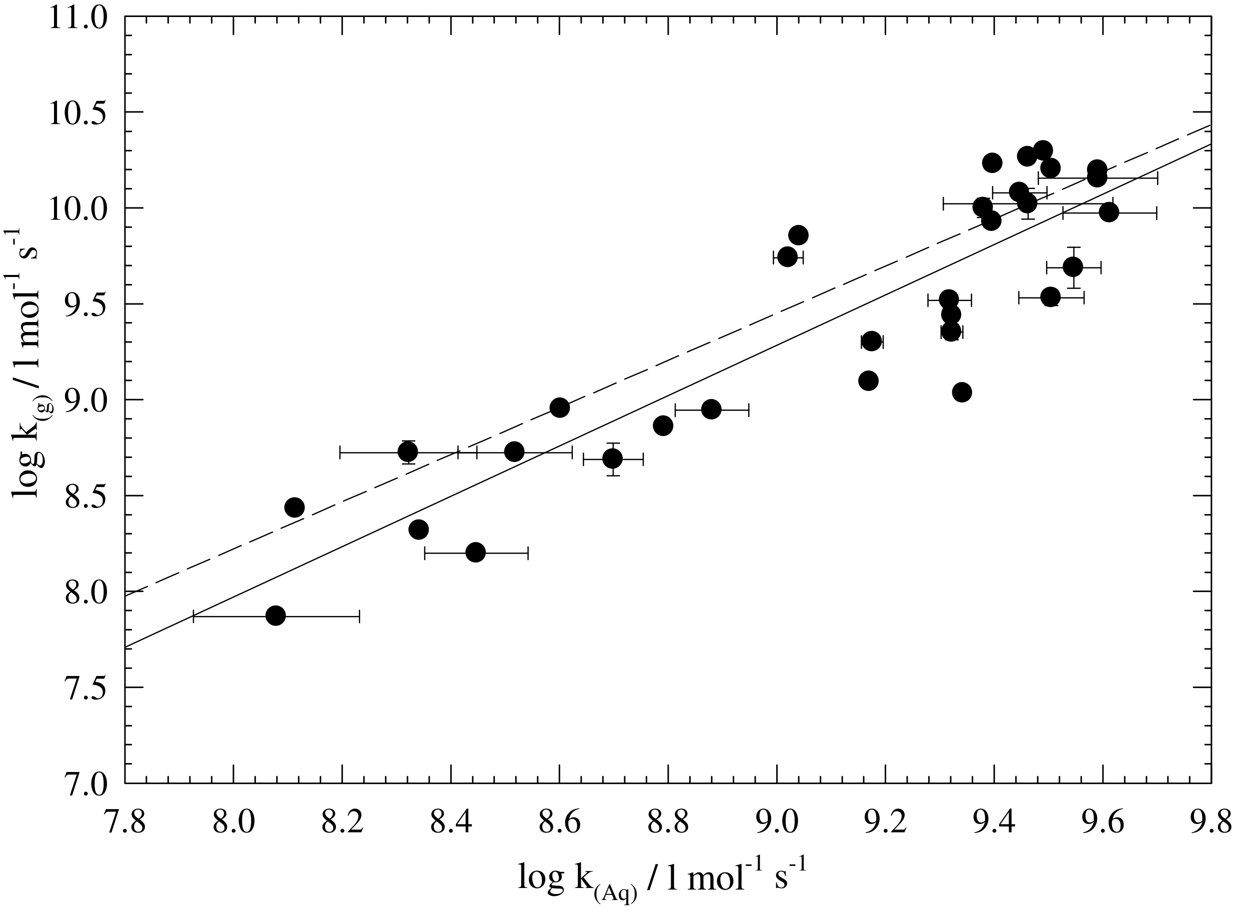

Figure 7: Plot of measured room temperature gas phase rate constants for the H-abstraction reactions of OH with a series of organic compounds versus corresponding aqueous phase rate constants. (—): Regression line, (---): 1:1 reactivity correlation.

Sasho Gligorovski, is an Associate Prof. in the “Laboratoire de Chimie de l’Environnement” at the Aix Marseille University, France. He obtained his Ph.D. at 2005 under supervision of Hartmut Herrmann at the Institute for Tropospheric Research, Leipzig, Germany followed by one year of postdoc (2005-2006) with Christian George at IRCELYON. In 2006 he was enrolled as an Assistant Professor at the Aix Marseille University where in 2012 he finished his habilitation thesis.

His research interest aim to elucidate the kinetics, mechanisms, and photochemistry of gas phase, aqueous phase and heterogeneous reactions occurring at the surface of particles, and on various indoor surfaces. He designed and organized the first field campaign aiming at the first experimental confirmation of OH radicals in the indoor atmospheres.

Rafal Strekowski holds a doctoral degree in Atmospheric Sciences from Georgia Institute of Technology, Atlanta, U.S.A.. He is now an Associate Professor in the *Laboratoire de Chimie de L'Environnement* at the Aix-Marseille University, Marseilles, France. Current research interests include gas phase reaction kinetic processes that are particularly important in the Earth's troposphere and stratosphere. Another focus of research effort is on aerosol speciation and formation processes that are particularly important in marine environments and of nuclear industry safety interest.

Dr. Stephane Barbati is an Associate Professor in the “Laboratoire de Chimie de l’Environnement” at the Aix Marseille University, France. He obtained his Ph.D. in Physical-Chemistry (1997) in the field of free radicals in organic chemistry under the supervision of Prof. Dr. Tordo. He joined his actual laboratory in 1998. His research interests focus on chemical reaction mechanisms in environmental chemistry. He is the author of two patent licenses in the field of water treatment technology.

Davide Vione (b. 1974) got his PhD in Chemistry in 2001 from the University of Torino, Italy, where he is associate professor in the Department of Chemistry since 2011. His main research interests focus on the photochemical processes taking place in surface waters and atmospheric aerosols. In 2003 he received the Young Researcher Award from the European Association of Chemistry and the Environment, of which he is presently (2013 -) a board member. He authored over 170 scientific articles, with h-index = 30 (Scopus, October 2015).